NOVEL METHODS FOR THE TIME-DEPENDENT MAXWELL'S EQUATIONS AND THEIR APPLICATIONS

by

Sidney Shields

April 20, 2017

This dissertation was prepared by using the class file unlvmathesis.cls according to the requirement of dissertation format of the Graduate College of the University of Nevada at Las Vegas, USA.

unlvmathesis.cls: A LaTeX Class for UNLV–MATH thesis and dissertation.

Version: 2.0

Authors: Anthony D. Holmes and Hongtao Yang

Dates: March 13, 2010 & April 29, 2014

NOVEL METHODS FOR THE TIME-DEPENDENT MAXWELL'S EQUATIONS AND THEIR APPLICATIONS

by

Sidney Shields

Bachelor of Science in Mathematics
Pacific Union College, Angwin, CA
2011

A dissertation submitted in partial fulfillment of
the requirements for the

Doctor of Philosophy - Mathematical Sciences

Department of Mathematical Sciences
College of Sciences
The Graduate College

University of Nevada, Las Vegas
May 2017

For Albert E. Watson,
1931-2013

ABSTRACT

NOVEL METHODS FOR THE TIME-DEPENDENT MAXWELL'S EQUATIONS AND THEIR APPLICATIONS

by

Sidney Shields

Dr. Jichun Li, Examination Committee Chair
Professor, Mathematics
University of Nevada, Las Vegas, USA

This dissertation investigates three different mathematical models based on the time-domain Maxwell's equations using three different numerical methods: a Yee scheme using a non-uniform grid, a nodal discontinuous Galerkin (nDG) method, and a newly developed discontinuous Galerkin method named the weak Galerkin (WG) method. The non-uniform Yee scheme is first applied to an electromagnetic metamaterial model. Stability and superconvergence error results are proved for the method, which are then confirmed through numerical results. Additionally, a numerical simulation of backwards wave propagation through a negative-index metamaterial is given using the presented method. Next, the nDG method is used to simulate signal propagation through a corrugated coaxial cable through the use of axisymmetric Maxwell's equations. Stability and error analysis are performed for the semi-discrete method, and are verified through numerical results. The nDG method is then used to simulate signal propagation through coaxial cables with a number of different corrugations. Finally, the WG method is developed for the standard time-domain Maxwell's equations. Similar to the other methods, stability and error analysis are performed on the method and are verified through a number of numerical experiments.

ACKNOWLEDGEMENTS

First and foremost I would like to thank my adviser professor Jichun Li for not only his patience with me, but for his constant support of my future career goals.

I am grateful to Eric Machorro, Aaron Luteman, and Michal Odyniec for their constant advice and mentoring while I worked at NSTec. Because of them, my time there has given me indispensable experience for my future research.

I must also thank the members of my advisory committee, professors Monika Neda, Hongtao Yang, Pengtao Sun, and Yi-Tung Chen for their guidance and time.

My fellow graduate students have also been a great source of inspiration during my time at UNLV. I would like to specifically thank Daniel Corral, Anthony Sellari, Sean Breckling, and Jaicheng (Jason) Cai for their willingness to discuss problems with me among other things.

Finally, I would also like to acknowledge the enormous amount of support my family has given me throughout my career as a graduate student. I would like to thank my mother Marilyn for her unending words of encouragement, as well as my sister Andrea for her continuous friendship and random visits. Most of all I would like to thank my fiancée Sara: her continuous love and support were a great source of motivation when things got tough.

This manuscript has been authored by National Security Technologies, LLC, under Contract No. DE-AC52-06NA25946 with the U.S. Department of Energy, National Nuclear Security Administration, Office of Defense Programs (NA-10). The United States Government retains and the publisher, by accepting the work for pub-

TABLE OF CONTENTS

LIST OF FIGURES

CHAPTER 1

INTRODUCTION

One field of physics that benefits greatly from numerical methods is electromagnetics. The behavior of electric field $\mathbf{E}$ and magnetic field $\mathbf{B}$ can be described by a set of PDEs called Maxwell's equations. Maxwell's equations are a set of coupled partial differential equations describing the wave propagation in a specific material with permittivity ϵ and permeability μ:

$$\nabla \times \mathbf{E} = -\frac{\partial \mathbf{B}}{\partial t}, \quad \nabla \times \mathbf{H} = \frac{\partial \mathbf{D}}{\partial t} + \mathbf{j}, \tag{1.1a}$$

$$\nabla \cdot \mathbf{D} = \rho \quad , \quad \nabla \cdot \mathbf{B} = 0 \quad , \tag{1.1b}$$

supplemented with the following constitutive relations:

$$\mathbf{B} = \mu \mathbf{H}, \quad \mathbf{j} = \sigma \mathbf{E}, \quad \mathbf{D} = \epsilon \mathbf{E}. \tag{1.2}$$

Here $\mathbf{E}$ models the electric field, $\mathbf{B}$ describes the magnetic flux density, $\mathbf{H}$ represents the magnetic field, $\mathbf{D}$ is the displacement current density, σ is the electric conductivity, and ρ is the charge density. Because this set of PDEs is dependent on time as well as space, it is often converted to the frequency domain through a Fourier transform to reduce the complexity of them. However, if these PDEs are left in the time domain when being solved numerically, the divergence free conditions are then enforced implicitly and can be ignored. The following chapters will only concern numerical methods for solving Maxwell's equations in the time domain, though methods for solving the equations in the frequency domain do exist.

Often, under certain conditions, numerical methods will converge faster than expected; this phenomena is called superconvergence. The superconvergence study of finite element methods (FEMs) started in the early 1970s, over the years many interesting results have been proved mainly for a variety of equations such as elliptic Bank and Xu (2004a,b); Cao (2014); Celiker et al. (2012); Li and Wheeler (2000), parabolic Chen et al. (1998), hyperbolic Adjerid and Baccouch (2007); Guo et al. (2015), KdV Arnold and Winther (1982), and Stokes equations Wang and Ye (2001). More details on superconvergence can be found in classic books such as Chen and Huang (1995); Krizek et al. (1998); Lin and Yan (1996); Wahlbin (1995). As for Maxwell's equations in vacuum, in 1994 Monk carried out the first superconvergence analysis for FEMs Monk (1994), and for finite difference method together with Süli Monk and Süli (1994). Later more superconvergence results have been obtained on Cartesian grids solved with edge elements Lin and Yan (1999); Lin and Li (2008), nonconforming FEMs Qiao et al. (2011); Shi and Pei (2009), discontinuous Galerkin methods Chung et al. (2013), and finite volume methods Chung et al. (2003); Nicolaides and Wang (1998).

Inspired by the many exotic potential applications of metamaterials (cf. Craster and Guenneau (2013); Engheta and Ziolkowski (2006); Li and Huang (2013) and references therein), the study of metamaterials has been of significant interest as of late in the field of electromagnetics. The term "metamaterial" is a broad term that describes any material with special properties that are not found in nature. Because these materials are not natural, they must be specially engineered to have these properties. One specific type of metamaterial that is of interest is the negative-

index metamaterial. This material is characterized by having frequency dependent permittivitty and permeability, resulting in a negative index of refraction. To model this frequency dependent permittivitty and permeability, one can employ either the Drude model, Lorenz model, or a mixture of the two. Additionally, these definitions can be converted into the time-domain as shown in (Li and Huang (2013)).

In the chapter 2 of this dissertation we extend this superconvergence analysis to the Yee finite difference time-domain (FDTD) method with a non-uniform rectangular grid for the time-domain Drude model for metamaterials. To the best of our knowledge, superconvergence analysis for FDTD methods for Maxwell's equations are restricted to uniform rectangular grids (cf. Bokil and Gibson (2012); Chen et al. (2008); Gao and Zhang (2011); Hong et al. (2014); Li et al. (2013)). However, in Monk and Süli (1994) they extend this superconvergence result to an FDTD method with a non-uniform grid. As a continuation of their work with superconvergence analysis on FDTD methods with non-uniform grids, we extend their technique to the more complicated Drude metamaterial model found in Li (2007).

The next application that was solved through the use of Maxwell's equations is the corrugated coaxial cable model. Due to the long standing and widespread usage of coaxial cables, there are many published papers on modeling wave and signal propagation through coaxial cables. Various methods Sen and Wheeler (1998); Schüppert (1988), ranging from using experimental data to mathematical models, have been developed for transmission lines. For coaxial cables the two most common methods of mathematically modeling signal and wave propagation through the cables are to solve either the telegrapher's equations Ramo et al. (1994) (developed by Oliver Heaviside

in the 1880s) or Maxwell's equations.

The telegrapher's equations treat the conductors in the coaxial cable as an infinite series of two-port elementary components, each representing an infinitesimally short segment of the transmission line. Each segment of the line is modeled by a circuit with four elementary components: a resistor and inductor in series, a shunt capacitor between the two conductors, and a shunt resistor between the two conductors Ulaby (2007). The following telegrapher's equations are used to model the voltage V and current I of the transmitted signal on a transmission line with resistance R, inductance L, capacitance C, and conductance G:

$$\frac{\partial V}{\partial x}(x,t) = -L\frac{\partial I}{\partial t}(x,t) - RI(x,t),$$
$$\frac{\partial I}{\partial x}(x,t) = -C\frac{\partial V}{\partial t}(x,t) - GV(x,t).$$

Note that the telegrapher's equations are a coupled system of two one-dimensional partial differential equations (PDEs), making them quite simple and efficient to solve. However, since the telegrapher's equations are a one-dimensional representation of the coaxial cable, they do not take into account the geometry of the cable. Hence if the cable's cross section changes at different locations such as the corrugated cable, then the effects of the corrugation cannot be accounted for without adding in an artificial term. In Imperiale and Joly (2014), Imperiale and Joly derived the telegrapher's model via an asymptotic analysis from 3-D Maxwell's equations for a lossy coaxial cable whose cross section is not homogeneous.

To account for the variable cross section cables, we resort to solving the Maxwell's equations in three-dimensional (3-D) space. However, this PDE system is much more

complex and computationally intensive to solve than the telegrapher's equations. To reduce the computational cost and consider notions of the fact that many coaxial cables of interest have rotational symmetry about the z-axis (i.e. the angular component has no effect on the electric or magnetic fields), we often reduce the 3-D problem to a 2-D problem whose domain is the length-wise cross-section (the red part in Figure 1.1).

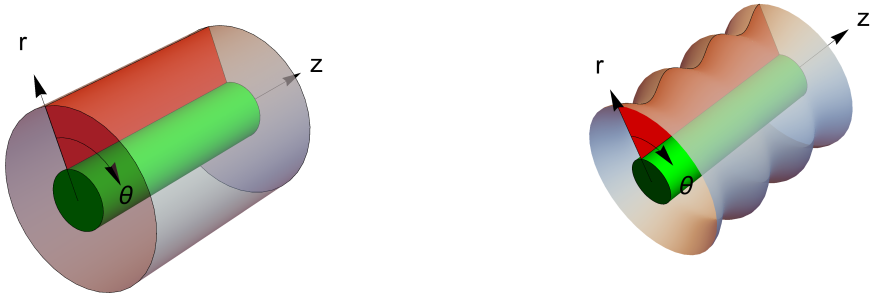

Figure 1.1. (Left) A 3-D view of a coaxial cable. Red rectangle: cross-sectional domain; Green cylinder: inner conductor; Grey cylinder: outer conductor. (Right) A 3-D view of a corrugated coaxial cable. Red rectangle: cross-sectional domain.

Although there has been previous work concerning the numerical modeling of corrugated coaxial cables Böcklin et al. (2009); Blank et al. (2013); Imperiale and Joly (2014), we aim to explore the effects of these corrugations in more detail in chapter 3. Following the work of Blank et al. (2013), we consider the axisymmetric Maxwell's equations in cylindrical coordinates, and extend their work to the corrugated cable model. Similar to their work, we solve these equations using a nodal Discontinuous

Galerkin method (cf. Hesthaven and Warburton (2008); Li and Hesthaven (2014); Li et al. (2012)). However, because they do not perform any analysis on their proposed scheme, we provide stability and error analysis for the semi-discrete scheme.

Finally, a new numerical method for PDEs, named the weak Galerkin (WG) method, was developed to spatially solve Maxwell's equations. The Weak Galerkin (WG) finite element method was initially developed by Wang and Ye Wang and Ye (2013, 2014) for solving the second order elliptic equations. The main idea is to approximate the differential operators in partial differential equations (PDEs) through the use of a new notion of discrete weak derivatives, which will be defined later (in Section 4.2). This concept offers a new paradigm for solving various PDEs, and applications have been extended to the biharmonic equations Mu et al. (2014); Wang and Wang (2015), Stokes equations Wang and Ye (2016), parabolic equations Li and Wang (2013), and time-harmonic Maxwell's equations Mu et al. (2015a), etc. The WG method is a newcomer to the ever growing family of various popular discontinuous Galerkin (DG) methods Oden et al. (1998); Babuśka et al. (1999); Arnold et al. (0102), such as the hybridizable discontinuous Galerkin method (HDG) Cockburn et al. (2009), the discontinuous Pertrov-Galerkin (DPG) method Demkowicz and Gopalakrishnan (2011); Chan et al. (2014), and the local discontinuous Galerkin (LDG) method Cockburn and Shu (1998). Some DG methods are closely related, for example, many differences and similarities between HDG and WG methods have been addressed in Chen et al. (2015); Mu et al. (2015b).

Since this method had only been applied to Maxwell's equations once, in the frequency domain Mu et al. (2015a), we decided to extend it to the standard set of

time-dependent Maxwell's equations. The goal here was to lay down a framework of analysis for the new method before continuing on to more difficult models. Therefore, in chapter 4 we propose a semi-discrete and a fully-discrete WG scheme for the time-dependent Maxwell's equations. In addition to this, we provide stability and convergence results for each of these schemes.

The rest of this dissertation is organized as follows. In chapter 2, we first propose semi-discrete and fully-discrete finite difference schemes on non-uniform rectangular meshes. Then we prove the discrete stability, and the second order convergence rate in space (which is superconvergent) for all field variables for both schemes in the discrete L_2 norm. Afterwards, we provide numerical results to confirm the superconvergence and solve a benchmark backwards wave propagation problem. In chapter 3 we extend the nodal Discontinuous Galerkin method for the axisymmetric Maxwell's equations proposed in Blank et al. (2013) to the cable model. Then we prove a stability and a convergence result for the aforementioned semi-discrete scheme. After, we support our results with numerical tests, in addition to providing a benchmark problem for signal propagation through corrugated coaxial cables. In chapter 4 we propose a semi-discrete and a fully-discrete weak Galerkin scheme for the time-domain Maxwell's equations. For each scheme we provide stability and convergence results. Then, we support our results with numerical tests. Finally, in chapter 5 we conclude and summarize the results provided in this dissertation.

CHAPTER 2

THE YEE SCHEME FOR METAMATERIAL MAXWELL'S EQUATIONS ON NON-UNIFORM RECTANGULAR MESHES

2.1 Introduction

In Li (2009), Li developed a finite element time-domain (FETD) method for solving the Drude metamaterial model (2.1)-(2.4) shown below, and proved that the scheme has an optimal error estimate $O(h) + O(\tau^2)$ in the L^2-norm for the lowest-order edge element, i.e., converges first order in space, and second order in time. But numerical results of Li (2009) showed the superconvergence rate $O(h^2)$ on non-uniform rectangular grids. The observed superconvergence phenomena were proved later for both 2D and 3D models solved by the FETD method on non-uniform rectangular and cubic grids in Huang et al. (2012) and Huang et al. (2011), respectively.

Compared to the superconvergence results obtained for Maxwell's equations by FEMs, some superconvergences have also proved for the finite difference time-domain (FDTD) methods (cf. Bokil and Gibson (2012); Chen et al. (2008); Gao and Zhang (2011); Hong et al. (2014); Li et al. (2013)). However, all papers except Monk and Süli Monk and Süli (1994) are restricted to uniform rectangular grids. In this chapter, we extend Monk and Süli's technique to the more complicated Maxwell's equations in metamaterials. First, we prove that similar superconvergence results hold true for the metamaterial Maxwell's equations solved by the FDTD method on staggered non-

uniform rectangular grids. Our proof is more succinct than Monk and Süli (1994). Second, we present the complete proofs for both the semi- and fully-discrete schemes (i.e, the true Yee scheme), while Monk and Süli (1994) only showed the proof for the semi-discrete scheme. To our best knowledge, this is the first superconvergence result obtained on Yee scheme for Maxwell's equations in metamaterial.

The rest of this chapter is organized as follows. In Sect. 2, we first derive a semi-discrete finite difference scheme on non-uniform rectangular meshes from a variational form, which will be used late in the error analysis. Then we prove the discrete stability, and the second order convergence rate in space (which is superconvergent) for all field variables in the discrete L_2 norm. In Sect. 3, we consider the fully-discrete scheme on non-uniform rectangular meshes. Detailed analysis is present for the discrete stability, and the error estimate which is second order in both time and spatial variables. Numerical results are presented in Sect. 4 to support our theoretical analysis. We conclude the chapter in Sect. 5. The research presented in this chapter was previously published as Li and Shields (2016) where I was the 2nd author.

2.2 The semi-discrete scheme

Consider the metamaterial model Li (2007):

$$\epsilon_0 \frac{\partial \boldsymbol{E}}{\partial t} = \nabla \times \boldsymbol{H} - \boldsymbol{J} \tag{2.1}$$

$$\mu_0 \frac{\partial \boldsymbol{H}}{\partial t} = -\nabla \times \boldsymbol{E} - \boldsymbol{K} \tag{2.2}$$

$$\frac{1}{\epsilon_0 \omega_{pe}^2} \frac{\partial \boldsymbol{J}}{\partial t} + \frac{\Gamma_e}{\epsilon_0 \omega_{pe}^2} \boldsymbol{J} = \boldsymbol{E} \tag{2.3}$$

$$\frac{1}{\mu_0\omega_{pm}^2}\frac{\partial \boldsymbol{K}}{\partial t}+\frac{\Gamma_m}{\mu_0\omega_{pm}^2}\boldsymbol{K}=\boldsymbol{H} \tag{2.4}$$

supplemented with the perfect conduct (PEC) boundary condition

$$\boldsymbol{n}\times\boldsymbol{E}=\boldsymbol{0} \quad \text{on } \partial\Omega, \tag{2.5}$$

and the initial conditions

$$\boldsymbol{E}(\boldsymbol{x},0)=\boldsymbol{E}_0(\boldsymbol{x}),\quad \boldsymbol{H}(\boldsymbol{x},0)=\boldsymbol{H}_0(\boldsymbol{x}),\quad \boldsymbol{J}(\boldsymbol{x},0)=\boldsymbol{J}_0(\boldsymbol{x}),\quad \boldsymbol{K}(\boldsymbol{x},0)=\boldsymbol{K}_0(\boldsymbol{x}), \tag{2.6}$$

where $\boldsymbol{n}$ denotes the outward unit normal vector, $\boldsymbol{E}_0(\boldsymbol{x}), \boldsymbol{H}_0(\boldsymbol{x}), \boldsymbol{J}_0(\boldsymbol{x})$ and $\boldsymbol{K}_0(\boldsymbol{x})$ are some given proper functions.

To avoid the technicality of the proof for 3D problems, below we only consider the 2D case of (2.1)-(2.6), in which $\boldsymbol{E}=(E_x,E_y), \boldsymbol{H}=H_z:=H, \boldsymbol{J}=(J_x,J_y), \boldsymbol{K}=K_z$, and the curls $\nabla\times\boldsymbol{E}=\frac{\partial E_y}{\partial x}-\frac{\partial E_x}{\partial y}$ and $\nabla\times H=(\frac{\partial H}{\partial y},-\frac{\partial H}{\partial x})'$. Here the subindices x,y and z denote the components in the x,y and z directions, respectively. For simplicity, we consider the rectangular domain $\Omega=[a,b]\times[c,d]$, which is discretized by a non-uniform grid

$$a=x_0<x_1<\cdots<x_{N_x}=b,\quad c=y_0<y_1<\cdots<y_{N_y}=d.$$

We like to emphasize that our proof and the obtained results can be similarly extend to 3D problem.

Following the classic FDTD scheme, we choose the unknowns E_x (and J_x) at the mid-points of the horizontal edges, E_y (and J_y) at the mid-points of the vertical edges, and H (and K) at the element centers (cf. Fig.2.1). Hence we can denote the corresponding approximate solutions (we suppress the explicit dependence on time

t):

$$E_{x,i+\frac{1}{2},j}, \quad J_{x,i+\frac{1}{2},j}, \quad i = 0, \cdots, N_x - 1, \ j = 0, \cdots, N_y,$$

$$E_{y,i,j+\frac{1}{2}}, \quad J_{y,i,j+\frac{1}{2}}, \quad j = 0, \cdots, N_y - 1, \ i = 0, \cdots, N_x,$$

$$H_{i+\frac{1}{2},j+\frac{1}{2}}, \quad K_{i+\frac{1}{2},j+\frac{1}{2}}, \quad i = 0, \cdots, N_x - 1, \ j = 0, \cdots, N_y - 1.$$

For convenience, we denote the following three types of rectangles

$$T_{ij} = (x_i, x_{i+1}) \times (y_j, y_{j+1}), \ T_{i-\frac{1}{2},j} = (x_{i-\frac{1}{2}}, x_{i+\frac{1}{2}}) \times (y_j, y_{j+1}),$$

$$T_{i,j-\frac{1}{2}} = (x_i, x_{i+1}) \times (y_{j-\frac{1}{2}}, y_{j+\frac{1}{2}}),$$

and the corresponding areas $|T_{ij}|, |T_{i-\frac{1}{2},j}|$ and $|T_{i,j-\frac{1}{2}}|$, respectively. To distinguish the role of non-uniform mesh, we denote $h_x = \max_{0 \le i \le N_x - 1}(x_{i+1} - x_i)$ and $h_y = \max_{0 \le j \le N_y - 1}(y_{j+1} - y_j)$ for the maximal mesh sizes in the x and y directions, respectively. The global mesh size will be denoted by $h = \max(h_x, h_y)$.

Integrating the x-component of (2.1) on $T_{i,j-\frac{1}{2}}$ (for any $0 \le i \le N_x - 1, 1 \le j \le N_y - 1$), we obtain

$$\int_{x_i}^{x_{i+1}} \int_{y_{j-\frac{1}{2}}}^{y_{j+\frac{1}{2}}} \epsilon_0 \frac{\partial E_x}{\partial t} = \int_{x_i}^{x_{i+1}} [H(x, y_{j+\frac{1}{2}}, t) - H(x, y_{j-\frac{1}{2}}, t)] dx - \int_{x_i}^{x_{i+1}} \int_{y_{j-\frac{1}{2}}}^{y_{j+\frac{1}{2}}} J_x. \quad (2.7)$$

Approximating those integrals in (2.7) by the mid-point quadrature rule, we have

$$\epsilon_0 |T_{i,j-\frac{1}{2}}| \cdot \frac{\partial E_x}{\partial t}|_{i+\frac{1}{2},j} = (x_{i+1} - x_i)(H_{i+\frac{1}{2},j+\frac{1}{2}} - H_{i+\frac{1}{2},j-\frac{1}{2}}) - |T_{i,j-\frac{1}{2}}| J_{x,i+\frac{1}{2},j}. \quad (2.8)$$

Similarly, integrating the y-component of (2.1) on $T_{i-\frac{1}{2},j}$ (for any $1 \le i \le N_x - 1, 0 \le j \le N_y - 1$) yields

$$\int_{x_{i-\frac{1}{2}}}^{x_{i+\frac{1}{2}}} \int_{y_j}^{y_{j+1}} \epsilon_0 \frac{\partial E_y}{\partial t} = -\int_{y_j}^{y_{j+1}} [H(x_{i+\frac{1}{2}}, y, t) - H(x_{i-\frac{1}{2}}, y, t)] dy - \int_{x_{i-\frac{1}{2}}}^{x_{i+\frac{1}{2}}} \int_{y_j}^{y_{j+1}} J_y. \quad (2.9)$$

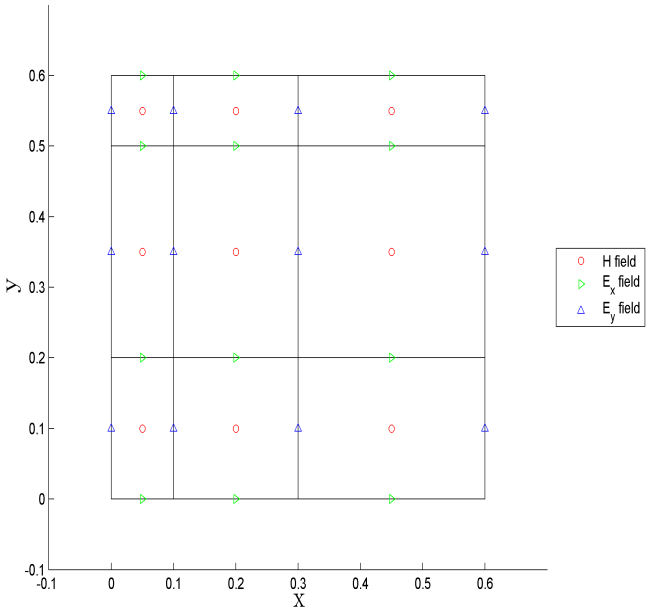

Figure 2.1. The exemplary grid for solving 2D Maxwell's equations.

Approximating those integrals in (2.9) by the mid-point quadrature rule, we have

$$\epsilon_0|T_{i-\frac{1}{2},j}|\cdot\frac{\partial E_y}{\partial t}|_{i,j+\frac{1}{2}}=-(y_{j+1}-y_j)(H_{i+\frac{1}{2},j+\frac{1}{2}}-H_{i-\frac{1}{2},j+\frac{1}{2}})-|T_{i-\frac{1}{2},j}|J_{y,i,j+\frac{1}{2}}. \quad (2.10)$$

By the same technique, integrating (2.2) on T_{ij} (for any $0\le i\le N_x-1, 0\le j\le N_y-1$) yields

$$\int_{x_i}^{x_{i+1}}\int_{y_j}^{y_{j+1}}\mu_0\frac{\partial H}{\partial t}=-\int_{x_i}^{x_{i+1}}\int_{y_j}^{y_{j+1}}(\frac{\partial E_y}{\partial x}-\frac{\partial E_x}{\partial y})-\int_{x_i}^{x_{i+1}}\int_{y_j}^{y_{j+1}}K. \quad (2.11)$$

Further application of the mid-point quadrature rule leads to

$$\begin{aligned}\mu_0|T_{ij}|\cdot\frac{\partial H}{\partial t}|_{i+\frac{1}{2},j+\frac{1}{2}}&=-(y_{j+1}-y_j)(E_{y,i+1,j+\frac{1}{2}}-E_{y,i,j+\frac{1}{2}})\\&+(x_{i+1}-x_i)(E_{x,i+\frac{1}{2},j+1}-E_{x,i+\frac{1}{2},j})-|T_{ij}|\cdot K_{i+\frac{1}{2},j+\frac{1}{2}}. \quad (2.12)\end{aligned}$$

Integrating the x-component of (2.3) on $T_{i,j-\frac{1}{2}}$ (for any $0\le i\le N_x-1, 1\le j\le$

$N_y - 1$), we obtain

$$\int_{x_i}^{x_{i+1}} \int_{y_{j-\frac{1}{2}}}^{y_{j+\frac{1}{2}}} \frac{1}{\epsilon_0 \omega_{pe}^2} \frac{\partial J_x}{\partial t} + \int_{x_i}^{x_{i+1}} \int_{y_{j-\frac{1}{2}}}^{y_{j+\frac{1}{2}}} \frac{\Gamma_e}{\epsilon_0 \omega_{pe}^2} J_x = \int_{x_i}^{x_{i+1}} \int_{y_{j-\frac{1}{2}}}^{y_{j+\frac{1}{2}}} E_x. \tag{2.13}$$

Approximating (2.13) by the mid-point quadrature rule, we have

$$|T_{i,j-\frac{1}{2}}| \cdot \frac{1}{\epsilon_0 \omega_{pe}^2} \frac{\partial J_x}{\partial t}|_{i+\frac{1}{2},j} + |T_{i,j-\frac{1}{2}}| \cdot \frac{\Gamma_e}{\epsilon_0 \omega_{pe}^2} J_{x,i+\frac{1}{2},j} = |T_{i,j-\frac{1}{2}}| \cdot E_{x,i+\frac{1}{2},j}. \tag{2.14}$$

Integrating the y-component of (2.3) on $T_{i-\frac{1}{2},j}$ (for any $1 \leq i \leq N_x - 1, 0 \leq j \leq N_y - 1$), and using the mid-point quadrature rule, we obtain

$$|T_{i-\frac{1}{2},j}| \cdot \frac{1}{\epsilon_0 \omega_{pe}^2} \frac{\partial J_y}{\partial t}|_{i,j+\frac{1}{2}} + |T_{i-\frac{1}{2},j}| \cdot \frac{\Gamma_e}{\epsilon_0 \omega_{pe}^2} J_{y,i,j+\frac{1}{2}} = |T_{i-\frac{1}{2},j}| \cdot E_{y,i,j+\frac{1}{2}}. \tag{2.15}$$

Similarly, integrating (2.4) on T_{ij} (for any $0 \leq i \leq N_x - 1, 0 \leq j \leq N_y - 1$), and using the mid-point quadrature rule, we obtain

$$|T_{ij}| \cdot \frac{1}{\mu_0 \omega_{pm}^2} \frac{\partial K}{\partial t}|_{i+\frac{1}{2},j+\frac{1}{2}} + |T_{ij}| \cdot \frac{\Gamma_m}{\mu_0 \omega_{pm}^2} K_{i+\frac{1}{2},j+\frac{1}{2}} = |T_{ij}| \cdot H_{i+\frac{1}{2},j+\frac{1}{2}}. \tag{2.16}$$

The stability analysis

We define the following mesh-dependent energy norms

$$\begin{aligned}
||E_x||_E^2 &= \sum_{\substack{0 \leq i \leq N_x - 1 \\ 1 \leq j \leq N_y - 1}} |T_{i,j-\frac{1}{2}}| \cdot |E_{x,i+\frac{1}{2},j}|^2, \\
||E_y||_E^2 &= \sum_{\substack{1 \leq i \leq N_x - 1 \\ 0 \leq j \leq N_y - 1}} |T_{i-\frac{1}{2},j}| \cdot |E_{y,i,j+\frac{1}{2}}|^2, \\
||H||_H^2 &= \sum_{\substack{0 \leq i \leq N_x - 1 \\ 0 \leq j \leq N_y - 1}} |T_{ij}| \cdot |H_{i+\frac{1}{2},j+\frac{1}{2}}|^2, \\
||J_x||_J^2 &= \sum_{\substack{0 \leq i \leq N_x - 1 \\ 1 \leq j \leq N_y - 1}} |T_{i,j-\frac{1}{2}}| \cdot |J_{x,i+\frac{1}{2},j}|^2, \\
||J_y||_J^2 &= \sum_{\substack{1 \leq i \leq N_x - 1 \\ 0 \leq j \leq N_y - 1}} |T_{i-\frac{1}{2},j}| \cdot |J_{y,i,j+\frac{1}{2}}|^2,
\end{aligned}$$

$$||K||_K^2 = \sum_{\substack{0\le i\le N_x-1\\ 0\le j\le N_y-1}} |T_{ij}|\cdot |K_{i+\frac{1}{2},j+\frac{1}{2}}|^2.$$

First, we can prove the following energy conservation for our semi-discrete scheme.

Theorem 2.21. The solution of the semi-discrete scheme (2.8)-(2.16) satisfies the global energy identity:

$$\begin{aligned}
&\frac{1}{2}[\epsilon_0(||E_x||_E^2+||E_y||_E^2)+\mu_0||H||_H^2+\frac{1}{\epsilon_0\omega_{pe}^2}(||J_x||_J^2+||J_y||_J^2)\\
&\quad+\frac{1}{\mu_0\omega_{pm}^2}||K||_K^2](t)+\int_0^t[\frac{\Gamma_e}{\epsilon_0\omega_{pe}^2}(||J_x||_J^2+||J_y||_J^2)+\frac{\Gamma_m}{\mu_0\omega_{pm}^2}||K||_K^2]dt\\
=\;&\frac{1}{2}[\epsilon_0(||E_x||_E^2+||E_y||_E^2)+\mu_0||H||_H^2+\frac{1}{\epsilon_0\omega_{pe}^2}(||J_x||_J^2+||J_y||_J^2)\\
&\quad+\frac{1}{\mu_0\omega_{pm}^2}||K||_K^2](0) \qquad (2.17)
\end{aligned}$$

holds true for any $t\in[0,T]$.

Proof. Multiplying (2.8) by $E_{x,i+\frac{1}{2},j}$, (2.10) by $E_{y,i,j+\frac{1}{2}}$, (2.12) by $H_{i+\frac{1}{2},j+\frac{1}{2}}$, (2.14) by $J_{x,i+\frac{1}{2},j}$, (2.15) by $J_{y,i,j+\frac{1}{2}}$, and (2.16) by $K_{i+\frac{1}{2},j+\frac{1}{2}}$, summing up each over its corresponding rectangular elements, then adding all results together, we obtain the sum of the right hand side as

$$\begin{aligned}
RHS\;=\;&\sum_{\substack{0\le i\le N_x-1\\ 1\le j\le N_y-1}}(x_{i+1}-x_i)(H_{i+\frac{1}{2},j+\frac{1}{2}}-H_{i+\frac{1}{2},j-\frac{1}{2}})E_{x,i+\frac{1}{2},j}\\
&-\sum_{\substack{1\le i\le N_x-1\\ 0\le j\le N_y-1}}(y_{j+1}-y_j)(H_{i+\frac{1}{2},j+\frac{1}{2}}-H_{i-\frac{1}{2},j+\frac{1}{2}})E_{y,i,j+\frac{1}{2}}\\
&-\sum_{\substack{0\le i\le N_x-1\\ 0\le j\le N_y-1}}(y_{j+1}-y_j)(E_{y,i+1,j+\frac{1}{2}}-E_{y,i,j+\frac{1}{2}})H_{i+\frac{1}{2},j+\frac{1}{2}}\\
&+\sum_{\substack{0\le i\le N_x-1\\ 0\le j\le N_y-1}}(x_{i+1}-x_i)(E_{x,i+\frac{1}{2},j+1}-E_{x,i+\frac{1}{2},j})H_{i+\frac{1}{2},j+\frac{1}{2}}\\
=\;&\sum_{0\le i\le N_x-1}(x_{i+1}-x_i)\sum_{0\le j\le N_y-1}[H_{i+\frac{1}{2},j+\frac{1}{2}}E_{x,i+\frac{1}{2},j+1}-H_{i+\frac{1}{2},j-\frac{1}{2}}E_{x,i+\frac{1}{2},j}]
\end{aligned}$$

$$
\begin{aligned}
& - \sum_{0\le j\le N_y-1}(y_{j+1}-y_j)\sum_{0\le i\le N_x-1}[H_{i+\frac{1}{2},j+\frac{1}{2}}E_{y,i+1,j+\frac{1}{2}} - H_{i-\frac{1}{2},j+\frac{1}{2}}E_{y,i,j+\frac{1}{2}}] \\
= & \sum_{0\le i\le N_x-1}(x_{i+1}-x_i)[H_{i+\frac{1}{2},N_y-\frac{1}{2}}E_{x,i+\frac{1}{2},N_y} - H_{i+\frac{1}{2},-\frac{1}{2}}E_{x,i+\frac{1}{2},0}] \\
& - \sum_{0\le j\le N_y-1}(y_{j+1}-y_j)[H_{N_x-\frac{1}{2},j+\frac{1}{2}}E_{y,N_x,j+\frac{1}{2}} - H_{-\frac{1}{2},j+\frac{1}{2}}E_{y,0,j+\frac{1}{2}}] \\
= & \ 0, \qquad (2.18)
\end{aligned}
$$

where we used the PEC boundary condition (2.5), which in our 2D case is equivalent to

$$
E_{x,i+\frac{1}{2},N_y} = E_{x,i+\frac{1}{2},0} = 0, \quad E_{y,N_x,j+\frac{1}{2}} = E_{y,0,j+\frac{1}{2}} = 0, \qquad (2.19)
$$

for all i and j.

Using the above defined energy norms, the sum of the left hand side corresponding to the above operation is given as

$$
\begin{aligned}
LHS \ = \ & \frac{1}{2}\frac{d}{dt}[\epsilon_0(||E_x||_E^2 + ||E_y||_E^2) + \mu_0||H||_H^2 + \frac{1}{\epsilon_0\omega_{pe}^2}(||J_x||_J^2 + ||J_y||_J^2) \\
& + \frac{1}{\mu_0\omega_{pm}^2}||K||_K^2] + \frac{\Gamma_e}{\epsilon_0\omega_{pe}^2}(||J_x||_J^2 + ||J_y||_J^2) + \frac{\Gamma_m}{\mu_0\omega_{pm}^2}||K||_K^2. \qquad (2.20)
\end{aligned}
$$

Equating (2.18) and (2.20), and integrating the resultant leads to the global conservation identity. □

Dropping the non-negative terms on the left hand side of (2.17), we can easily obtain the stability for our semi-discrete scheme.

Lemma 2.21. For any $t \in [0, T]$, the solution of the semi-discrete scheme (2.8)-(2.16) satisfies the following stability:

$$
\begin{aligned}
& [\epsilon_0(||E_x||_E^2 + ||E_y||_E^2) + \mu_0||H||_H^2 \\
& \quad + \frac{1}{\epsilon_0\omega_{pe}^2}(||J_x||_J^2 + ||J_y||_J^2) + \frac{1}{\mu_0\omega_{pm}^2}||K||_K^2](t)
\end{aligned}
$$

$$\leq \quad [\epsilon_0(||E_x||_E^2 + ||E_y||_E^2) + \mu_0||H||_H^2 + \frac{1}{\epsilon_0\omega_{pe}^2}(||J_x||_J^2 + ||J_y||_J^2) + \frac{1}{\mu_0\omega_{pm}^2}||K||_K^2](0). \tag{2.21}$$

The error estimate

To make the error analysis easy to follow, we denote the errors by their corresponding script letters. For example, the error of E_x at point $(x_{i+\frac{1}{2}}, y_j, t)$ is denoted by $\mathcal{E}_{x,i+\frac{1}{2},j} = E_x(x_{i+\frac{1}{2}}, y_j, t) - E_{x,i+\frac{1}{2},j}$, where $E_x(x_{i+\frac{1}{2}}, y_j, t)$ and $E_{x,i+\frac{1}{2},j}$ denote the exact and numerical solutions of E_x at point $(x_{i+\frac{1}{2}}, y_j, t)$, respectively. Similarly, we denote errors

$$\mathcal{E}_{y,i,j+\frac{1}{2}} = E_y(x_i, y_{j+\frac{1}{2}}, t) - E_{y,i,j+\frac{1}{2}}, \quad \mathcal{H}_{i+\frac{1}{2},j+\frac{1}{2}} = H(x_{i+\frac{1}{2}}, y_{j+\frac{1}{2}}, t) - H_{i+\frac{1}{2},j+\frac{1}{2}},$$

$$\mathcal{J}_{x,i+\frac{1}{2},j} = J_x(x_{i+\frac{1}{2}}, y_j, t) - J_{x,i+\frac{1}{2},j}, \quad \mathcal{J}_{y,i,j+\frac{1}{2}} = J_y(x_i, y_{j+\frac{1}{2}}, t) - J_{y,i,j+\frac{1}{2}},$$

$$\mathcal{K}_{i+\frac{1}{2},j+\frac{1}{2}} = K(x_{i+\frac{1}{2}}, y_{j+\frac{1}{2}}, t) - K_{i+\frac{1}{2},j+\frac{1}{2}}.$$

By the definition of errors, and from (2.7) and (2.8), we obtain

$$\begin{aligned}
\epsilon_0|T_{i,j-\frac{1}{2}}| \cdot \frac{\partial \mathcal{E}_x}{\partial t}|_{i+\frac{1}{2},j} &= \epsilon_0(\iint_{T_{i,j-\frac{1}{2}}} \frac{\partial E_x}{\partial t}(x_{i+\frac{1}{2}}, y_j, t) - |T_{i,j-\frac{1}{2}}| \cdot \frac{\partial E_x}{\partial t}|_{i+\frac{1}{2},j}) \\
&= \epsilon_0(\iint_{T_{i,j-\frac{1}{2}}} \frac{\partial E_x}{\partial t}(x_{i+\frac{1}{2}}, y_j, t) - \iint_{T_{i,j-\frac{1}{2}}} \frac{\partial E_x}{\partial t}(x, y, t)) \\
&\quad + \int_{x_i}^{x_{i+1}} (H(x, y_{j+\frac{1}{2}}, t) - H(x, y_{j-\frac{1}{2}}, t))dx - \iint_{T_{i,j-\frac{1}{2}}} J_x(x, y, t) \\
&\quad -(x_{i+1} - x_i)(H_{i+\frac{1}{2},j+\frac{1}{2}} - H_{i+\frac{1}{2},j-\frac{1}{2}}) + |T_{i,j-\frac{1}{2}}| \cdot J_{x,i+\frac{1}{2},j} \\
&= \epsilon_0(\iint_{T_{i,j-\frac{1}{2}}} \frac{\partial E_x}{\partial t}(x_{i+\frac{1}{2}}, y_j, t) - \iint_{T_{i,j-\frac{1}{2}}} \frac{\partial E_x}{\partial t}(x, y, t)) \\
&\quad +(x_{i+1} - x_i)(\mathcal{H}_{i+\frac{1}{2},j+\frac{1}{2}} - \mathcal{H}_{i+\frac{1}{2},j-\frac{1}{2}}) + \int_{x_i}^{x_{i+1}} (H(x, y_{j+\frac{1}{2}}, t) - H(x, y_{j-\frac{1}{2}}, t))dx \\
&\quad -(x_{i+1} - x_i)(H(x_{i+\frac{1}{2}}, y_{j+\frac{1}{2}}, t) - H(x_{i+\frac{1}{2}}, y_{j-\frac{1}{2}}, t)) - |T_{i,j-\frac{1}{2}}| \cdot \mathcal{J}_{x,i+\frac{1}{2},j}
\end{aligned}$$

$$+\iint_{T_{i,j-\frac{1}{2}}} J_x(x_{i+\frac{1}{2}},y_j,t)-\iint_{T_{i,j-\frac{1}{2}}} J_x(x,y,t),$$

which leads to the error equation for E_x:

$$\begin{aligned}
\epsilon_0|T_{i,j-\frac{1}{2}}|\cdot\frac{\partial \mathcal{E}_x}{\partial t}|_{i+\frac{1}{2},j} &= (x_{i+1}-x_i)(\mathcal{H}_{i+\frac{1}{2},j+\frac{1}{2}}-\mathcal{H}_{i+\frac{1}{2},j-\frac{1}{2}})-|T_{i,j-\frac{1}{2}}|\cdot\mathcal{J}_{x,i+\frac{1}{2},j}\\
&+\epsilon_0(\iint_{T_{i,j-\frac{1}{2}}}(\frac{\partial E_x}{\partial t}(x_{i+\frac{1}{2}},y_j,t)-\frac{\partial E_x}{\partial t}(x,y,t))\\
&+[\int_{x_i}^{x_{i+1}}(H(x,y_{j+\frac{1}{2}},t)-H(x,y_{j-\frac{1}{2}},t))dx\\
&-\int_{x_i}^{x_{i+1}}(H(x_{i+\frac{1}{2}},y_{j+\frac{1}{2}},t)-H(x_{i+\frac{1}{2}},y_{j-\frac{1}{2}},t))dx]\\
&+\iint_{T_{i,j-\frac{1}{2}}}(J_x(x_{i+\frac{1}{2}},y_j,t)-J_x(x,y,t))\\
:= \;& (x_{i+1}-x_i)(\mathcal{H}_{i+\frac{1}{2},j+\frac{1}{2}}-\mathcal{H}_{i+\frac{1}{2},j-\frac{1}{2}})-|T_{i,j-\frac{1}{2}}|\cdot\mathcal{J}_{x,i+\frac{1}{2},j}\\
&+r_{1,ij}+r_{2,ij}+r_{3,ij}.
\end{aligned}\tag{2.22}$$

Similarly, we can obtain the error equation for E_y:

$$\begin{aligned}
\epsilon_0|T_{i-\frac{1}{2},j}|\cdot\frac{\partial \mathcal{E}_y}{\partial t}|_{i,j+\frac{1}{2}} &= -(y_{j+1}-y_j)(\mathcal{H}_{i+\frac{1}{2},j+\frac{1}{2}}-\mathcal{H}_{i-\frac{1}{2},j+\frac{1}{2}})-|T_{i-\frac{1}{2},j}|\cdot\mathcal{J}_{y,i,j+\frac{1}{2}}\\
&+\epsilon_0\iint_{T_{i-\frac{1}{2},j}}(\frac{\partial E_y}{\partial t}(x_i,y_{j+\frac{1}{2}},t)-\frac{\partial E_y}{\partial t}(x,y,t))\\
&-[\int_{y_j}^{y_{j+1}}(H(x_{i+\frac{1}{2}},y,t)-H(x_{i-\frac{1}{2}},y,t))dy\\
&-\int_{y_j}^{y_{j+1}}(H(x_{i+\frac{1}{2}},y_{j+\frac{1}{2}},t)-H(x_{i-\frac{1}{2}},y_{j+\frac{1}{2}},t))dy]\\
&+\iint_{T_{i-\frac{1}{2},j}}(J_y(x_i,y_{j+\frac{1}{2}},t)-J_y(x,y,t))\\
:= \;& -(y_{j+1}-y_j)(\mathcal{H}_{i+\frac{1}{2},j+\frac{1}{2}}-\mathcal{H}_{i-\frac{1}{2},j+\frac{1}{2}})-|T_{i-\frac{1}{2},j}|\cdot\mathcal{J}_{y,i,j+\frac{1}{2}}\\
&+r_{4,ij}+r_{5,ij}+r_{6,ij}.
\end{aligned}\tag{2.23}$$

By the same technique, we can obtain the error equation for H:

$$\mu_0|T_{ij}|\cdot\frac{\partial \mathcal{H}}{\partial t}|_{i+\frac{1}{2},j+\frac{1}{2}}=-(y_{j+1}-y_j)(\mathcal{E}_{y,i+1,j+\frac{1}{2}}-\mathcal{E}_{y,i,j+\frac{1}{2}})$$

$$
\begin{aligned}
&+(x_{i+1}-x_i)(\mathcal{E}_{x,i+\frac{1}{2},j+1}-\mathcal{E}_{x,i+\frac{1}{2},j})-|T_{ij}|\cdot\mathcal{K}_{i+\frac{1}{2},j+\frac{1}{2}}\\
&+\mu_0\iint_{T_{ij}}(\frac{\partial H}{\partial t}(x_{i+\frac{1}{2}},y_{j+\frac{1}{2}},t)-\frac{\partial H}{\partial t}(x,y,t))\\
&-[\int_{y_j}^{y_{j+1}}(E_y(x_{i+1},y,t)-E_y(x_i,y,t))dy\\
&-\int_{y_j}^{y_{j+1}}(E_y(x_{i+1},y_{j+\frac{1}{2}},t)-E_y(x_i,y_{j+\frac{1}{2}},t))dy]\\
&+\iint_{T_{ij}}(K(x_{i+\frac{1}{2}},y_{j+\frac{1}{2}},t)-K(x,y,t))\\
:=\;&-(y_{j+1}-y_j)(\mathcal{E}_{y,i+1,j+\frac{1}{2}}-\mathcal{E}_{y,i,j+\frac{1}{2}})\\
&+(x_{i+1}-x_i)(\mathcal{E}_{x,i+\frac{1}{2},j+1}-\mathcal{E}_{x,i+\frac{1}{2},j})-|T_{ij}|\cdot\mathcal{K}_{i+\frac{1}{2},j+\frac{1}{2}}\\
&+r_{7,ij}+r_{8,ij}+r_{9,ij}.
\end{aligned}
\tag{2.24}
$$

The error equations for $\boldsymbol{J}$ and K are easily obtained and given respectively by:

$$
\begin{aligned}
&|T_{i,j-\frac{1}{2}}|\cdot\frac{1}{\epsilon_0\omega_{pe}^2}\frac{\partial\mathcal{J}_x}{\partial t}|_{i+\frac{1}{2},j}+\frac{\Gamma_e}{\epsilon_0\omega_{pe}^2}|T_{i,j-\frac{1}{2}}|\cdot\mathcal{J}_{x,i+\frac{1}{2},j}\\
=\;&|T_{i,j-\frac{1}{2}}|\cdot\mathcal{E}_{x,i+\frac{1}{2},j}+\frac{1}{\epsilon_0\omega_{pe}^2}\iint_{T_{i,j-\frac{1}{2}}}(\frac{\partial J_x}{\partial t}(x_{i+\frac{1}{2}},y_j,t)-\frac{\partial J_x}{\partial t}(x,y,t))\\
&+\frac{\Gamma_e}{\epsilon_0\omega_{pe}^2}\iint_{T_{i,j-\frac{1}{2}}}(J_x(x_{i+\frac{1}{2}},y_j,t)-J_x(x,y,t))\\
&-\iint_{T_{i,j-\frac{1}{2}}}(E_x(x_{i+\frac{1}{2}},y_j,t)-E_x(x,y,t))\\
:=\;&|T_{i,j-\frac{1}{2}}|\cdot\mathcal{E}_{x,i+\frac{1}{2},j}+r_{10,ij}+r_{11,ij}+r_{12,ij},
\end{aligned}
\tag{2.25}
$$

$$
\begin{aligned}
&|T_{i-\frac{1}{2},j}|\cdot\frac{1}{\epsilon_0\omega_{pe}^2}\frac{\partial\mathcal{J}_y}{\partial t}|_{i,j+\frac{1}{2}}+\frac{\Gamma_e}{\epsilon_0\omega_{pe}^2}|T_{i-\frac{1}{2},j}|\cdot\mathcal{J}_{y,i,j+\frac{1}{2}}\\
=\;&|T_{i-\frac{1}{2},j}|\cdot\mathcal{E}_{y,i,j+\frac{1}{2}}+\frac{1}{\epsilon_0\omega_{pe}^2}\iint_{T_{i-\frac{1}{2},j}}(\frac{\partial J_y}{\partial t}(x_i,y_{j+\frac{1}{2}},t)-\frac{\partial J_y}{\partial t}(x,y,t))\\
&+\frac{\Gamma_e}{\epsilon_0\omega_{pe}^2}\iint_{T_{i-\frac{1}{2},j}}(J_y(x_i,y_{j+\frac{1}{2}},t)-J_y(x,y,t))\\
&-\iint_{T_{i-\frac{1}{2},j}}(E_y(x_i,y_{j+\frac{1}{2}},t)-E_y(x,y,t))
\end{aligned}
$$

$$:= \quad |T_{i-\frac{1}{2},j}| \cdot \mathcal{E}_{y,i,j+\frac{1}{2}} + r_{13,ij} + r_{14,ij} + r_{15,ij}, \tag{2.26}$$

and

$$\begin{aligned}
&|T_{ij}| \cdot \frac{1}{\mu_0\omega_{pm}^2}\frac{\partial \mathcal{K}}{\partial t}|_{i+\frac{1}{2},j+\frac{1}{2}} + \frac{\Gamma_m}{\mu_0\omega_{pm}^2}|T_{ij}| \cdot \mathcal{K}_{i+\frac{1}{2},j+\frac{1}{2}} \\
= \quad & |T_{ij}| \cdot \mathcal{H}_{i+\frac{1}{2},j+\frac{1}{2}} + \frac{1}{\mu_0\omega_{pm}^2}\iint_{T_{ij}} (\frac{\partial K}{\partial t}(x_{i+\frac{1}{2}}, y_{j+\frac{1}{2}}, t) - \frac{\partial K}{\partial t}(x,y,t)) \\
& + \frac{\Gamma_m}{\mu_0\omega_{pm}^2}\iint_{T_{ij}} (K(x_{i+\frac{1}{2}}, y_{j+\frac{1}{2}}, t) - K(x,y,t)) \\
& + \iint_{T_{ij}} (H(x_{i+\frac{1}{2}}, y_{j+\frac{1}{2}}, t) - H(x,y,t)) \\
:= \quad & |T_{ij}| \cdot \mathcal{H}_{i+\frac{1}{2},j+\frac{1}{2}} + r_{16,ij} + r_{17,ij} + r_{18,ij}.
\end{aligned} \tag{2.27}$$

With the above preparations, we can obtain the following superconvergence result.

Theorem 2.22. Suppose that the solution of the model problem (2.1)-(2.6) possesses the following regularity property:

$$E_x, E_y, H \in C([0,T]; C^3(\overline{\Omega})) \cap C^1([0,T]; C^2(\overline{\Omega})),$$

$$J_x, J_y, K \in C([0,T]; C^2(\overline{\Omega})) \cap C^1([0,T]; C^2(\overline{\Omega})).$$

Under the assumption that if the following initial error

$$\begin{aligned}
[\epsilon_0(||\mathcal{E}_x||_E^2 + ||\mathcal{E}_y||_E^2) + \mu_0||\mathcal{H}||_H^2 + \frac{1}{\epsilon_0\omega_{pe}^2}(||\mathcal{J}_x||_J^2 + ||\mathcal{J}_y||_J^2) + \frac{1}{\mu_0\omega_{pm}^2}||\mathcal{K}||_K^2](0) \\
\leq C(h_x^2 + h_y^2)^2,
\end{aligned} \tag{2.28}$$

holds true, then we have

$$\begin{aligned}
\max_{0\leq t\leq T}[\epsilon_0(||\mathcal{E}_x||_E^2 + ||\mathcal{E}_y||_E^2) + \mu_0||\mathcal{H}||_H^2 + \frac{1}{\epsilon_0\omega_{pe}^2}(||\mathcal{J}_x||_J^2 + ||\mathcal{J}_y||_J^2) + \frac{1}{\mu_0\omega_{pm}^2}||\mathcal{K}||_K^2(t)] \\
\leq CT(h_x^2 + h_y^2)^2.
\end{aligned} \tag{2.29}$$

Proof. By the Taylor expansion, for any function f we can easily prove that

$$\begin{aligned}
&\iint_{T_{i,j-\frac{1}{2}}} (f(x,y,t) - f(x_{i+\frac{1}{2}}, y_j, t))dxdy \\
&= \iint_{T_{i,j-\frac{1}{2}}} [(x - x_{i+\frac{1}{2}})\frac{\partial f}{\partial x}(p_*) + (y - y_j)\frac{\partial f}{\partial y}(p_*) + \frac{1}{2}(x - x_{i+\frac{1}{2}})^2\frac{\partial^2 f}{\partial x^2}(p_1) \\
&\quad +(x - x_{i+\frac{1}{2}})(y - y_j)\frac{\partial^2 f}{\partial x \partial y}(p_2) + \frac{1}{2}(y - y_j)^2\frac{\partial^2 f}{\partial y^2}(p_3)] \\
&\leq \iint_{T_{i,j-\frac{1}{2}}} C[h_x^2|\frac{\partial^2 f}{\partial x^2}|_\infty + h_y^2|\frac{\partial^2 f}{\partial y^2}|_\infty], \qquad (2.30)
\end{aligned}$$

where we denote $p_* = (x_{i+\frac{1}{2}}, y_j, t)$, and p_1, p_2 and p_3 for some midpoints between p_* and (x, y, t).

Applying (2.30) to $f = \frac{\partial E_x}{\partial t}$, we obtain

$$r_{1,ij} = (O(h_x^2)|\frac{\partial^3 E_x}{\partial t \partial x^2}|_\infty + O(h_y^2)|\frac{\partial^3 E_x}{\partial t \partial y^2}|_\infty) \cdot |T_{i,j-\frac{1}{2}}|.$$

It is easy to see that for any function f, we have

$$\begin{aligned}
&|\int_{y_j}^{y_{j+1}} (f(y) - f(y_{j+\frac{1}{2}})dy| \\
&= |\int_{y_j}^{y_{j+1}} [(y - y_{j+\frac{1}{2}})\frac{\partial f}{\partial y}(y_{j+\frac{1}{2}}) + \int_{y_{j+\frac{1}{2}}}^{y} (y - \eta)\frac{\partial^2 f}{\partial y^2}(\eta)d\eta]dy| \\
&= |\int_{y_j}^{y_{j+1}} [\int_{y_{j+\frac{1}{2}}}^{y} (y - \eta)\frac{\partial^2 f}{\partial y^2}(\eta)d\eta]dy| \\
&\leq Ch_y^2 \int_{y_j}^{y_{j+1}} |\frac{\partial^2 f}{\partial y^2}(\eta)|d\eta \leq Ch_y^3|\frac{\partial^2 f}{\partial y^2}(\eta)|_\infty, \qquad (2.31)
\end{aligned}$$

which leads to

$$\sum_{0\leq i\leq N_x-1} \sum_{0\leq j\leq N_y-1} |\int_{y_j}^{y_{j+1}} (f(y) - f(y_{j+\frac{1}{2}})dy| \leq Ch|\frac{\partial^2 f}{\partial y^2}(\eta)|_\infty. \qquad (2.32)$$

Applying (2.32) to each single integral in (2.22)-(2.27), we will only obtain $O(h)$ convergence rate. This was pointed out by Monk and Süli in Monk and Süli (1994).

They managed to prove the $O(h^2)$ rate by using a special structure of the local errors. Here we will use a simpler method to prove $O(h^2)$ error estimate.

Note that

$$\begin{aligned}
&\int_{x_i}^{x_{i+1}} (H(x, y_{j+\frac{1}{2}}, t) - H(x, y_{j-\frac{1}{2}}, t))dx \\
&\quad - \int_{x_i}^{x_{i+1}} (H(x_{i+\frac{1}{2}}, y_{j+\frac{1}{2}}, t) - H(x_{i+\frac{1}{2}}, y_{j-\frac{1}{2}}, t))dx \\
&= \int_{x_i}^{x_{i+1}} [\int_{y_{j-\frac{1}{2}}}^{y_{j+\frac{1}{2}}} (\frac{\partial H}{\partial y}(x, y, t) - \frac{\partial H}{\partial y}(x_{i+\frac{1}{2}}, y, t))dy]dx = O(h_x^2)|\frac{\partial^3 H}{\partial y \partial x^2}|_\infty |T_{i,j-\frac{1}{2}}|,
\end{aligned}$$

which leads to

$$r_{2,ij} = O(h_x^2)|\frac{\partial^3 H}{\partial y \partial x^2}|_\infty \cdot |T_{i,j-\frac{1}{2}}|.$$

We like to remark that we can reduce the regularity requirement if we use the integral residue as shown in (2.30).

Applying (2.30) to $f = J_x$, we obtain

$$r_{3,ij} = (O(h_x^2)|\frac{\partial^2 J_x}{\partial x^2}|_\infty + O(h_y^2)|\frac{\partial^2 J_x}{\partial y^2}|_\infty) \cdot |T_{i,j-\frac{1}{2}}|.$$

By carrying out the above technique to the E_y error equation, we have

$$\begin{aligned}
r_{4,ij} &= (O(h_x^2)|\frac{\partial^3 E_y}{\partial t \partial x^2}|_\infty + O(h_y^2)|\frac{\partial^3 E_y}{\partial t \partial y^2}|_\infty) \cdot |T_{i-\frac{1}{2},j}|, \\
r_{5,ij} &= -\iint_{T_{i-\frac{1}{2},j}} (\frac{\partial H}{\partial x}(x, y, t) - \frac{\partial H}{\partial x}(x, y_{j+\frac{1}{2}}, t)) = O(h_y^2)|\frac{\partial^3 H}{\partial x \partial y^2}|_\infty |T_{i-\frac{1}{2},j}|, \\
r_{6,ij} &= (O(h_x^2)|\frac{\partial^2 J_y}{\partial x^2}|_\infty + O(h_y^2)|\frac{\partial^2 J_y}{\partial y^2}|_\infty) \cdot |T_{i-\frac{1}{2},j}|.
\end{aligned}$$

Using the same technique to the H error equation, we have

$$\begin{aligned}
r_{7,ij} &= (O(h_x^2)|\frac{\partial^3 H}{\partial t \partial x^2}|_\infty + O(h_y^2)|\frac{\partial^3 H}{\partial t \partial y^2}|_\infty) \cdot |T_{ij}|, \\
r_{8,ij} &= -\iint_{T_{ij}} (\frac{\partial E_y}{\partial x}(x, y, t) - \frac{\partial E_y}{\partial x}(x, y_{j+\frac{1}{2}}, t)) = O(h_y^2)|\frac{\partial^3 E_y}{\partial x \partial y^2}|_\infty |T_{ij}|, \\
r_{9,ij} &= (O(h_x^2)|\frac{\partial^2 K}{\partial x^2}|_\infty + O(h_y^2)|\frac{\partial^2 K}{\partial y^2}|_\infty) \cdot |T_{ij}|.
\end{aligned}$$

Similarly, we can obtain the following estimates for the J_x, J_y and K error equations, respectively,

$$
\begin{aligned}
r_{10,ij} &= (O(h_x^2)|\frac{\partial^3 J_x}{\partial t \partial x^2}|_\infty + O(h_y^2)|\frac{\partial^3 J_x}{\partial t \partial y^2}|_\infty) \cdot |T_{i,j-\frac{1}{2}}|, \\
r_{11,ij} &= (O(h_x^2)|\frac{\partial^2 J_x}{\partial x^2}|_\infty + O(h_y^2)|\frac{\partial^2 J_x}{\partial y^2}|_\infty) \cdot |T_{i,j-\frac{1}{2}}|, \\
r_{12,ij} &= (O(h_x^2)|\frac{\partial^2 E_x}{\partial x^2}|_\infty + O(h_y^2)|\frac{\partial^2 E_x}{\partial y^2}|_\infty) \cdot |T_{i,j-\frac{1}{2}}|,
\end{aligned}
$$

$$
\begin{aligned}
r_{13,ij} &= (O(h_x^2)|\frac{\partial^3 J_y}{\partial t \partial x^2}|_\infty + O(h_y^2)|\frac{\partial^3 J_y}{\partial t \partial y^2}|_\infty) \cdot |T_{i-\frac{1}{2},j}|, \\
r_{14,ij} &= (O(h_x^2)|\frac{\partial^2 J_y}{\partial x^2}|_\infty + O(h_y^2)|\frac{\partial^2 J_y}{\partial y^2}|_\infty) \cdot |T_{i-\frac{1}{2},j}|, \\
r_{15,ij} &= (O(h_x^2)|\frac{\partial^2 E_y}{\partial x^2}|_\infty + O(h_y^2)|\frac{\partial^2 E_y}{\partial y^2}|_\infty) \cdot |T_{i-\frac{1}{2},j}|,
\end{aligned}
$$

and

$$
\begin{aligned}
r_{16,ij} &= (O(h_x^2)|\frac{\partial^3 K}{\partial t \partial x^2}|_\infty + O(h_y^2)|\frac{\partial^3 K}{\partial t \partial y^2}|_\infty) \cdot |T_{ij}|, \\
r_{17,ij} &= (O(h_x^2)|\frac{\partial^2 K}{\partial x^2}|_\infty + O(h_y^2)|\frac{\partial^2 K}{\partial y^2}|_\infty) \cdot |T_{ij}|, \\
r_{18,ij} &= (O(h_x^2)|\frac{\partial^2 H}{\partial x^2}|_\infty + O(h_y^2)|\frac{\partial^2 H}{\partial y^2}|_\infty) \cdot |T_{ij}|.
\end{aligned}
$$

Denote the error energy

$$
Q(t) = [\epsilon_0(||\mathcal{E}_x||_E^2 + ||\mathcal{E}_y||_E^2) + \mu_0||\mathcal{H}||_H^2 + \frac{1}{\epsilon_0\omega_{pe}^2}(||\mathcal{J}_x||_J^2 + ||\mathcal{J}_y||_J^2) + \frac{1}{\mu_0\omega_{pm}^2}||\mathcal{K}||_K^2](t).
$$

Multiplying $\mathcal{E}_{x,i+\frac{1}{2},j}$ to (2.22), $\mathcal{E}_{y,i,j+\frac{1}{2}}$ to (2.23), $\mathcal{H}_{i+\frac{1}{2},j+\frac{1}{2}}$ to (2.24), $\mathcal{J}_{x,i+\frac{1}{2},j}$ to (2.25), $\mathcal{J}_{y,i,j+\frac{1}{2}}$ to (2.26), $\mathcal{K}_{i+\frac{1}{2},j+\frac{1}{2}}$ to (2.27), summing up the results for all i and j, using estimates such as the following:

$$
\begin{aligned}
\sum_{\substack{0\le i\le N_x-1 \\ 1\le j\le N_y-1}} r_{1,ij}\mathcal{E}_{x,i+\frac{1}{2},j} &\le \sum_{\substack{0\le i\le N_x-1 \\ 1\le j\le N_y-1}} [\delta|T_{i,j-\frac{1}{2}}| \cdot |\mathcal{E}_{x,i+\frac{1}{2},j}|^2 + \frac{1}{4\delta}(O(h_x^2) + O(h_y^2))^2|T_{i,j-\frac{1}{2}}|] \\
&\le \delta||\mathcal{E}_x||_E^2 + \frac{1}{4\delta}(O(h_x^2) + O(h_y^2))^2,
\end{aligned}
$$

and using the estimate (2.18) with E and H replaced by $\mathcal{E}$ and $\mathcal{H}$, respectively, we obtain

$$\frac{1}{2}\frac{d}{dt}Q(t) + \frac{\Gamma_e}{\epsilon_0\omega_{pe}^2}(||\mathcal{J}_x||_J^2 + ||\mathcal{J}_y||_J^2) + \frac{\Gamma_m}{\mu_0\omega_{pm}^2}||\mathcal{K}||_K^2 \leq C(h_x^2 + h_y^2)^2 + \frac{\delta}{2}Q(t),$$

where $\delta > 0$ is a small constant.

Integrating the above inequality from 0 to t, we have

$$Q(t) \leq Q(0) + C(h_x^2 + h_y^2)^2 t + \delta \int_0^t Q(s)ds. \tag{2.33}$$

Suppose that t_* achieves the maximum of $Q(s)$ on the interval $[0, t]$, i.e.,

$$\max_{0\leq s\leq t} Q(s) = Q(t_*)$$

. Using $t = t_*$ in (2.33), we obtain

$$Q(t_*) \leq Q(0) + C(h_x^2 + h_y^2)^2 t_* + \delta t_* Q(t_*). \tag{2.34}$$

Choosing δ small enough such that $\delta t_* < 1$, and using the assumption (2.81), we complete the proof. □

2.3 The fully discrete scheme

To construct a fully discrete scheme, we divide the time interval $[0, T]$ into $N_t + 2$ uniform intervals, i.e., we have discrete times $0 = t_0 < t_1 < \cdots < t_{N_t+2} = T$.

Approximating those time directives properly in the semi-discrete schemes (2.8), (2.10), (2.12), (2.14), (2.15), and (2.16), we can obtain the following fully-discrete scheme: Given initial approximations $E^0_{x,i+\frac{1}{2},j}, E^0_{y,i,j+\frac{1}{2}}$, $H^{\frac{1}{2}}_{i+\frac{1}{2},j+\frac{1}{2}}, J^{\frac{1}{2}}_{x,i+\frac{1}{2},j}, J^{\frac{1}{2}}_{y,i,j+\frac{1}{2}}$,

$K^1_{i+\frac{1}{2},j+\frac{1}{2}}$, for any $0 \le n \le N_t$, solve $E^{n+1}_{x,i+\frac{1}{2},j}, E^{n+1}_{y,i,j+\frac{1}{2}}$, $H^{n+\frac{3}{2}}_{i+\frac{1}{2},j+\frac{1}{2}}, J^{n+\frac{3}{2}}_{x,i+\frac{1}{2},j}, J^{n+\frac{3}{2}}_{y,i,j+\frac{1}{2}}$, $K^{n+2}_{i+\frac{1}{2},j+\frac{1}{2}}$ from:

$$\epsilon_0 \frac{E^{n+1}_{x,i+\frac{1}{2},j} - E^n_{x,i+\frac{1}{2},j}}{\tau} = \frac{H^{n+\frac{1}{2}}_{i+\frac{1}{2},j+\frac{1}{2}} - H^{n+\frac{1}{2}}_{i+\frac{1}{2},j-\frac{1}{2}}}{y_{j+\frac{1}{2}} - y_{j-\frac{1}{2}}} - J^{n+\frac{1}{2}}_{x,i+\frac{1}{2},j}, \tag{2.35}$$

$$\epsilon_0 \frac{E^{n+1}_{y,i,j+\frac{1}{2}} - E^n_{y,i,j+\frac{1}{2}}}{\tau} = -\frac{H^{n+\frac{1}{2}}_{i+\frac{1}{2},j+\frac{1}{2}} - H^{n+\frac{1}{2}}_{i-\frac{1}{2},j+\frac{1}{2}}}{x_{i+\frac{1}{2}} - x_{i-\frac{1}{2}}} - J^{n+\frac{1}{2}}_{y,i,j+\frac{1}{2}}, \tag{2.36}$$

$$\mu_0 \frac{H^{n+\frac{3}{2}}_{i+\frac{1}{2},j+\frac{1}{2}} - H^{n+\frac{1}{2}}_{i+\frac{1}{2},j+\frac{1}{2}}}{\tau} = -\frac{E^{n+1}_{y,i+1,j+\frac{1}{2}} - E^{n+1}_{y,i,j+\frac{1}{2}}}{x_{i+1} - x_i} + \frac{E^{n+1}_{x,i+\frac{1}{2},j+1} - E^{n+1}_{x,i+\frac{1}{2},j}}{y_{j+1} - y_j} - K^{n+1}_{i+\frac{1}{2},j+\frac{1}{2}}, \tag{2.37}$$

$$\frac{1}{\epsilon_0 \omega^2_{pe}} \frac{J^{n+\frac{3}{2}}_{x,i+\frac{1}{2},j} - J^{n+\frac{1}{2}}_{x,i+\frac{1}{2},j}}{\tau} + \frac{\Gamma_e}{\epsilon_0 \omega^2_{pe}} \frac{J^{n+\frac{3}{2}}_{x,i+\frac{1}{2},j} + J^{n+\frac{1}{2}}_{x,i+\frac{1}{2},j}}{2} = E^{n+1}_{x,i+\frac{1}{2},j}, \tag{2.38}$$

$$\frac{1}{\epsilon_0 \omega^2_{pe}} \frac{J^{n+\frac{3}{2}}_{y,i,j+\frac{1}{2}} - J^{n+\frac{1}{2}}_{y,i,j+\frac{1}{2}}}{\tau} + \frac{\Gamma_e}{\epsilon_0 \omega^2_{pe}} \frac{J^{n+\frac{3}{2}}_{y,i,j+\frac{1}{2}} + J^{n+\frac{1}{2}}_{y,i,j+\frac{1}{2}}}{2} = E^{n+1}_{y,i,j+\frac{1}{2}}, \tag{2.39}$$

$$\frac{1}{\mu_0 \omega^2_{pm}} \frac{K^{n+2}_{i+\frac{1}{2},j+\frac{1}{2}} - K^{n+1}_{i+\frac{1}{2},j+\frac{1}{2}}}{\tau} + \frac{\Gamma_m}{\mu_0 \omega^2_{pm}} \frac{K^{n+2}_{i+\frac{1}{2},j+\frac{1}{2}} + K^{n+1}_{i+\frac{1}{2},j+\frac{1}{2}}}{2} = H^{n+\frac{3}{2}}_{i+\frac{1}{2},j+\frac{1}{2}}. \tag{2.40}$$

Let $C_v = 1/\sqrt{\epsilon_0 \mu_0}$ be the wave propagation speed in free space. For any grid function $u_{i,j}$, let us denote the backward difference operators ∇_x and ∇_y:

$$\nabla_x u_{i+1,j} = \frac{u_{i+1,j} - u_{i,j}}{x_{i+1} - x_i}, \quad \nabla_y u_{i,j+1} = \frac{u_{i,j+1} - u_{i,j}}{y_{j+1} - y_j}.$$

Furthermore, we denote the constant $C_{inv} > 0$ satisfying the inverse inequality

$$||\nabla_x u|| \le C_{inv} h_x^{-1} ||u||, \quad ||\nabla_y u|| \le C_{inv} h_y^{-1} ||u||, \tag{2.41}$$

for any energy norm defined earlier.

The stability analysis

Theorem 2.31. Assume that the time step size τ satisfies the constraint

$$\tau \leq \min(\frac{C_{inv}h_y}{2C_v}, \frac{C_{inv}h_x}{2C_v}, \frac{1}{2\omega_{pe}}, \frac{1}{2\omega_{pm}}), \tag{2.42}$$

then the solution of the fully discrete scheme (2.35)-(2.40) satisfies the following stability: For any $1 \leq n \leq N_t$,

$$\begin{aligned}
&\epsilon_0(||E_x^{n+1}||_E^2 + ||E_y^{n+1}||_E^2) + \mu_0||H^{n+\frac{3}{2}}||_H^2 \\
&\quad + \frac{1}{\epsilon_0\omega_{pe}^2}(||J_x^{n+\frac{3}{2}}||_J^2 + ||J_y^{n+\frac{3}{2}}||_J^2) + \frac{1}{\mu_0\omega_{pm}^2}||K^{n+2}||_K^2 \\
\leq\ & C[\epsilon_0(||E_x^0||_E^2 + ||E_y^0||_E^2) + \mu_0||H^{\frac{1}{2}}||_H^2 \\
&\quad + \frac{1}{\epsilon_0\omega_{pe}^2}(||J_x^{\frac{1}{2}}||_J^2 + ||J_y^{\frac{1}{2}}||_J^2) + \frac{1}{\mu_0\omega_{pm}^2}||K^1||_K^2],
\end{aligned} \tag{2.43}$$

where the constant $C > 0$ is independent of τ, h_x and h_y.

Proof. Multiplying (2.35) by $\tau|T_{i,j-\frac{1}{2}}|(E_{x,i+\frac{1}{2},j}^{n+1} + E_{x,i+\frac{1}{2},j}^{n})$, (2.36) by $\tau|T_{i-\frac{1}{2},j}|(E_{y,i,j+\frac{1}{2}}^{n+1} + E_{y,i,j+\frac{1}{2}}^{n})$, (2.37) by $\tau|T_{ij}|(H_{i+\frac{1}{2},j+\frac{1}{2}}^{n+\frac{3}{2}} + H_{i+\frac{1}{2},j+\frac{1}{2}}^{n+\frac{1}{2}})$, (2.38) by $\tau|T_{i,j-\frac{1}{2}}|(J_{x,i+\frac{1}{2},j}^{n+\frac{3}{2}} + J_{x,i+\frac{1}{2},j}^{n+\frac{1}{2}})$, (2.39) by $\tau|T_{i-\frac{1}{2},j}|(J_{y,i,j+\frac{1}{2}}^{n+\frac{3}{2}} + J_{y,i,j+\frac{1}{2}}^{n+\frac{1}{2}})$, (2.40) by $\tau|T_{ij}|(K_{i+\frac{1}{2},j+\frac{1}{2}}^{n+2} + K_{i+\frac{1}{2},j+\frac{1}{2}}^{n+1})$, then summing up the results, we obtain the sum of the right hand side as

$$\begin{aligned}
RHS \ =\ & \tau \sum_{\substack{0\leq i\leq N_x-1 \\ 1\leq j\leq N_y-1}} [(x_{i+1}-x_i)(H_{i+\frac{1}{2},j+\frac{1}{2}}^{n+\frac{1}{2}} - H_{i+\frac{1}{2},j-\frac{1}{2}}^{n+\frac{1}{2}}) \\
&\qquad - J_{x,i+\frac{1}{2},j}^{n+\frac{1}{2}}|T_{i,j-\frac{1}{2}}|](E_{x,i+\frac{1}{2},j}^{n+1} + E_{x,i+\frac{1}{2},j}^{n}) \\
&+\tau \sum_{\substack{1\leq i\leq N_x-1 \\ 0\leq j\leq N_y-1}} [-(y_{j+1}-y_j)(H_{i+\frac{1}{2},j+\frac{1}{2}}^{n+\frac{1}{2}} - H_{i-\frac{1}{2},j+\frac{1}{2}}^{n+\frac{1}{2}}) \\
&\qquad - J_{y,i,j+\frac{1}{2}}^{n+\frac{1}{2}}|T_{i-\frac{1}{2},j}|](E_{y,i,j+\frac{1}{2}}^{n+1} + E_{y,i,j+\frac{1}{2}}^{n})
\end{aligned}$$

$$
\begin{aligned}
&+\tau \sum_{\substack{0\le i\le N_x-1\\ 0\le j\le N_y-1}} [-(y_{j+1}-y_j)(E^{n+1}_{y,i+1,j+\frac{1}{2}} - E^{n+1}_{y,i,j+\frac{1}{2}}) \\
&\qquad +(x_{i+1}-x_i)(E^{n+1}_{x,i+\frac{1}{2},j+1} - E^{n+1}_{x,i+\frac{1}{2},j})\\
&-K^{n+1}_{i+\frac{1}{2},j+\frac{1}{2}}|T_{ij}|](H^{n+\frac{3}{2}}_{i+\frac{1}{2},j+\frac{1}{2}} + H^{n+\frac{1}{2}}_{i+\frac{1}{2},j+\frac{1}{2}})\\
&+\tau \sum_{\substack{0\le i\le N_x-1\\ 1\le j\le N_y-1}} E^{n+1}_{x,i+\frac{1}{2},j}\cdot|T_{i,j-\frac{1}{2}}|(J^{n+\frac{3}{2}}_{x,i+\frac{1}{2},j} + J^{n+\frac{1}{2}}_{x,i+\frac{1}{2},j})\\
&+\tau \sum_{\substack{1\le i\le N_x-1\\ 0\le j\le N_y-1}} E^{n+1}_{y,i,j+\frac{1}{2}}\cdot|T_{i-\frac{1}{2},j}|(J^{n+\frac{3}{2}}_{y,i,j+\frac{1}{2}} + J^{n+\frac{1}{2}}_{y,i,j+\frac{1}{2}})\\
&+\tau \sum_{\substack{0\le i\le N_x-1\\ 0\le j\le N_y-1}} H^{n+\frac{3}{2}}_{i+\frac{1}{2},j+\frac{1}{2}}\cdot|T_{ij}|(K^{n+2}_{i+\frac{1}{2},j+\frac{1}{2}} + K^{n+1}_{i+\frac{1}{2},j+\frac{1}{2}}).
\end{aligned}
$$

Regrouping those terms in RHS, we rewrite RHS as

$$
\begin{aligned}
RHS \;=\;& \tau \sum_{0\le i\le N_x-1}(x_{i+1}-x_i)\sum_{1\le j\le N_y-1}[(H^{n+\frac{1}{2}}_{i+\frac{1}{2},j+\frac{1}{2}} - H^{n+\frac{1}{2}}_{i+\frac{1}{2},j-\frac{1}{2}})(E^{n+1}_{x,i+\frac{1}{2},j}\\
&\qquad +E^{n}_{x,i+\frac{1}{2},j})\\
&+(E^{n+1}_{x,i+\frac{1}{2},j+1} - E^{n+1}_{x,i+\frac{1}{2},j})(H^{n+\frac{3}{2}}_{i+\frac{1}{2},j+\frac{1}{2}} + H^{n+\frac{1}{2}}_{i+\frac{1}{2},j+\frac{1}{2}})]\\
&+\tau \sum_{0\le j\le N_y-1}(y_{j+1}-y_j)\sum_{1\le i\le N_x-1}[(H^{n+\frac{1}{2}}_{i-\frac{1}{2},j+\frac{1}{2}} - H^{n+\frac{1}{2}}_{i+\frac{1}{2},j+\frac{1}{2}})(E^{n+1}_{y,i,j+\frac{1}{2}}\\
&\qquad +E^{n}_{y,i,j+\frac{1}{2}})\\
&+(E^{n+1}_{y,i,j+\frac{1}{2}} - E^{n+1}_{y,i+1,j+\frac{1}{2}})(H^{n+\frac{3}{2}}_{i+\frac{1}{2},j+\frac{1}{2}} + H^{n+\frac{1}{2}}_{i+\frac{1}{2},j+\frac{1}{2}})]\\
&+\tau \sum_{\substack{0\le i\le N_x-1\\ 1\le j\le N_y-1}} |T_{i,j-\frac{1}{2}}|[-J^{n+\frac{1}{2}}_{x,i+\frac{1}{2},j}(E^{n+1}_{x,i+\frac{1}{2},j} + E^{n}_{x,i+\frac{1}{2},j})\\
&\qquad +(J^{n+\frac{3}{2}}_{x,i+\frac{1}{2},j} + J^{n+\frac{1}{2}}_{x,i+\frac{1}{2},j})E^{n+1}_{x,i+\frac{1}{2},j}]\\
&+\tau \sum_{\substack{1\le i\le N_x-1\\ 0\le j\le N_y-1}} |T_{i-\frac{1}{2},j}|[-J^{n+\frac{1}{2}}_{y,i,j+\frac{1}{2}}(E^{n+1}_{y,i,j+\frac{1}{2}} + E^{n}_{y,i,j+\frac{1}{2}})\\
&\qquad +(J^{n+\frac{3}{2}}_{y,i,j+\frac{1}{2}} + J^{n+\frac{1}{2}}_{y,i,j+\frac{1}{2}})E^{n+1}_{y,i,j+\frac{1}{2}}]\\
&+\tau \sum_{\substack{0\le i\le N_x-1\\ 0\le j\le N_y-1}} |T_{ij}|[-K^{n+1}_{i+\frac{1}{2},j+\frac{1}{2}}(H^{n+\frac{3}{2}}_{i+\frac{1}{2},j+\frac{1}{2}} + H^{n+\frac{1}{2}}_{i+\frac{1}{2},j+\frac{1}{2}})
\end{aligned}
$$

$$
\begin{aligned}
&+H^{n+\frac{3}{2}}_{i+\frac{1}{2},j+\frac{1}{2}}(K^{n+2}_{i+\frac{1}{2},j+\frac{1}{2}}+K^{n+1}_{i+\frac{1}{2},j+\frac{1}{2}})] \\
:= \quad \tau\Bigg[&\sum_{0\le i\le N_x-1}(x_{i+1}-x_i)R_1 \\
&+\sum_{0\le j\le N_y-1}(y_{j+1}-y_j)R_2+R_3+R_4+R_5\Bigg]. \qquad (2.44)
\end{aligned}
$$

To evaluate the above RHS, below we evaluate each term separately. First, note that

$$
\begin{aligned}
\sum_{n=0}^{N_t}R_1 &= \sum_{n=0}^{N_t}\sum_{0\le j\le N_y-1}[(H^{n+\frac{1}{2}}_{i+\frac{1}{2},j+\frac{1}{2}}-H^{n+\frac{1}{2}}_{i+\frac{1}{2},j-\frac{1}{2}})(E^{n+1}_{x,i+\frac{1}{2},j}+E^{n}_{x,i+\frac{1}{2},j}) \\
&\quad +(E^{n+1}_{x,i+\frac{1}{2},j+1}-E^{n+1}_{x,i+\frac{1}{2},j})(H^{n+\frac{3}{2}}_{i+\frac{1}{2},j+\frac{1}{2}}+H^{n+\frac{1}{2}}_{i+\frac{1}{2},j+\frac{1}{2}})] \\
&= \sum_{n=0}^{N_t}\sum_{0\le j\le N_y-1}[(H^{n+\frac{1}{2}}_{i+\frac{1}{2},j+\frac{1}{2}}E^{n}_{x,i+\frac{1}{2},j}-H^{n+\frac{3}{2}}_{i+\frac{1}{2},j+\frac{1}{2}}E^{n+1}_{x,i+\frac{1}{2},j}) \\
&\quad +(H^{n+\frac{1}{2}}_{i+\frac{1}{2},j+\frac{1}{2}}E^{n+1}_{x,i+\frac{1}{2},j+1}-H^{n+\frac{1}{2}}_{i+\frac{1}{2},j-\frac{1}{2}}E^{n+1}_{x,i+\frac{1}{2},j})] \\
&\quad +\sum_{n=0}^{N_t}\sum_{0\le j\le N_y-1}[(H^{n+\frac{3}{2}}_{i+\frac{1}{2},j+\frac{1}{2}}E^{n+1}_{x,i+\frac{1}{2},j+1}-H^{n+\frac{1}{2}}_{i+\frac{1}{2},j+\frac{1}{2}}E^{n}_{x,i+\frac{1}{2},j+1}) \\
&\quad +(H^{n+\frac{1}{2}}_{i+\frac{1}{2},j+\frac{1}{2}}E^{n}_{x,i+\frac{1}{2},j+1}-H^{n+\frac{1}{2}}_{i+\frac{1}{2},j-\frac{1}{2}}E^{n}_{x,i+\frac{1}{2},j})] \\
&= \sum_{0\le j\le N_y-1}(H^{\frac{1}{2}}_{i+\frac{1}{2},j+\frac{1}{2}}E^{0}_{x,i+\frac{1}{2},j}-H^{N_t+\frac{3}{2}}_{i+\frac{1}{2},j+\frac{1}{2}}E^{N_t+1}_{x,i+\frac{1}{2},j}) \\
&\quad +\sum_{n=0}^{N_t}(H^{n+\frac{1}{2}}_{i+\frac{1}{2},N_y+\frac{1}{2}}E^{n+1}_{x,i+\frac{1}{2},N_y}-H^{n+\frac{1}{2}}_{i+\frac{1}{2},-\frac{1}{2}}E^{n+1}_{x,i+\frac{1}{2},0}) \\
&\quad +\sum_{0\le j\le N_y-1}(H^{N_t+\frac{3}{2}}_{i+\frac{1}{2},j+\frac{1}{2}}E^{N_t+1}_{x,i+\frac{1}{2},j+1}-H^{\frac{1}{2}}_{i+\frac{1}{2},j+\frac{1}{2}}E^{0}_{x,i+\frac{1}{2},j+1}) \\
&\quad +\sum_{n=0}^{N_t}(H^{n+\frac{1}{2}}_{i+\frac{1}{2},N_y+\frac{1}{2}}E^{n}_{x,i+\frac{1}{2},N_y})-H^{n+\frac{1}{2}}_{i+\frac{1}{2},-\frac{1}{2}}E^{n}_{x,i+\frac{1}{2},0}) \\
&= \sum_{0\le j\le N_y-1}(H^{\frac{1}{2}}_{i+\frac{1}{2},j+\frac{1}{2}}E^{0}_{x,i+\frac{1}{2},j}-H^{N_t+\frac{3}{2}}_{i+\frac{1}{2},j+\frac{1}{2}}E^{N_t+1}_{x,i+\frac{1}{2},j}) \\
&\quad +\sum_{0\le j\le N_y-1}(H^{N_t+\frac{3}{2}}_{i+\frac{1}{2},j+\frac{1}{2}}E^{N_t+1}_{x,i+\frac{1}{2},j+1}-H^{\frac{1}{2}}_{i+\frac{1}{2},j+\frac{1}{2}}E^{0}_{x,i+\frac{1}{2},j+1}) \\
&= \sum_{0\le j\le N_y-1}(y_{j+1}-y_j)(H^{N_t+\frac{3}{2}}_{i+\frac{1}{2},j+\frac{1}{2}}\nabla_y E^{N_t+1}_{x,i+\frac{1}{2},j+1}
\end{aligned}
$$

$$-H^{\frac{1}{2}}_{i+\frac{1}{2},j+\frac{1}{2}}\nabla_y E^0_{x,i+\frac{1}{2},j+1}), \tag{2.45}$$

where we used the PEC boundary condition (2.19) in the second last step, and the backward difference operator ∇_y in the last step. Note that in the first step, we extended the original sum of $1 \le j \le N_y - 1$ to $0 \le j \le N_y - 1$. Even though $H^{n+\frac{1}{2}}_{i+\frac{1}{2},-\frac{1}{2}}$ has subindex out of the original bound, its product with $E^{n+1}_{x,i+\frac{1}{2},0} + E^n_{x,i+\frac{1}{2},0} = 0$ (by the PEC boundary condition (2.19)) is still zero.

The term R_2 can be evaluated as follows:

$$\begin{aligned}
\sum_{n=0}^{N_t} R_2 &= \sum_{n=0}^{N_t}\sum_{0\le i\le N_x-1}[(H^{n+\frac{1}{2}}_{i-\frac{1}{2},j+\frac{1}{2}} - H^{n+\frac{1}{2}}_{i+\frac{1}{2},j+\frac{1}{2}})(E^{n+1}_{y,i,j+\frac{1}{2}} + E^n_{y,i,j+\frac{1}{2}}) \\
&\quad +(E^{n+1}_{y,i,j+\frac{1}{2}} - E^{n+1}_{y,i+1,j+\frac{1}{2}})(H^{n+\frac{3}{2}}_{i+\frac{1}{2},j+\frac{1}{2}} + H^{n+\frac{1}{2}}_{i+\frac{1}{2},j+\frac{1}{2}})] \\
&= \sum_{n=0}^{N_t}\sum_{0\le i\le N_x-1}[(H^{n+\frac{1}{2}}_{i-\frac{1}{2},j+\frac{1}{2}}E^{n+1}_{y,i,j+\frac{1}{2}} - H^{n+\frac{1}{2}}_{i+\frac{1}{2},j+\frac{1}{2}}E^{n+1}_{y,i+1,j+\frac{1}{2}}) \\
&\quad +(-H^{n+\frac{1}{2}}_{i+\frac{1}{2},j+\frac{1}{2}}E^n_{y,i,j+\frac{1}{2}} + H^{n+\frac{3}{2}}_{i+\frac{1}{2},j+\frac{1}{2}}E^{n+1}_{y,i,j+\frac{1}{2}})] \\
&\quad +\sum_{n=0}^{N_t}\sum_{0\le i\le N_x-1}[(H^{n+\frac{1}{2}}_{i-\frac{1}{2},j+\frac{1}{2}}E^n_{y,i,j+\frac{1}{2}} - H^{n+\frac{1}{2}}_{i+\frac{1}{2},j+\frac{1}{2}}E^n_{y,i+1,j+\frac{1}{2}}) \\
&\quad +(H^{n+\frac{1}{2}}_{i+\frac{1}{2},j+\frac{1}{2}}E^n_{y,i+1,j+\frac{1}{2}} - H^{n+\frac{3}{2}}_{i+\frac{1}{2},j+\frac{1}{2}}E^{n+1}_{y,i+1,j+\frac{1}{2}})] \\
&= \sum_{n=0}^{N_t}(H^{n+\frac{1}{2}}_{-\frac{1}{2},j+\frac{1}{2}}E^{n+1}_{y,0,j+\frac{1}{2}} - H^{n+\frac{1}{2}}_{N_x-\frac{1}{2},j+\frac{1}{2}}E^{n+1}_{y,N_x,j+\frac{1}{2}}) \\
&\quad +\sum_{0\le i\le N_x-1}(-H^{\frac{1}{2}}_{i+\frac{1}{2},j+\frac{1}{2}}E^0_{y,i,j+\frac{1}{2}} + H^{N_t+\frac{3}{2}}_{i+\frac{1}{2},j+\frac{1}{2}}E^{N_t+1}_{y,i,j+\frac{1}{2}}) \\
&\quad +\sum_{n=0}^{N_t}(H^{n+\frac{1}{2}}_{-\frac{1}{2},j+\frac{1}{2}}E^n_{y,0,j+\frac{1}{2}} - H^{n+\frac{1}{2}}_{N_x+\frac{1}{2},j+\frac{1}{2}}E^n_{y,N_x,j+\frac{1}{2}}) \\
&\quad +\sum_{0\le i\le N_x-1}(H^{\frac{1}{2}}_{i+\frac{1}{2},j+\frac{1}{2}}E^0_{y,i+1,j+\frac{1}{2}} - H^{N_t+\frac{3}{2}}_{i+\frac{1}{2},j+\frac{1}{2}}E^{N_t+1}_{y,i+1,j+\frac{1}{2}}) \\
&= \sum_{0\le i\le N_x-1}(-H^{\frac{1}{2}}_{i+\frac{1}{2},j+\frac{1}{2}}E^0_{y,i,j+\frac{1}{2}} + H^{N_t+\frac{3}{2}}_{i+\frac{1}{2},j+\frac{1}{2}}E^{N_t+1}_{y,i,j+\frac{1}{2}}) \\
&\quad +\sum_{0\le i\le N_x-1}(H^{\frac{1}{2}}_{i+\frac{1}{2},j+\frac{1}{2}}E^0_{y,i+1,j+\frac{1}{2}} - H^{N_t+\frac{3}{2}}_{i+\frac{1}{2},j+\frac{1}{2}}E^{N_t+1}_{y,i+1,j+\frac{1}{2}})
\end{aligned}$$

$$= \sum_{0\le i\le N_x-1} (x_{i+1}-x_i)(-H^{N_t+\frac{3}{2}}_{i+\frac{1}{2},j+\frac{1}{2}} \nabla_x E^{N_t+1}_{y,i+1,j+\frac{1}{2}} + H^{\frac{1}{2}}_{i+\frac{1}{2},j+\frac{1}{2}} \nabla_x E^{0}_{y,i+1,j+\frac{1}{2}}), \tag{2.46}$$

where the PEC boundary condition (2.19) was used in the second last step, and the backward difference operator ∇_x was used in the last step. Here similarly to R_1, in the first step we extended the original sum of $1 \le i \le N_x - 1$ to $0 \le i \le N_x - 1$. Even though $H^{n+\frac{1}{2}}_{-\frac{1}{2},j+\frac{1}{2}}$ has subindex out of the original bound, its product with $E^{n+1}_{y,0,j+\frac{1}{2}} + E^{n}_{y,0,j+\frac{1}{2}} = 0$ (by the PEC boundary condition (2.19)) is still zero.

Similarly, we can evaluate the rest terms in RHS (2.44) as follows.

$$\begin{aligned}\sum_{n=0}^{N_t} R_3 &= \sum_{n=0}^{N_t} \sum_{\substack{0\le i\le N_x-1\\ 0\le j\le N_y-1}} |T_{i,j-\frac{1}{2}}|[-J^{n+\frac{1}{2}}_{x,i+\frac{1}{2},j}(E^{n+1}_{x,i+\frac{1}{2},j} + E^{n}_{x,i+\frac{1}{2},j}) \\ &\quad + (J^{n+\frac{3}{2}}_{x,i+\frac{1}{2},j} + J^{n+\frac{1}{2}}_{x,i+\frac{1}{2},j}) E^{n+1}_{x,i+\frac{1}{2},j}] \\ &= \sum_{\substack{0\le i\le N_x-1\\ 0\le j\le N_y-1}} |T_{i,j-\frac{1}{2}}|(J^{N_t+\frac{3}{2}}_{x,i+\frac{1}{2},j} E^{N_t+1}_{x,i+\frac{1}{2},j} - J^{\frac{1}{2}}_{x,i+\frac{1}{2},j} E^{0}_{x,i+\frac{1}{2},j}),\end{aligned} \tag{2.47}$$

$$\begin{aligned}\sum_{n=0}^{N_t} R_4 &= \sum_{n=0}^{N_t} \sum_{\substack{0\le i\le N_x-1\\ 0\le j\le N_y-1}} |T_{i-\frac{1}{2},j}|[-J^{n+\frac{1}{2}}_{y,i,j+\frac{1}{2}}(E^{n+1}_{y,i,j+\frac{1}{2}} + E^{n}_{y,i,j+\frac{1}{2}}) \\ &\quad + (J^{n+\frac{3}{2}}_{y,i,j+\frac{1}{2}} + J^{n+\frac{1}{2}}_{y,i,j+\frac{1}{2}}) E^{n+1}_{y,i,j+\frac{1}{2}}] \\ &= \sum_{\substack{0\le i\le N_x-1\\ 0\le j\le N_y-1}} |T_{i-\frac{1}{2},j}|(J^{N_t+\frac{3}{2}}_{y,i,j+\frac{1}{2}} E^{N_t+1}_{y,i,j+\frac{1}{2}} - J^{\frac{1}{2}}_{y,i,j+\frac{1}{2}} E^{0}_{y,i,j+\frac{1}{2}}),\end{aligned} \tag{2.48}$$

and

$$\begin{aligned}\sum_{n=0}^{N_t} R_5 &= \sum_{n=0}^{N_t} \sum_{\substack{0\le i\le N_x-1\\ 0\le j\le N_y-1}} |T_{ij}|[-K^{n+1}_{i+\frac{1}{2},j+\frac{1}{2}}(H^{n+\frac{3}{2}}_{i+\frac{1}{2},j+\frac{1}{2}} + H^{n+\frac{1}{2}}_{i+\frac{1}{2},j+\frac{1}{2}}) \\ &\quad + H^{n+\frac{3}{2}}_{i+\frac{1}{2},j+\frac{1}{2}}(K^{n+2}_{i+\frac{1}{2},j+\frac{1}{2}} + K^{n+1}_{i+\frac{1}{2},j+\frac{1}{2}})]\end{aligned}$$

$$= \sum_{\substack{0\le i\le N_x-1\\ 0\le j\le N_y-1}} |T_{ij}|(H^{N_t+\frac{3}{2}}_{i+\frac{1}{2},j+\frac{1}{2}} K^{N_t+2}_{i+\frac{1}{2},j+\frac{1}{2}} - H^{\frac{1}{2}}_{i+\frac{1}{2},j+\frac{1}{2}} K^{1}_{i+\frac{1}{2},j+\frac{1}{2}}). \quad (2.49)$$

Summing up (2.44) from $n = 0$ to N_t, then substituting the estimates (2.45)-(2.49), and using the energy norm notations, we have

$$\begin{aligned}
&\epsilon_0(||E_x^{N_t+1}||_E^2 - ||E_x^0||_E^2) + \epsilon_0(||E_y^{N_t+1}||_E^2 - ||E_y^0||_E^2) + \mu_0(||H^{N_t+\frac{3}{2}}||_H^2 - ||H^{\frac{1}{2}}||_H^2)\\
&\quad + \frac{1}{\epsilon_0\omega_{pe}^2}(||J_x^{N_t+\frac{3}{2}}||_J^2 - ||J_x^{\frac{1}{2}}||_J^2) + \frac{1}{\epsilon_0\omega_{pe}^2}(||J_y^{N_t+\frac{3}{2}}||_J^2 - ||J_y^{\frac{1}{2}}||_J^2)\\
&\quad + \frac{1}{\mu_0\omega_{pm}^2}(||K^{N_t+2}||_K^2 - ||K^1||_K^2)\\
\le\ & \tau \sum_{\substack{0\le i\le N_x-1\\ 0\le j\le N_y-1}} |T_{ij}|(H^{N_t+\frac{3}{2}}_{i+\frac{1}{2},j+\frac{1}{2}} \nabla_y E^{N_t+1}_{x,i+\frac{1}{2},j+1} - H^{\frac{1}{2}}_{i+\frac{1}{2},j+\frac{1}{2}} \nabla_y E^{0}_{x,i+\frac{1}{2},j+1})\\
&\quad + \tau \sum_{\substack{0\le i\le N_x-1\\ 0\le j\le N_y-1}} |T_{ij}|(-H^{N_t+\frac{3}{2}}_{i+\frac{1}{2},j+\frac{1}{2}} \nabla_x E^{N_t+1}_{y,i+1,j+\frac{1}{2}} + H^{\frac{1}{2}}_{i+\frac{1}{2},j+\frac{1}{2}} \nabla_x E^{0}_{y,i+1,j+\frac{1}{2}})\\
&\quad + \tau \sum_{\substack{0\le i\le N_x-1\\ 0\le j\le N_y-1}} |T_{i,j-\frac{1}{2}}|(J^{N_t+\frac{3}{2}}_{x,i+\frac{1}{2},j} E^{N_t+1}_{x,i+\frac{1}{2},j} - J^{\frac{1}{2}}_{x,i+\frac{1}{2},j} E^{0}_{x,i+\frac{1}{2},j})\\
&\quad + \tau \sum_{\substack{0\le i\le N_x-1\\ 0\le j\le N_y-1}} |T_{i-\frac{1}{2},j}|(J^{N_t+\frac{3}{2}}_{y,i,j+\frac{1}{2}} E^{N_t+1}_{y,i,j+\frac{1}{2}} - J^{\frac{1}{2}}_{y,i,j+\frac{1}{2}} E^{0}_{y,i,j+\frac{1}{2}})\\
&\quad + \tau \sum_{\substack{0\le i\le N_x-1\\ 0\le j\le N_y-1}} |T_{ij}|(H^{N_t+\frac{3}{2}}_{i+\frac{1}{2},j+\frac{1}{2}} K^{N_t+2}_{i+\frac{1}{2},j+\frac{1}{2}} - H^{\frac{1}{2}}_{i+\frac{1}{2},j+\frac{1}{2}} K^{1}_{i+\frac{1}{2},j+\frac{1}{2}}). \quad (2.50)
\end{aligned}$$

Now we just need to bound those right hand side terms of (2.50). Using the Cauchy-Schwarz inequality and the inverse estimate (2.41), we have

$$\begin{aligned}
&\tau \sum_{\substack{0\le i\le N_x-1\\ 0\le j\le N_y-1}} |T_{ij}| \cdot H^{N_t+\frac{3}{2}}_{i+\frac{1}{2},j+\frac{1}{2}} \nabla_y E^{N_t+1}_{x,i+\frac{1}{2},j+1}\\
\le\ & \tau\Big(\sum_{\substack{0\le i\le N_x-1\\ 0\le j\le N_y-1}} |T_{ij}| \cdot |H^{N_t+\frac{3}{2}}_{i+\frac{1}{2},j+\frac{1}{2}}|^2\Big)^{1/2}\Big(\sum_{\substack{0\le i\le N_x-1\\ 0\le j\le N_y-1}} |T_{ij}| \cdot |\nabla_y E^{N_t+1}_{x,i+\frac{1}{2},j+1}|^2\Big)^{1/2}\\
=\ & \tau||H^{N_t+\frac{3}{2}}||_H||\nabla_y E_x^{N_t+1}||_E \le \delta\mu_0||H^{N_t+\frac{3}{2}}||_H^2\\
&\quad + \frac{1}{4\delta} \cdot \frac{(\tau C_{inv} h_y^{-1})^2}{\mu_0\epsilon_0} \cdot \epsilon_0||E_x^{N_t+1}||_E^2. \quad (2.51)
\end{aligned}$$

Similarly, we can obtain

$$\tau \sum_{\substack{0\le i\le N_x-1\\ 0\le j\le N_y-1}} |T_{ij}| \cdot H^{N_t+\frac{3}{2}}_{i+\frac{1}{2},j+\frac{1}{2}} \nabla_x E^{N_t+1}_{y,i+1,j+\frac{1}{2}}$$

$$\le \delta\mu_0 ||H^{N_t+\frac{3}{2}}||^2_H + \frac{1}{4\delta}\cdot\frac{(\tau C_{inv}h_x^{-1})^2}{\mu_0\epsilon_0}\cdot\epsilon_0||E_y^{N_t+1}||^2_E. \qquad (2.52)$$

By the similar technique, we can prove that

$$\tau \sum_{\substack{0\le i\le N_x-1\\ 1\le j\le N_y-1}} |T_{i,j-\frac{1}{2}}| \cdot J^{N_t+\frac{3}{2}}_{x,i+\frac{1}{2},j} E^{N_t+1}_{x,i+\frac{1}{2},j}$$

$$\le \tau||J_x^{N_t+\frac{3}{2}}||_J||E_x^{N_t+1}||_E \le \frac{\tau\omega_{pe}}{2}(\frac{1}{\epsilon_0\omega_{pe}^2}||J_x^{N_t+\frac{3}{2}}||^2_J + \epsilon_0||E_x^{N_t+1}||^2_E), \qquad (2.53)$$

$$\tau \sum_{\substack{1\le i\le N_x-1\\ 0\le j\le N_y-1}} |T_{i-\frac{1}{2},j}| \cdot J^{N_t+\frac{3}{2}}_{y,i,j+\frac{1}{2}} E^{N_t+1}_{y,i,j+\frac{1}{2}}$$

$$\le \tau||J_y^{N_t+\frac{3}{2}}||_J||E_y^{N_t+1}||_E \le \frac{\tau\omega_{pe}}{2}(\frac{1}{\epsilon_0\omega_{pe}^2}||J_y^{N_t+\frac{3}{2}}||^2_J + \epsilon_0||E_y^{N_t+1}||^2_E), \qquad (2.54)$$

and

$$\tau \sum_{\substack{0\le i\le N_x-1\\ 0\le j\le N_y-1}} |T_{ij}| \cdot H^{N_t+\frac{3}{2}}_{i+\frac{1}{2},j+\frac{1}{2}} K^{N_t+2}_{i+\frac{1}{2},j+\frac{1}{2}}$$

$$\le \tau||H^{N_t+\frac{3}{2}}||_H||K^{N_t+2}||_K \le \frac{\tau\omega_{pm}}{2}(\mu_0||H^{N_t+\frac{3}{2}}||^2_H + \frac{1}{\mu_0\omega_{pm}^2}||K^{N_t+2}||^2_K). \qquad (2.55)$$

Substituting the estimates (2.51)-(2.55) into (2.50), then choosing δ and τ small enough so that the left hand side terms of (2.50) can control those corresponding terms on the right hand side. A specific choice can be

$$\delta = \frac{1}{4},\ \tau \le \frac{C_{inv}h_y}{2C_v},\ \tau \le \frac{C_{inv}h_x}{2C_v},\ \tau \le \frac{1}{2\omega_{pe}},\ \tau \le \frac{1}{2\omega_{pm}}.$$

This completes the proof. □

The error estimate

To make the error analysis easy to follow, we denote the errors by their corresponding script letters. For example, the error of E_x at point $(x_{i+\frac{1}{2}}, y_j, t_n)$ is denoted by $\mathcal{E}^n_{x,i+\frac{1}{2},j} = E_x(x_{i+\frac{1}{2}}, y_j, t_n) - E^n_{x,i+\frac{1}{2},j}$, where $E_x(x_{i+\frac{1}{2}}, y_j, t_n)$ and $E^n_{x,i+\frac{1}{2},j}$ denote the exact and numerical solutions of E_x at point $(x_{i+\frac{1}{2}}, y_j, t_n)$, respectively. Similar error notations given below will be used for other variables:

$$\mathcal{E}^n_{y,i,j+\frac{1}{2}}, \quad \mathcal{H}^{n+\frac{1}{2}}_{i+\frac{1}{2},j+\frac{1}{2}}, \quad \mathcal{J}^{n+\frac{1}{2}}_{x,i+\frac{1}{2},j}, \quad \mathcal{J}^{n+\frac{1}{2}}_{y,i,j+\frac{1}{2}}, \quad \mathcal{K}^{n+1}_{i+\frac{1}{2},j+\frac{1}{2}}.$$

The error equation for E_x

Multiplying (2.35) by $|T_{i,j-\frac{1}{2}}|$ (the area of rectangle $T_{i,j-\frac{1}{2}}$), we can rewrite (2.35) as follows:

$$\frac{\epsilon_0|T_{i,j-\frac{1}{2}}|}{\tau}(E^{n+1}_{x,i+\frac{1}{2},j} - E^n_{x,i+\frac{1}{2},j}) = (x_{i+1} - x_i)(H^{n+\frac{1}{2}}_{i+\frac{1}{2},j+\frac{1}{2}} - H^{n+\frac{1}{2}}_{i+\frac{1}{2},j-\frac{1}{2}}) - |T_{i,j-\frac{1}{2}}|J^{n+\frac{1}{2}}_{x,i+\frac{1}{2},j},$$

from which we can easily obtain the error equation for E_x:

$$\begin{aligned}&\frac{\epsilon_0|T_{i,j-\frac{1}{2}}|}{\tau}(\mathcal{E}^{n+1}_{x,i+\frac{1}{2},j} - \mathcal{E}^n_{x,i+\frac{1}{2},j})\\ &\qquad = (x_{i+1} - x_i)(\mathcal{H}^{n+\frac{1}{2}}_{i+\frac{1}{2},j+\frac{1}{2}} - \mathcal{H}^{n+\frac{1}{2}}_{i+\frac{1}{2},j-\frac{1}{2}}) - |T_{i,j-\frac{1}{2}}|\mathcal{J}^{n+\frac{1}{2}}_{x,i+\frac{1}{2},j} + R_1, \quad (2.56)\end{aligned}$$

where the local truncation error term R_1 is given by

$$\begin{aligned}R_1 = &\frac{\epsilon_0|T_{i,j-\frac{1}{2}}|}{\tau}(E_x(x_{i+\frac{1}{2}}, y_j, t_{n+1}) - E_x(x_{i+\frac{1}{2}}, y_j, t_n))\\ &-(x_{i+1} - x_i)(H(x_{i+\frac{1}{2}}, y_{j+\frac{1}{2}}, t_{n+\frac{1}{2}}) - H(x_{i+\frac{1}{2}}, y_{j-\frac{1}{2}}, t_{n+\frac{1}{2}}))\\ &+|T_{i,j-\frac{1}{2}}|J_x(x_{i+\frac{1}{2}}, y_j, t_{n+\frac{1}{2}}). \quad (2.57)\end{aligned}$$

Integrating (2.7) from $t = t_n$ to t_{n+1} and dividing the resultant by τ, we have

$$\begin{aligned}
&\frac{\epsilon_0}{\tau}\iint_{T_{i,j-\frac{1}{2}}}(E_x(x,y,t_{n+1})-E_x(x,y,t_n))dxdy \qquad (2.58)\\
&= \frac{1}{\tau}\int_{t_n}^{t_{n+1}}\int_{x_i}^{x_{i+1}}(H(x,y_{j+\frac{1}{2}},t)-H(x,y_{j-\frac{1}{2}},t))dxdt\\
&\quad -\frac{1}{\tau}\int_{t_n}^{t_{n+1}}\iint_{T_{i,j-\frac{1}{2}}}J_x(x,y,t)dxdydt.
\end{aligned}$$

Subtracting (2.58) from (2.57), we can rewrite R_1 as follows:

$$\begin{aligned}
R_1 &= \frac{\epsilon_0}{\tau}\iint_{T_{i,j-\frac{1}{2}}}\Big[(E_x(x_{i+\frac{1}{2}},y_j,t_{n+1})-E_x(x,y,t_{n+1}))\\
&\quad -(E_x(x_{i+\frac{1}{2}},y_j,t_n)-E_x(x,y,t_n))\Big]dxdy\\
&\quad -\{\int_{x_i}^{x_{i+1}}(H(x_{i+\frac{1}{2}},y_{j+\frac{1}{2}},t_{n+\frac{1}{2}})-H(x_{i+\frac{1}{2}},y_{j-\frac{1}{2}},t_{n+\frac{1}{2}}))dx\\
&\quad -\frac{1}{\tau}\int_{t_n}^{t_{n+1}}\int_{x_i}^{x_{i+1}}(H(x,y_{j+\frac{1}{2}},t)-H(x,y_{j-\frac{1}{2}},t))dxdt\}\\
&\quad +\left[\iint_{T_{i,j-\frac{1}{2}}}J_x(x_{i+\frac{1}{2}},y_j,t_{n+\frac{1}{2}})dxdy-\frac{1}{\tau}\int_{t_n}^{t_{n+1}}\iint_{T_{i,j-\frac{1}{2}}}J_x(x,y,t)dxdydt\right]\\
&= R_{11}+R_{12}+R_{13}. \qquad (2.59)
\end{aligned}$$

Following the same technique used for deriving (2.30), for any function f we can prove that

$$\begin{aligned}
&\iint_{T_{i,j-\frac{1}{2}}}(f(x,y,t_{n+1})-f(x_{i+\frac{1}{2}},y_j,t_{n+1}))dxdy\\
&\quad -\iint_{T_{i,j-\frac{1}{2}}}(f(x,y,t_n)-f(x_{i+\frac{1}{2}},y_j,t_n))dxdy\\
&= \iint_{T_{i,j-\frac{1}{2}}}[\frac{1}{2}(x-x_{i+\frac{1}{2}})^2(\frac{\partial^2 f}{\partial x^2}(q_1,t_{n+1})-\frac{\partial^2 f}{\partial x^2}(q_1,t_n))\\
&\quad +\frac{1}{2}(y-y_j)^2(\frac{\partial^2 f}{\partial y^2}(q_2,t_{n+1})-\frac{\partial^2 f}{\partial y^2}(q_2,t_n))]dxdy\\
&= \tau\iint_{T_{i,j-\frac{1}{2}}}\left[\frac{1}{2}(x-x_{i+\frac{1}{2}})^2\frac{\partial^3 f}{\partial t\partial x^2}(q_1,t_*)\right.\\
&\quad \left.+\frac{1}{2}(y-y_j)^2\frac{\partial^3 f}{\partial t\partial y^2}(q_2,t_*)\right]dxdy, \qquad (2.60)
\end{aligned}$$

where we denote q_1 and q_2 for some points between $(x_{i+\frac{1}{2}}, y_j)$ and (x, y), and t_* for some point between t_n and t_{n+1}. In the last step we used the following Taylor expansion

$$g(t_{n+1}) - g(t_n) = \tau \frac{\partial g}{\partial t}(t_*)$$

with $g = \frac{\partial^2 f}{\partial x^2}$ and $g = \frac{\partial^2 f}{\partial y^2}$, respectively.

Applying (2.60) with $f = E_x$, we can bound R_{11} as follows:

$$\begin{aligned} R_{11} &= \frac{\epsilon_0}{\tau} \iint_{T_{i,j-\frac{1}{2}}} \left[\frac{1}{2}(x - x_{i+\frac{1}{2}})^2 \tau \frac{\partial^3 E_x}{\partial t \partial x^2}(q_1, t_*) + \frac{1}{2}(y - y_j)^2 \tau \frac{\partial^3 E_x}{\partial t \partial y^2}(q_2, t_*) \right] dxdy \\ &= (O(h_x^2) |\frac{\partial^3 E_x}{\partial t \partial x^2}|_\infty + O(h_y^2) |\frac{\partial^3 E_x}{\partial t \partial y^2}|_\infty) |T_{i,j-\frac{1}{2}}|. \end{aligned}$$

Similarly, by the Taylor expansion, we can estimate R_{12} as follows:

$$\begin{aligned} R_{12} &= -\int_{x_i}^{x_{i+1}} \int_{y_{j-\frac{1}{2}}}^{y_{j+\frac{1}{2}}} \frac{\partial H}{\partial y}(x_{i+\frac{1}{2}}, y, t_{n+\frac{1}{2}}) dydx \\ &\quad + \frac{1}{\tau} \int_{t_n}^{t_{n+1}} \int_{x_i}^{x_{i+1}} \int_{y_{j-\frac{1}{2}}}^{y_{j+\frac{1}{2}}} \frac{\partial H}{\partial y}(x, y, t) dydxdt \\ &= -\int_{x_i}^{x_{i+1}} \int_{y_{j-\frac{1}{2}}}^{y_{j+\frac{1}{2}}} \left[\frac{\partial H}{\partial y}(x_{i+\frac{1}{2}}, y, t_{n+\frac{1}{2}}) - \frac{\partial H}{\partial y}(x, y, t_{n+\frac{1}{2}}) \right] dydx \\ &\quad + \int_{x_i}^{x_{i+1}} \int_{y_{j-\frac{1}{2}}}^{y_{j+\frac{1}{2}}} \frac{1}{\tau} \int_{t_n}^{t_{n+1}} \left[\frac{\partial H}{\partial y}(x, y, t) - \frac{\partial H}{\partial y}(x, y, t_{n+\frac{1}{2}}) \right] dtdydx \\ &= \iint_{T_{i,j-\frac{1}{2}}} \frac{1}{2}(x - x_{i+\frac{1}{2}})^2 \frac{\partial^3 H}{\partial x^2 \partial y}(x_*, y, t_{n+\frac{1}{2}}) dxdy \\ &\quad + \iint_{T_{i,j-\frac{1}{2}}} \frac{1}{\tau} \int_{t_n}^{t_{n+1}} \frac{1}{2}(t - t_{n+\frac{1}{2}})^2 \frac{\partial^3 H}{\partial t^2 \partial y}(x, y, t_*) dtdydx \\ &= (O(h_x^2) |\frac{\partial^3 H}{\partial x^2 \partial y}|_\infty + O(\tau^2) |\frac{\partial^3 H}{\partial t^2 \partial y}|_\infty) |T_{i,j-\frac{1}{2}}|, \end{aligned}$$

where x_* is some number between $x_{i+\frac{1}{2}}$ and x, and t_* is some number between $t_{n+\frac{1}{2}}$ and t.

Using exactly the same argument, we can estimate R_{13} as follows:

$$\begin{aligned} R_{13} &= \iint_{T_{i,j-\frac{1}{2}}} (J_x(x_{i+\frac{1}{2}}, y_j, t_{n+\frac{1}{2}}) - J_x(x, y, t_{n+\frac{1}{2}}))dxdy \\ &\quad + \frac{1}{\tau}\int_{t_n}^{t_{n+1}} \iint_{T_{i,j-\frac{1}{2}}} (J_x(x, y, t_{n+\frac{1}{2}}) - J_x(x, y, t))dxdydt \\ &= (O(h_x^2)|\frac{\partial^2 J_x}{\partial x^2}|_\infty + O(h_y^2)|\frac{\partial^2 J_x}{\partial y^2}|_\infty + O(\tau^2)|\frac{\partial^2 J_x}{\partial t^2}|_\infty)|T_{i,j-\frac{1}{2}}|. \end{aligned}$$

The error equation for E_y

Multiplying (2.36) by $|T_{i-\frac{1}{2},j}|$, we can easily derive the error equation for E_y:

$$\begin{aligned} &\frac{\epsilon_0|T_{i-\frac{1}{2},j}|}{\tau}(\mathcal{E}^{n+1}_{y,i,j+\frac{1}{2}} - \mathcal{E}^{n}_{y,i,j+\frac{1}{2}}) \\ &\quad = -(y_{j+1} - y_j)(\mathcal{H}^{n+\frac{1}{2}}_{i+\frac{1}{2},j+\frac{1}{2}} - \mathcal{H}^{n+\frac{1}{2}}_{i-\frac{1}{2},j+\frac{1}{2}}) - |T_{i-\frac{1}{2},j}|\mathcal{J}^{n+\frac{1}{2}}_{y,i,j+\frac{1}{2}} + R_2, \end{aligned} \tag{2.61}$$

where the local truncation error R_2 is given by

$$\begin{aligned} R_2 &= \frac{\epsilon_0|T_{i-\frac{1}{2},j}|}{\tau}(E_y(x_i, y_{j+\frac{1}{2}}, t_{n+1}) - E_y(x_i, y_{j+\frac{1}{2}}, t_n)) \\ &\quad + (y_{j+1} - y_j)(H(x_{i+\frac{1}{2}}, y_{j+\frac{1}{2}}, t_{n+\frac{1}{2}}) - H(x_{i-\frac{1}{2}}, y_{j+\frac{1}{2}}, t_{n+\frac{1}{2}})) \\ &\quad + |T_{i-\frac{1}{2},j}|J_y(x_i, y_{j+\frac{1}{2}}, t_{n+\frac{1}{2}}). \end{aligned} \tag{2.62}$$

Integrating (2.9) from $t = t_n$ to t_{n+1} and dividing the resultant by τ, we have

$$\begin{aligned} &\frac{\epsilon_0}{\tau}\iint_{T_{i-\frac{1}{2},j}} (E_y(x, y, t_{n+1}) - E_y(x, y, t_n))dxdy \\ &= -\frac{1}{\tau}\int_{t_n}^{t_{n+1}}\int_{y_j}^{y_{j+1}} (H(x_{i+\frac{1}{2}}, y, t) - H(x_{i-\frac{1}{2}}, y, t))dydt \\ &\quad -\frac{1}{\tau}\int_{t_n}^{t_{n+1}} \iint_{T_{i-\frac{1}{2},j}} J_y(x, y, t)dxdydt. \end{aligned} \tag{2.63}$$

Subtracting (2.63) from (2.62), we can rewrite R_2 as follows:

$$\begin{aligned} R_2 &= \frac{\epsilon_0}{\tau}\iint_{T_{i-\frac{1}{2},j}} \Big[(E_y(x_i, y_{j+\frac{1}{2}}, t_{n+1}) - E_y(x, y, t_{n+1})) \\ &\quad -(E_y(x_i, y_{j+\frac{1}{2}}, t_n) - E_y(x, y, t_n))\Big]\, dxdy \\ &\quad - \{\int_{y_j}^{y_{j+1}} (H(x_{i+\frac{1}{2}}, y_{j+\frac{1}{2}}, t_{n+\frac{1}{2}}) - H(x_{i-\frac{1}{2}}, y_{j+\frac{1}{2}}, t_{n+\frac{1}{2}}))dy \\ &\quad - \frac{1}{\tau}\int_{t_n}^{t_{n+1}}\int_{y_j}^{y_{j+1}} (H(x_{i+\frac{1}{2}}, y, t) - H(x_{i-\frac{1}{2}}, y, t))dydt\} \\ &\quad + \left[\iint_{T_{i-\frac{1}{2},j}} J_y(x_i, y_{j+\frac{1}{2}}, t_{n+\frac{1}{2}})dxdy - \frac{1}{\tau}\int_{t_n}^{t_{n+1}}\iint_{T_{i-\frac{1}{2},j}} J_y(x, y, t)dxdydt\right] \\ &= R_{21} + R_{22} + R_{23}. \end{aligned} \tag{2.64}$$

Following exactly the same technique developed above for R_1, we can show that

$$\begin{aligned} R_{21} &= (O(h_x^2)|\frac{\partial^3 E_y}{\partial t \partial x^2}|_\infty + O(h_y^2)|\frac{\partial^3 E_y}{\partial t \partial y^2}|_\infty)|T_{i-\frac{1}{2},j}|, \\ R_{22} &= (O(h_y^2)|\frac{\partial^3 H}{\partial y^2 \partial x}|_\infty + O(\tau^2)|\frac{\partial^3 H}{\partial t^2 \partial x}|_\infty)|T_{i-\frac{1}{2},j}|, \\ R_{23} &= (O(h_x^2)|\frac{\partial^2 J_y}{\partial x^2}|_\infty + O(h_y^2)|\frac{\partial^2 J_y}{\partial y^2}|_\infty + O(\tau^2)|\frac{\partial^2 J_y}{\partial t^2}|_\infty)|T_{i-\frac{1}{2},j}|. \end{aligned}$$

The error equation for H

Multiplying (2.37) by $|T_{i,j}|$, we can easily obtain the error equation for H:

$$\begin{aligned} &\frac{\mu_0|T_{i,j}|}{\tau}(\mathcal{H}_{i+\frac{1}{2},j+\frac{1}{2}}^{n+\frac{3}{2}} - \mathcal{H}_{i+\frac{1}{2},j+\frac{1}{2}}^{n+\frac{1}{2}}) = -(y_{j+1} - y_j)(\mathcal{E}_{y,i+1,j+\frac{1}{2}}^{n+1} - \mathcal{E}_{y,i,j+\frac{1}{2}}^{n+1}) \\ &\quad +(x_{i+1} - x_i)(\mathcal{E}_{x,i+\frac{1}{2},j+1}^{n+1} - \mathcal{E}_{x,i+\frac{1}{2},j}^{n+1}) - |T_{i,j}|\mathcal{K}_{i+\frac{1}{2},j+\frac{1}{2}}^{n+1} + R_3, \end{aligned} \tag{2.65}$$

where the local truncation error R_3 is given by

$$\begin{aligned} R_3 &= \frac{\mu_0|T_{i,j}|}{\tau}(H(x_{i+\frac{1}{2}}, y_{j+\frac{1}{2}}, t_{n+\frac{3}{2}}) - H(x_{i+\frac{1}{2}}, y_{j+\frac{1}{2}}, t_{n+\frac{1}{2}})) \\ &\quad +(y_{j+1} - y_j)(E_y(x_{i+1}, y_{j+\frac{1}{2}}, t_{n+1}) - E_y(x_i, y_{j+\frac{1}{2}}, t_{n+1})) \\ &\quad -(x_{i+1} - x_i)(E_x(x_{i+\frac{1}{2}}, y_{j+1}, t_{n+1}) - E_x(x_{i+\frac{1}{2}}, y_j, t_{n+1})) \end{aligned} \tag{2.66}$$

$$+|T_{i,j}|K(x_{i+\frac{1}{2}}, y_{j+\frac{1}{2}}, t_{n+1}).$$

Integrating (2.11) from $t = t_{n+\frac{1}{2}}$ to $t_{n+\frac{3}{2}}$ and dividing the resultant by τ, we obtain

$$\begin{aligned}
&\frac{\mu_0}{\tau}\iint_{T_{i,j}}(H(x,y,t_{n+\frac{3}{2}}) - H(x,y,t_{n+\frac{1}{2}}))dxdy \\
&= -\frac{1}{\tau}\int_{t_{n+\frac{1}{2}}}^{t_{n+\frac{3}{2}}}\iint_{T_{i,j}}(\frac{\partial E_y}{\partial x} - \frac{\partial E_x}{\partial y})(x,y,t)dxdydt \\
&\quad -\frac{1}{\tau}\int_{t_{n+\frac{1}{2}}}^{t_{n+\frac{3}{2}}}\iint_{T_{i,j}} K(x,y,t)dxdydt. \qquad (2.67)
\end{aligned}$$

Subtracting (2.67) from (2.66), we can rewrite R_3 as follows:

$$\begin{aligned}
R_3 &= \frac{\mu_0}{\tau}\iint_{T_{i,j}}\{(H(x_{i+\frac{1}{2}}, y_{j+\frac{1}{2}}, t_{n+\frac{3}{2}}) - H(x,y,t_{n+\frac{3}{2}})) \\
&\qquad -(H(x_{i+\frac{1}{2}}, y_{j+\frac{1}{2}}, t_{n+\frac{1}{2}}) - H(x,y,t_{n+\frac{1}{2}}))\}dxdy \\
&\quad +\{\iint_{T_{i,j}}(\frac{\partial E_y}{\partial x}(x, y_{j+\frac{1}{2}}, t_{n+1}) - \frac{\partial E_x}{\partial y}(x_{i+\frac{1}{2}}, y, t_{n+1}))dxdy \\
&\quad -\frac{1}{\tau}\int_{t_{n+\frac{1}{2}}}^{t_{n+\frac{3}{2}}}\iint_{T_{i,j}}(\frac{\partial E_y}{\partial x}(x,y,t) - \frac{\partial E_x}{\partial y}(x,y,t))dxdydt\} \\
&\quad +\{\iint_{T_{i,j}} K(x_{i+\frac{1}{2}}, y_{j+\frac{1}{2}}, t_{n+1})dxdy - \frac{1}{\tau}\int_{t_{n+\frac{1}{2}}}^{t_{n+\frac{3}{2}}}\iint_{T_{i,j}} K(x,y,t)dxdydt\} \\
&= R_{31} + R_{32} + R_{33}. \qquad (2.68)
\end{aligned}$$

By the Taylor expansion, we can obtain

$$\begin{aligned}
R_{31} &= (O(h_x^2)|\frac{\partial^3 H}{\partial t \partial x^2}|_\infty + O(h_y^2)|\frac{\partial^3 H}{\partial t \partial y^2}|_\infty)|T_{i,j}|, \\
R_{32} &= (O(h_y^2)|\frac{\partial^3 E_y}{\partial y^2 \partial x}|_\infty + O(\tau^2)|\frac{\partial^3 E_y}{\partial t^2 \partial x}|_\infty + O(h_x^2)|\frac{\partial^3 E_x}{\partial x^2 \partial y}|_\infty \\
&\qquad +O(\tau^2)|\frac{\partial^3 E_x}{\partial t^2 \partial y}|_\infty)|T_{i,j}|, \\
R_{33} &= (O(h_x^2)|\frac{\partial^2 K}{\partial x^2}|_\infty + O(h_y^2)|\frac{\partial^2 K}{\partial y^2}|_\infty + O(\tau^2)|\frac{\partial^2 K}{\partial t^2}|_\infty)|T_{i,j}|.
\end{aligned}$$

The error equation for J_x

Multiplying (2.38) by $|T_{i,j-\frac{1}{2}}|$, we easily derive the error equation for J_x:

$$\frac{|T_{i,j-\frac{1}{2}}|}{\tau\epsilon_0\omega_{pe}^2}(\mathcal{J}_{x,i+\frac{1}{2},j}^{n+\frac{3}{2}}-\mathcal{J}_{x,i+\frac{1}{2},j}^{n+\frac{1}{2}})+\frac{\Gamma_e|T_{i,j-\frac{1}{2}}|}{2\epsilon_0\omega_{pe}^2}(\mathcal{J}_{x,i+\frac{1}{2},j}^{n+\frac{3}{2}}+\mathcal{J}_{x,i+\frac{1}{2},j}^{n+\frac{1}{2}})$$
$$=|T_{i,j-\frac{1}{2}}|\mathcal{E}_{x,i+\frac{1}{2},j}^{n+1}+R_4, \tag{2.69}$$

where the local truncation error R_4 is given by

$$\begin{aligned}R_4 &= \frac{|T_{i,j-\frac{1}{2}}|}{\tau\epsilon_0\omega_{pe}^2}(J_x(x_{i+\frac{1}{2}},y_j,t_{n+\frac{3}{2}})-J_x(x_{i+\frac{1}{2}},y_j,t_{n+\frac{1}{2}}))\\ &\quad+\frac{\Gamma_e|T_{i,j-\frac{1}{2}}|}{2\epsilon_0\omega_{pe}^2}(J_x(x_{i+\frac{1}{2}},y_j,t_{n+\frac{3}{2}})+J_x(x_{i+\frac{1}{2}},y_j,t_{n+\frac{1}{2}}))\\ &\quad-|T_{i,j-\frac{1}{2}}|E_x(x_{i+\frac{1}{2}},y_j,t_{n+1}).\end{aligned} \tag{2.70}$$

Integrating (2.13) from $t=t_{n+\frac{1}{2}}$ to $t_{n+\frac{3}{2}}$ and dividing the resultant by τ, we have

$$\begin{aligned}&\frac{1}{\tau\epsilon_0\omega_{pe}^2}\iint_{T_{i,j-\frac{1}{2}}}(J_x(x,y,t_{n+\frac{3}{2}})-J_x(x,y,t_{n+\frac{1}{2}}))dxdy\\ &\quad+\frac{\Gamma_e}{\tau\epsilon_0\omega_{pe}^2}\int_{t_{n+\frac{1}{2}}}^{t_{n+\frac{3}{2}}}\iint_{T_{i,j-\frac{1}{2}}}J_x(x,y,t)dxdydt\\ &=\frac{1}{\tau}\int_{t_{n+\frac{1}{2}}}^{t_{n+\frac{3}{2}}}\iint_{T_{i,j-\frac{1}{2}}}E_x(x,y,t)dxdydt.\end{aligned} \tag{2.71}$$

Subtracting (2.71) from (2.70), we can rewrite R_4 as follows:

$$\begin{aligned}R_4 &= \frac{1}{\tau\epsilon_0\omega_{pe}^2}\iint_{T_{i,j-\frac{1}{2}}}\{(J_x(x_{i+\frac{1}{2}},y_j,t_{n+\frac{3}{2}})-J_x(x,y,t_{n+\frac{3}{2}}))\\ &\quad-(J_x(x_{i+\frac{1}{2}},y_j,t_{n+\frac{1}{2}})-J_x(x,y,t_{n+\frac{1}{2}}))\}dxdy\\ &\quad+\frac{\Gamma_e}{\epsilon_0\omega_{pe}^2}\{\iint_{T_{i,j-\frac{1}{2}}}\frac{1}{2}(J_x(x_{i+\frac{1}{2}},y_j,t_{n+\frac{3}{2}})+J_x(x_{i+\frac{1}{2}},y_j,t_{n+\frac{1}{2}}))dxdy\\ &\quad-\frac{1}{\tau}\int_{t_{n+\frac{1}{2}}}^{t_{n+\frac{3}{2}}}\iint_{T_{i,j-\frac{1}{2}}}J_x(x,y,t)dxdydt\}\\ &\quad-\{\iint_{T_{i,j-\frac{1}{2}}}E_x(x_{i+\frac{1}{2}},y_j,t_{n+1})dxdy-\frac{1}{\tau}\int_{t_{n+\frac{1}{2}}}^{t_{n+\frac{3}{2}}}\iint_{T_{i,j-\frac{1}{2}}}E_x(x,y,t)dxdydt\}\\ &= R_{41}+R_{42}+R_{43}.\end{aligned} \tag{2.72}$$

By the Taylor expansion, we easily have

$$
\begin{aligned}
R_{41} &= (O(h_x^2)|\frac{\partial^3 J_x}{\partial t \partial x^2}|_\infty + O(h_y^2)|\frac{\partial^3 J_x}{\partial t \partial y^2}|_\infty)|T_{i,j-\frac{1}{2}}|, \\
R_{42} &= \frac{\Gamma_e}{\epsilon_0 \omega_{pe}^2}\{\iint_{T_{i,j-\frac{1}{2}}} \frac{1}{2}(J_x(x_{i+\frac{1}{2}}, y_j, t_{n+\frac{3}{2}}) + J_x(x_{i+\frac{1}{2}}, y_j, t_{n+\frac{1}{2}}) \\
&\quad -J_x(x, y, t_{n+\frac{3}{2}}) - J_x(x, y, t_{n+\frac{1}{2}}))dxdy\} \\
&\quad + \iint_{T_{i,j-\frac{1}{2}}} \frac{1}{\tau}\int_{t_{n+\frac{1}{2}}}^{t_{n+\frac{3}{2}}} \{\frac{1}{2}(J_x(x, y, t_{n+\frac{3}{2}}) + J_x(x, y, t_{n+\frac{1}{2}})) - J_x(x, y, t)\}dtdxdy \\
&= (O(h_x^2)|\frac{\partial^2 J_x}{\partial x^2}|_\infty + O(h_y^2)|\frac{\partial^2 J_x}{\partial y^2}|_\infty + O(\tau^2)|\frac{\partial^2 J_x}{\partial t^2}|_\infty)|T_{i,j-\frac{1}{2}}|,
\end{aligned}
$$

where in the last step we used the property: For any function $f \in C^2([0,T])$,

$$
\frac{1}{\tau}\int_{t_{n+\frac{1}{2}}}^{t_{n+\frac{3}{2}}} \{\frac{1}{2}(f(t_{n+\frac{3}{2}}) + f(t_{n+\frac{1}{2}})) - f(t)\}dt = O(\tau^2)|\frac{\partial^2 f}{\partial t^2}|_\infty.
$$

Similarly, it is easy to show that

$$
R_{43} = (O(h_x^2)|\frac{\partial^2 E_x}{\partial x^2}|_\infty + O(h_y^2)|\frac{\partial^2 E_x}{\partial y^2}|_\infty + O(\tau^2)|\frac{\partial^2 E_x}{\partial t^2}|_\infty)|T_{i,j-\frac{1}{2}}|.
$$

The error equation for J_y

Following exactly the same technique used for the J_x equation, we easily obtain the error equation for J_y from (2.39):

$$
\begin{aligned}
&\frac{|T_{i-\frac{1}{2},j}|}{\tau\epsilon_0\omega_{pe}^2}(\mathcal{J}_{y,i,j+\frac{1}{2}}^{n+\frac{3}{2}} - \mathcal{J}_{y,i,j+\frac{1}{2}}^{n+\frac{1}{2}}) + \frac{\Gamma_e|T_{i-\frac{1}{2},j}|}{2\epsilon_0\omega_{pe}^2}(\mathcal{J}_{y,i,j+\frac{1}{2}}^{n+\frac{3}{2}} + \mathcal{J}_{y,i,j+\frac{1}{2}}^{n+\frac{1}{2}}) \\
&\qquad = |T_{i-\frac{1}{2},j}|\mathcal{E}_{y,i,j+\frac{1}{2}}^{n+1} + R_5, \qquad (2.73)
\end{aligned}
$$

where the local truncation error R_5 is given by

$$
\begin{aligned}
R_5 &= \frac{|T_{i-\frac{1}{2},j}|}{\tau\epsilon_0\omega_{pe}^2}(J_y(x_i, y_{j+\frac{1}{2}}, t_{n+\frac{3}{2}}) - J_y(x_i, y_{j+\frac{1}{2}}, t_{n+\frac{1}{2}})) \\
&\quad + \frac{\Gamma_e|T_{i-\frac{1}{2},j}|}{2\epsilon_0\omega_{pe}^2}(J_y(x_i, y_{j+\frac{1}{2}}, t_{n+\frac{3}{2}}) + J_y(x_i, y_{j+\frac{1}{2}}, t_{n+\frac{1}{2}})) \\
&\quad - |T_{i-\frac{1}{2},j}|E_y(x_i, y_{j+\frac{1}{2}}, t_{n+1}). \qquad (2.74)
\end{aligned}
$$

Integrating the y-component of (2.3) on $T_{i-\frac{1}{2},j}$, then integrating the resultant from $t = t_{n+\frac{1}{2}}$ to $t_{n+\frac{3}{2}}$ and dividing the resultant by τ, we have

$$\begin{aligned}
&\frac{1}{\tau\epsilon_0\omega_{pe}^2}\iint_{T_{i-\frac{1}{2},j}}(J_y(x,y,t_{n+\frac{3}{2}})-J_y(x,y,t_{n+\frac{1}{2}}))dxdy\\
&\quad+\frac{\Gamma_e}{\tau\epsilon_0\omega_{pe}^2}\int_{t_{n+\frac{1}{2}}}^{t_{n+\frac{3}{2}}}\iint_{T_{i-\frac{1}{2},j}}J_y(x,y,t)dxdydt\\
&=\frac{1}{\tau}\int_{t_{n+\frac{1}{2}}}^{t_{n+\frac{3}{2}}}\iint_{T_{i-\frac{1}{2},j}}E_y(x,y,t)dxdydt. \qquad (2.75)
\end{aligned}$$

Subtracting (2.75) from (2.74), we can rewrite R_5 as follows:

$$\begin{aligned}
R_5 &= \frac{1}{\tau\epsilon_0\omega_{pe}^2}\iint_{T_{i-\frac{1}{2},j}}\{(J_y(x_i,y_{j+\frac{1}{2}},t_{n+\frac{3}{2}})-J_y(x,y,t_{n+\frac{3}{2}}))\\
&\quad-(J_y(x_i,y_{j+\frac{1}{2}},t_{n+\frac{1}{2}})-J_y(x,y,t_{n+\frac{1}{2}}))\}dxdy\\
&\quad+\frac{\Gamma_e}{\epsilon_0\omega_{pe}^2}\{\iint_{T_{i-\frac{1}{2},j}}\frac{1}{2}(J_y(x_i,y_{j+\frac{1}{2}},t_{n+\frac{3}{2}})+J_y(x_i,y_{j+\frac{1}{2}},t_{n+\frac{1}{2}}))dxdy\\
&\quad-\frac{1}{\tau}\int_{t_{n+\frac{1}{2}}}^{t_{n+\frac{3}{2}}}\iint_{T_{i-\frac{1}{2},j}}J_y(x,y,t)dxdydt\}\\
&\quad-\{\iint_{T_{i-\frac{1}{2},j}}E_y(x_i,y_{j+\frac{1}{2}},t_{n+1})dxdy-\frac{1}{\tau}\int_{t_{n+\frac{1}{2}}}^{t_{n+\frac{3}{2}}}\iint_{T_{i-\frac{1}{2},j}}E_y(x,y,t)dxdydt\}\\
&= R_{51}+R_{52}+R_{53}. \qquad (2.76)
\end{aligned}$$

By the Taylor expansion, we can obtain

$$\begin{aligned}
R_{51} &= (O(h_x^2)|\frac{\partial^3 J_y}{\partial t\partial x^2}|_\infty+O(h_y^2)|\frac{\partial^3 J_y}{\partial t\partial y^2}|_\infty)|T_{i-\frac{1}{2},j}|,\\
R_{52} &= (O(h_x^2)|\frac{\partial^2 J_y}{\partial x^2}|_\infty+O(h_y^2)|\frac{\partial^2 J_y}{\partial y^2}|_\infty+O(\tau^2)|\frac{\partial^2 J_y}{\partial t^2}|_\infty)|T_{i-\frac{1}{2},j}|,\\
R_{53} &= (O(h_x^2)|\frac{\partial^2 E_y}{\partial x^2}|_\infty+O(h_y^2)|\frac{\partial^2 E_y}{\partial y^2}|_\infty+O(\tau^2)|\frac{\partial^2 E_y}{\partial t^2}|_\infty)|T_{i-\frac{1}{2},j}|.
\end{aligned}$$

The error equation for K

Similarly, we can obtain the error equation for K from (2.40):

$$\frac{|T_{i,j}|}{\tau\mu_0\omega_{pm}^2}(\mathcal{K}_{i+\frac{1}{2},j+\frac{1}{2}}^{n+2}-\mathcal{K}_{i+\frac{1}{2},j+\frac{1}{2}}^{n+1})+\frac{\Gamma_m|T_{i,j}|}{2\mu_0\omega_{pm}^2}(\mathcal{K}_{i+\frac{1}{2},j+\frac{1}{2}}^{n+2}+\mathcal{K}_{i+\frac{1}{2},j+\frac{1}{2}}^{n+1})$$

$$= |T_{i,j}|\mathcal{H}^{n+\frac{3}{2}}_{i+\frac{1}{2},j+\frac{1}{2}} + R_6, \tag{2.77}$$

where the local truncation error R_6 is given by

$$\begin{aligned} R_6 &= \frac{|T_{i,j}|}{\tau\mu_0\omega^2_{pm}}(K(x_{i+\frac{1}{2}}, y_{j+\frac{1}{2}}, t_{n+2}) - K(x_{i+\frac{1}{2}}, y_{j+\frac{1}{2}}, t_{n+1})) \\ &\quad + \frac{\Gamma_m|T_{i,j}|}{2\mu_0\omega^2_{pm}}(K(x_{i+\frac{1}{2}}, y_{j+\frac{1}{2}}, t_{n+2}) + K(x_{i+\frac{1}{2}}, y_{j+\frac{1}{2}}, t_{n+1})) \\ &\quad - |T_{i,j}|H(x_{i+\frac{1}{2}}, y_{j+\frac{1}{2}}, t_{n+\frac{3}{2}}). \end{aligned} \tag{2.78}$$

Integrating (2.4) on $T_{i,j}$, then integrating the resultant from $t = t_{n+1}$ to t_{n+2} and dividing the resultant by τ, we have

$$\begin{aligned} &\frac{1}{\tau\mu_0\omega^2_{pm}}\iint_{T_{i,j}}(K(x,y,t_{n+2}) - K(x,y,t_{n+1}))dxdy \\ &\quad + \frac{\Gamma_m}{\tau\mu_0\omega^2_{pm}}\int_{t_{n+1}}^{t_{n+2}}\iint_{T_{i,j}} K(x,y,t)dxdydt \\ &= \frac{1}{\tau}\int_{t_{n+1}}^{t_{n+2}}\iint_{T_{i,j}} H(x,y,t)dxdydt. \end{aligned} \tag{2.79}$$

Subtracting (2.79) from (2.78), we can rewrite R_6 as follows:

$$\begin{aligned} R_6 &= \frac{1}{\tau\mu_0\omega^2_{pm}}\iint_{T_{i,j}}\{(K(x_{i+\frac{1}{2}}, y_{j+\frac{1}{2}}, t_{n+2}) - K(x,y,t_{n+2})) \\ &\qquad -(K(x_{i+\frac{1}{2}}, y_{j+\frac{1}{2}}, t_{n+1}) - K(x,y,t_{n+1}))\}dxdy \\ &\quad + \frac{\Gamma_m}{\mu_0\omega^2_{pm}}\{\iint_{T_{i,j}}\frac{1}{2}(K(x_{i+\frac{1}{2}}, y_{j+\frac{1}{2}}, t_{n+2}) + K(x_{i+\frac{1}{2}}, y_{j+\frac{1}{2}}, t_{n+1}))dxdy \\ &\quad - \frac{1}{\tau}\int_{t_{n+1}}^{t_{n+2}}\iint_{T_{i,j}} K(x,y,t)dxdydt\} \\ &\quad - \{\iint_{T_{i,j}} H(x_{i+\frac{1}{2}}, y_{j+\frac{1}{2}}, t_{n+\frac{3}{2}})dxdy - \frac{1}{\tau}\int_{t_{n+1}}^{t_{n+2}}\iint_{T_{i,j}} H(x,y,t)dxdydt\} \\ &= R_{61} + R_{62} + R_{63}. \end{aligned} \tag{2.80}$$

By the Taylor expansion, we can obtain

$$R_{61} = (O(h_x^2)|\frac{\partial^3 K}{\partial t \partial x^2}|_\infty + O(h_y^2)|\frac{\partial^3 K}{\partial t \partial y^2}|_\infty)|T_{i,j}|,$$
$$R_{62} = (O(h_x^2)|\frac{\partial^2 K}{\partial x^2}|_\infty + O(h_y^2)|\frac{\partial^2 K}{\partial y^2}|_\infty + O(\tau^2)|\frac{\partial^2 K}{\partial t^2}|_\infty)|T_{i,j}|,$$
$$R_{63} = (O(h_x^2)|\frac{\partial^2 H}{\partial x^2}|_\infty + O(h_y^2)|\frac{\partial^2 H}{\partial y^2}|_\infty + O(\tau^2)|\frac{\partial^2 H}{\partial t^2}|_\infty)|T_{i,j}|.$$

The final error estimate

With the above preparations, we can now prove the major error estimate result.

Theorem 2.32. Suppose that the solution of (2.1)-(2.6) possesses the following regularity property:

$$E_x, E_y, H \in C([0,T]; C^3(\overline{\Omega})) \cap C^1([0,T]; C^2(\overline{\Omega})) \cap C^2([0,T]; C^1(\overline{\Omega})),$$
$$J_x, J_y, K \in C([0,T]; C^2(\overline{\Omega})) \cap C^1([0,T]; C^2(\overline{\Omega})) \cap C^2([0,T]; C(\overline{\Omega})).$$

If the initial error

$$||\mathcal{E}_x^0||_E + ||\mathcal{E}_y^0||_E + ||\mathcal{H}^{\frac{1}{2}}||_H + ||\mathcal{J}_x^{\frac{1}{2}}||_J + ||\mathcal{J}_y^{\frac{1}{2}}||_J + ||\mathcal{K}^1||_K \leq C(h_x^2 + h_y^2 + \tau^2), \quad (2.81)$$

holds true, then for any $1 \leq n \leq N_t$ we have

$$\begin{aligned} &\epsilon_0(||\mathcal{E}_x^{n+1}||_E^2 + ||\mathcal{E}_y^{n+1}||_E^2) + \mu_0||\mathcal{H}^{n+\frac{3}{2}}||_H^2 + \frac{1}{\epsilon_0\omega_{pe}^2}(||\mathcal{J}_x^{n+\frac{3}{2}}||_J^2 + ||\mathcal{J}_y^{n+\frac{3}{2}}||_J^2) \\ &\qquad + \frac{1}{\mu_0\omega_{pm}^2}||\mathcal{K}^{n+2}||_K^2 \\ \leq\ & C(h_x^2 + h_y^2 + \tau^2)^2, \end{aligned} \quad (2.82)$$

where the constant $C > 0$ is independent of τ, h_x and h_y.

Proof. Note that the error equations (2.56), (2.61), (2.65), (2.69), (2.73) and (2.77) have exactly the same form as (2.35)-(2.40) with extra right hand side terms

representing the errors introduced by time discretization and space discretization. Hence we can follow exactly the same technique developed in the proof of Theorem 2.31 to obtain (cf. (2.50)):

$$
\begin{aligned}
&\epsilon_0(||\mathcal{E}_x^{N_t+1}||_E^2 - ||\mathcal{E}_x^0||_E^2) + \epsilon_0(||\mathcal{E}_y^{N_t+1}||_E^2 - ||\mathcal{E}_y^0||_E^2) + \mu_0(||\mathcal{H}^{N_t+\frac{3}{2}}||_H^2 - ||\mathcal{H}^{\frac{1}{2}}||_H^2) \\
&\quad + \frac{1}{\epsilon_0\omega_{pe}^2}(||\mathcal{J}_x^{N_t+\frac{3}{2}}||_J^2 - ||\mathcal{J}_x^{\frac{1}{2}}||_J^2) + \frac{1}{\epsilon_0\omega_{pe}^2}(||\mathcal{J}_y^{N_t+\frac{3}{2}}||_J^2 - ||\mathcal{J}_y^{\frac{1}{2}}||_J^2) \\
&\quad + \frac{1}{\mu_0\omega_{pm}^2}(||\mathcal{K}^{N_t+2}||_K^2 - ||\mathcal{K}^1||_K^2) \\
\leq\ & \tau \sum_{\substack{0\le i\le N_x-1\\ 0\le j\le N_y-1}} |T_{ij}|(\mathcal{H}_{i+\frac{1}{2},j+\frac{1}{2}}^{N_t+\frac{3}{2}} \nabla_y \mathcal{E}_{x,i+\frac{1}{2},j+1}^{N_t+1} - \mathcal{H}_{i+\frac{1}{2},j+\frac{1}{2}}^{\frac{1}{2}} \nabla_y \mathcal{E}_{x,i+\frac{1}{2},j+1}^{0}) \\
&\quad + \tau \sum_{\substack{0\le i\le N_x-1\\ 0\le j\le N_y-1}} |T_{ij}|(-\mathcal{H}_{i+\frac{1}{2},j+\frac{1}{2}}^{N_t+\frac{3}{2}} \nabla_x \mathcal{E}_{y,i+1,j+\frac{1}{2}}^{N_t+1} + \mathcal{H}_{i+\frac{1}{2},j+\frac{1}{2}}^{\frac{1}{2}} \nabla_x \mathcal{E}_{y,i+1,j+\frac{1}{2}}^{0}) \\
&\quad + \tau \sum_{\substack{0\le i\le N_x-1\\ 0\le j\le N_y-1}} |T_{i,j-\frac{1}{2}}|(\mathcal{J}_{x,i+\frac{1}{2},j}^{N_t+\frac{3}{2}} \mathcal{E}_{x,i+\frac{1}{2},j}^{N_t+1} - \mathcal{J}_{x,i+\frac{1}{2},j}^{\frac{1}{2}} \mathcal{E}_{x,i+\frac{1}{2},j}^{0}) \\
&\quad + \tau \sum_{\substack{0\le i\le N_x-1\\ 0\le j\le N_y-1}} |T_{i-\frac{1}{2},j}|(\mathcal{J}_{y,i,j+\frac{1}{2}}^{N_t+\frac{3}{2}} \mathcal{E}_{y,i,j+\frac{1}{2}}^{N_t+1} - \mathcal{J}_{y,i,j+\frac{1}{2}}^{\frac{1}{2}} \mathcal{E}_{y,i,j+\frac{1}{2}}^{0}) \\
&\quad + \tau \sum_{\substack{0\le i\le N_x-1\\ 0\le j\le N_y-1}} |T_{ij}|(\mathcal{H}_{i+\frac{1}{2},j+\frac{1}{2}}^{N_t+\frac{3}{2}} \mathcal{K}_{i+\frac{1}{2},j+\frac{1}{2}}^{N_t+2} - \mathcal{H}_{i+\frac{1}{2},j+\frac{1}{2}}^{\frac{1}{2}} \mathcal{K}_{i+\frac{1}{2},j+\frac{1}{2}}^{1}) \\
&\quad + \tau \sum_{n=0}^{N_t} \sum_{\substack{0\le i\le N_x-1\\ 0\le j\le N_y-1}} R_1(\mathcal{E}_{x,i+\frac{1}{2},j}^{n+1} + \mathcal{E}_{x,i+\frac{1}{2},j}^{n}) + \tau \sum_{n=0}^{N_t} \sum_{\substack{0\le i\le N_x-1\\ 0\le j\le N_y-1}} R_2(\mathcal{E}_{y,i,j+\frac{1}{2}}^{n+1} + \mathcal{E}_{y,i,j+\frac{1}{2}}^{n}) \\
&\quad + \tau \sum_{n=0}^{N_t} \sum_{\substack{0\le i\le N_x-1\\ 0\le j\le N_y-1}} R_3(\mathcal{H}_{i+\frac{1}{2},j+\frac{1}{2}}^{n+\frac{3}{2}} + \mathcal{H}_{i+\frac{1}{2},j+\frac{1}{2}}^{n+\frac{1}{2}}) \\
&\quad + \tau \sum_{n=0}^{N_t} \sum_{\substack{0\le i\le N_x-1\\ 0\le j\le N_y-1}} R_4(\mathcal{J}_{x,i+\frac{1}{2},j}^{n+\frac{3}{2}} + \mathcal{J}_{x,i+\frac{1}{2},j}^{n+\frac{1}{2}}) \\
&\quad + \tau \sum_{n=0}^{N_t} \sum_{\substack{0\le i\le N_x-1\\ 0\le j\le N_y-1}} R_5(\mathcal{J}_{y,i,j+\frac{1}{2}}^{n+\frac{3}{2}} + \mathcal{J}_{y,i,j+\frac{1}{2}}^{n+\frac{1}{2}}) \\
&\quad + \tau \sum_{n=0}^{N_t} \sum_{\substack{0\le i\le N_x-1\\ 0\le j\le N_y-1}} R_6(\mathcal{K}_{i+\frac{1}{2},j+\frac{1}{2}}^{n+2} + \mathcal{K}_{i+\frac{1}{2},j+\frac{1}{2}}^{n+1}).
\end{aligned}
\tag{2.83}
$$

All terms except those containing R_i on the RHS of (2.83) can be bounded as in the proof of Theorem 2.3.1. The R_i terms can be easily bounded by the Cauchy-Schwarz inequality. For example, we have

$$\begin{aligned}
&\tau \sum_{n=0}^{N_t} \sum_{\substack{0\le i\le N_x-1\\ 0\le j\le N_y-1}} R_1(\mathcal{E}^{n+1}_{x,i+\frac{1}{2},j} + \mathcal{E}^{n}_{x,i+\frac{1}{2},j}) \\
\le\ & \tau \sum_{n=0}^{N_t} \sum_{\substack{0\le i\le N_x-1\\ 0\le j\le N_y-1}} |T_{i,j-\frac{1}{2}}| C(h_x^2+h_y^2+\tau^2)(|\mathcal{E}^{n+1}_{x,i+\frac{1}{2},j} + \mathcal{E}^{n}_{x,i+\frac{1}{2},j}|) \\
\le\ & \tau \sum_{n=0}^{N_t} \sum_{\substack{0\le i\le N_x-1\\ 0\le j\le N_y-1}} |T_{i,j-\frac{1}{2}}| \left[\frac{C}{\delta}(h_x^2+h_y^2+\tau^2)^2 + \frac{\delta}{2}(|\mathcal{E}^{n+1}_{x,i+\frac{1}{2},j}|^2 + |\mathcal{E}^{n}_{x,i+\frac{1}{2},j}|^2)\right] \\
\le\ & \frac{CT}{\delta}(h_x^2+h_y^2+\tau^2)^2 + \tau \sum_{n=0}^{N_t} \frac{\delta}{2}(||\mathcal{E}^{n+1}_{x,i+\frac{1}{2},j}||_E^2 + ||\mathcal{E}^{n}_{x,i+\frac{1}{2},j}||_E^2),
\end{aligned}$$

where we used the inequality $ab \le \frac{1}{\delta}a^2 + \frac{\delta}{4}b^2$, where the constant $\delta > 0$.

Choosing δ small enough so that $||\mathcal{E}^{N_t+1}_{x,i+\frac{1}{2},j}||_E^2$ etc can be bounded by the corresponding terms on the left hand side of (2.83). The proof is completed by using the discrete Gronwall inequality. □

2.4 Numerical results

In this section, we present two numerical examples. The first one is used to justify our theoretical analysis with an exact solution. The second one is a classic example showing the backward wave propagation phenomenon in metamaterial.

Example 1. In this example, we solve the 2D version of our model (2.1)-(2.4). More specifically, the governing equations are (with added source terms g_x, g_y, and

f):

$$\epsilon_0 \frac{\partial E_x}{\partial t} = \frac{\partial H_z}{\partial y} - J_x + g_x, \tag{2.84}$$

$$\epsilon_0 \frac{\partial E_y}{\partial t} = -\frac{\partial H_z}{\partial x} - J_y + g_y, \tag{2.85}$$

$$\mu_0 \frac{\partial H_z}{\partial t} = -\frac{\partial E_y}{\partial x} + \frac{\partial E_x}{\partial y} - K_z + f, \tag{2.86}$$

$$\frac{1}{\epsilon_0 \omega_{pe}^2} \frac{\partial J_x}{\partial t} + \frac{\Gamma_e}{\epsilon_0 \omega_{pe}^2} J_x = E_x, \tag{2.87}$$

$$\frac{1}{\epsilon_0 \omega_{pe}^2} \frac{\partial J_y}{\partial t} + \frac{\Gamma_e}{\epsilon_0 \omega_{pe}^2} J_y = E_y, \tag{2.88}$$

$$\frac{1}{\mu_0 \omega_{pm}^2} \frac{\partial K_z}{\partial t} + \frac{\Gamma_m}{\mu_0 \omega_{pm}^2} K_z = H_z. \tag{2.89}$$

To rigorously check the convergence rate, we choose the physical domain $\Omega = [0,1]^2$, and coefficients as follows:

$$\epsilon_0 = \mu_0 = 1, \quad \Gamma_m = \Gamma_e = \pi, \quad \omega_{pm} = \omega_{pe} = \pi$$

such that (2.84)–(2.89) has the exact solution:

$$\mathbf{E} \equiv \begin{pmatrix} E_x \\ E_y \end{pmatrix} = \begin{pmatrix} \cos(\pi x)\sin(\pi y)e^{-\pi t} \\ -\sin(\pi x)\cos(\pi y)e^{-\pi t} \end{pmatrix},$$

$$H_z = \cos(\pi x)\cos(\pi y)e^{-\pi t},$$

$$\mathbf{J} \equiv \begin{pmatrix} J_x \\ J_y \end{pmatrix} = \begin{pmatrix} \pi^2 t\cos(\pi x)\sin(\pi y)e^{-\pi t} \\ -\pi^2 t\sin(\pi x)\cos(\pi y)e^{-\pi t} \end{pmatrix},$$

$$K_z = \pi^2 t\cos(\pi x)\cos(\pi y)e^{-\pi t}.$$

The corresponding source terms are

$$g_x = \pi^2 t\cos(\pi x)\sin(\pi y)e^{-\pi t},$$

$$g_y = -\pi^2 t\sin(\pi x)\cos(\pi y)e^{-\pi t},$$

$$f = (-3\pi + \pi^2 t)\cos(\pi x)\cos(\pi y)e^{-\pi t}.$$

We build the 1D non-uniform mesh in the X-direction as $[0 : dx : 0.5 - dx, 0.5 : dx2 : 1]$, where $dx2 = dx/2$, and the 1D non-uniform mesh in the y-direction as $[0 : dy : 0.5 - dy, 0.5 : dy2 : 1]$, where $dy2 = dy/2$. The 2D non-uniform mesh is obtained by extending both 1D meshes to cover the whole domain Ω (see Fig. 2.2).

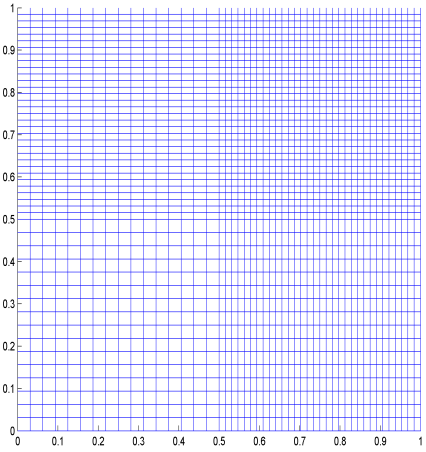

Figure 2.2. A non-uniform mesh with $dx = dy = 1/32$.

We solve the 2D problem (2.84)-(2.89) by our scheme (2.35)-(2.40) on a series of non-uniform meshes with $dx = dy = h$ varying from 1/4 to 1/128, with a fixed time step $\tau = 10^{-5}$, and ran for a total of 1000 time steps. The obtained errors for the main fields E_x, E_y and H_z at the 1000th time step in discrete energy norms are presented in Table 2.1, which shows clearly that they all converge in $O(h^2)$. This confirms our theoretical superconvergence rates $O(h_x^2 + h_y^2)$.

Example 2. In this example, we solve a classic example of wave propagation in metamaterial originally introduced by Ziolkowski Ziolkowski (2003) and lately solved by Huang, Li, and Yang with edge elements Huang et al. (2013). This example

Mesh	$\|\|H_z - H_{z,h}\|\|_H$	Rate	$\|\|E_x - E_{x,h}\|\|_{Ex}$	Rate	$\|\|E_y - E_{y,h}\|\|_{Ey}$	Rate
$h = 1/4$	5.283211E-04	—	2.824375E-04	—	2.824375E-04	—
$h = 1/8$	1.326984E-04	1.9933	7.266416E-05	1.9586	7.266416E-05	1.9586
$h = 1/16$	3.321344E-05	1.9983	1.839161E-05	1.9822	1.839161E-05	1.9822
$h = 1/32$	8.306978E-06	1.9994	4.622600E-06	1.9923	4.622600E-06	1.9923
$h = 1/64$	2.077415E-06	1.9995	1.158079E-06	1.9970	1.158079E-06	1.9970
$h = 1/128$	5.194356E-07	1.9998	2.897430E-07	1.9989	2.897430E-07	1.9989

Table 2.1. The errors of E_x, E_y, H_z obtained with $\tau = 10^{-5}$ on non-uniform meshes.

assumes that a metamaterial slab of size $[0.024, 0.054]m \times [0.002, 0.062]m$ is located inside a vacuum of size $[0, 0.07]m \times [0, 0.064]m$. An incident source wave is imposed as H_z field and is excited at $x = 0.004m$ and $y \in [0.025, 0.035]m$. The source wave varies in space as $e^{-(x-0.03)^2/(50h)^2}$ and in time as:

$$f(t) = \begin{cases} 0, & for \;\; t < 0, \\ g_1(t)\sin(\omega_0 t), & for \;\; 0 < t < mT_p, \\ \sin(\omega_0 t), & for \;\; mT_p < t < (m+k)T_p, \\ g_2(t)\sin(\omega_0 t), & for \;\; (m+k)T_p < t < (2m+k)T_p, \\ 0, & for \;\; t > (2m+k)T_p, \end{cases}$$

where the functions g_1 and g_2 are

$$g_1(t) = 10x_1^3 - 15x_1^4 + 6x_1^5, \quad x_1 = t/mT_p,$$

$$g_2(t) = 1 - (10x_2^3 - 15x_2^4 + 6x_2^5), \quad x_2 = (t - (m+k)T_p)/mT_p.$$

Here we denote $T_p = 1/f_0$ and $\omega_0 = 2\pi f_0$. In our simulation, we use $m = 2, k = 100, f_0 = 30$GHz.

We solved this model with our scheme (2.35)-(2.40) on a non-uniform mesh uniformly refined from a coarse mesh demonstrated in Fig. 2.3 (Top left). Here, we used time step size $\tau = 10^{-13}s = 0.1$ps (peco second), and 12 perfectly matched layers (PML) around the physical domain (cf. Huang et al. (2013)). The obtained H_z fields

at various time steps are presented in Fig. 2.3, which matches with what we obtained in Huang et al. (2013). The simulation shows that as wave enters into the metamaterial slab, the wave propagates backward due to the negative refractive index of the metamaterial.

2.5 Conclusions

In this chapter, we first develop the Yee scheme for solving the Maxwell's equations in metamaterials on nonuniform rectangular grids from the variational point of view. Then we show that the scheme achieves a second order superconvergence rate in space for both semi- and fully-discrete schemes. A numerical example supporting the theoretical analysis is presented first, then a popular backward wave propagation in metamaterial is simulated by Yee scheme on nonuniform rectangular grids. Similar techniques can be extended to more complicated metamaterial Maxwell's equations Li and Huang (2013), and detailed results will be presented in our future work.

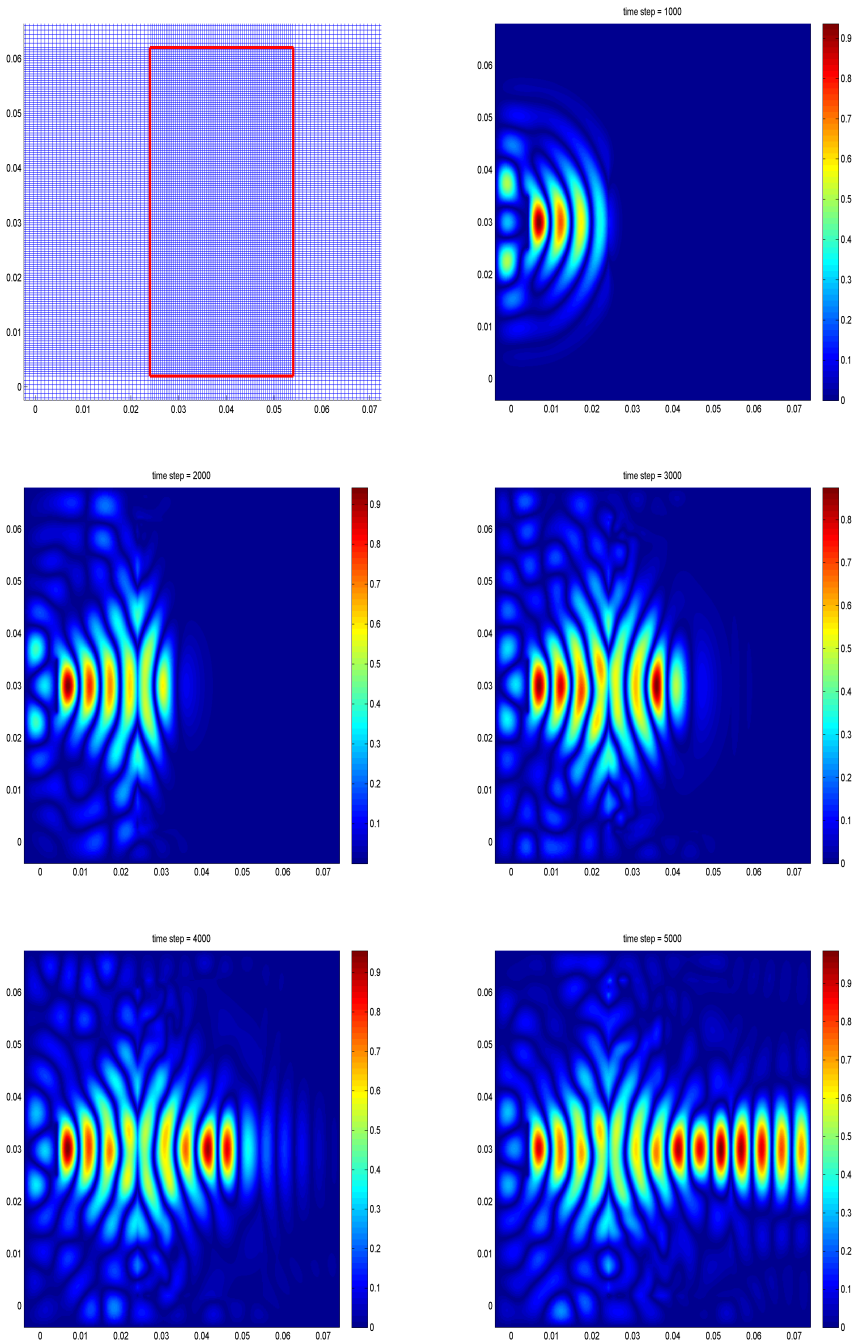

Figure 2.3. Example 2. A coarse mesh (the red rectangle shows the metamaterial slab), and contour plots of $|H_z|$ obtained with $\tau = 0.1ps$ at 1000, 2000, 3000, 4000, and 5000 time steps.

CHAPTER 3

A NODAL DISCONTINUOUS GALERKIN METHOD FOR THE STUDY OF SIGNAL PROPAGATION IN CORRUGATED COAXIAL CABLES

3.1 Introduction

Mathematical analysis of finite elements for axisymmetric Maxwell equations has been attracting an increasing interest since 2000. Ciarlet *et al.* initiated the study of axisymmetric Maxwell equations Ciarlet et al. (2000); Assous et al. (2002). Later, in 2006, a least-squares method for axisymmetric div-curl systems was analyzed D.M.Copeland and J.E.Pasciak (2006). In that same timeframe, multigrid methods were proposed and analyzed for axisymmetric Maxwell equations S.Borm and R.Hiptmair (2002); D.M.Copeland et al. (2010). Subsequently, finite element methods were developed and analyzed for solving time-dependent axisymmetric eddy current models Bermúdez et al. (2015, 2010).

The goal of this chapter is to explore the effect of corrugated coaxial cables on the electric pulse propagation in more detail than others Böcklin et al. (2009); Blank et al. (2013); Imperiale and Joly (2014). Here we estimate the effects of corrugation by solving Maxwell's equations in cylindrical coordinates to model the wave propagation between the two conductors of the corrugated coaxial cable. In Blank et al. (2013), the nodal discontinuous Galerkin method (e.g., Hesthaven and Warburton (2008); Li and Hesthaven (2014); Li et al. (2012)) was extended to solve the 2-D cylindrical

cooridinate Maxwell equations. However, Blank et al. (2013) does not provide any stability analysis nor error estimate of the method. Here, we first develop a similar method for our corrugated cable model, then we present a stability analysis and error estimate for the semi-discrete scheme. Finally, we use our algorithm to solve various corrugations and compare with the results obtained by the finite difference time domain (FDTD) method.

The rest of the chapter is organized as follows. In Section 2, we present the axisymmetric Maxwell equations and show that the energy of the system is conserved. In Section 3, we introduce the nodal discontinuous Galerkin (nDG) method in both semi- and fully-discrete forms. Stability and convergence of the semi-discrete scheme is established rigorously. In Section 4, we present extensive numerical results verifying the theoretical analysis and applying the method to the wave propagation problem in various corrugated coaxial cables. Conclusions are in Section 5. The research presented in this chapter was previously published as Li et al. (2017) where Jichun Li, Eric Machorro, and I were all equally contributing authors.

3.2 The governing equations

Replacing the curl operator in cartesian coordinates by that in cylindrical coordinates (r, θ, z), we can easily obtain the Maxwell's equations in cylindrical coordinates (cf. Blank et al. (2013)):

$$\frac{\partial E^r}{\partial t} - \frac{1}{r}\frac{\partial B^z}{\partial \theta} + \frac{\partial B^\theta}{\partial z} = 0 \tag{3.1}$$

$$\frac{\partial E^\theta}{\partial t} + \frac{\partial B^z}{\partial r} - \frac{\partial B^r}{\partial z} = 0 \tag{3.2}$$

$$\frac{\partial E^z}{\partial t} - \frac{1}{r}\left(\frac{\partial}{\partial r}\left(rB^\theta\right) - \frac{\partial B^r}{\partial \theta}\right) = 0 \tag{3.3}$$

$$\frac{\partial B^r}{\partial t} + \frac{1}{r}\frac{\partial E^z}{\partial \theta} - \frac{\partial E^\theta}{\partial z} = 0 \tag{3.4}$$

$$\frac{\partial B^\theta}{\partial t} - \frac{\partial E^z}{\partial r} + \frac{\partial E^r}{\partial z} = 0 \tag{3.5}$$

$$\frac{\partial B^z}{\partial t} + \frac{1}{r}\left(\frac{\partial}{\partial r}\left(rE^\theta\right) - \frac{\partial E^r}{\partial \theta}\right) = 0, \tag{3.6}$$

where (E^r, E^θ, E^z) and (B^r, B^θ, B^z) denote the electric and magnetic fields, respectively. For simplicity, we assume that the permittivity and permability both equal 1.

Below we only consider the 2-D cylindrical coordinate Maxwell's equations, which have three non-zero variables (E^r, E^z, B^θ), i.e., the non-zero varaibles are:

$$E^\theta = B^r = B^z = 0. \tag{3.7}$$

Furthermore, we assume that variables (E^r, E^z, B^θ) are independent of the azimuth angle θ, i.e.,

$$\frac{\partial E^r}{\partial \theta} = \frac{\partial E^z}{\partial \theta} = \frac{\partial B^\theta}{\partial \theta} = 0. \tag{3.8}$$

Finally, plugging (3.7) and (3.8) into equations (3.1)-(3.6) gives the following 2-D cylindrical coordinate formulation of Maxwell's equations for the problem of interest:

$$\frac{\partial E^r}{\partial t} = -\frac{\partial B^\theta}{\partial z} \tag{3.9}$$

$$\frac{\partial E^z}{\partial t} = \frac{1}{r}B^\theta + \frac{\partial B^\theta}{\partial r} \tag{3.10}$$

$$\frac{\partial B^\theta}{\partial t} = \frac{\partial E^z}{\partial r} - \frac{\partial E^r}{\partial z}. \tag{3.11}$$

For simplicity, we assume that the model equations (3.9)-(3.11) satisfy the perfect

conducting (PEC) boundary condition

$$\hat{\boldsymbol{\tau}} \cdot \boldsymbol{E} = 0 \quad \text{on } \partial\Omega, \tag{3.12}$$

for $\boldsymbol{E} = (E^z, E^r)$. Here and below $\hat{\boldsymbol{\tau}} = (n_r, -n_z)'$ and $\hat{\boldsymbol{n}} = (n_z, n_r)'$ denote the unit tangential and normal vectors on the physical boundary $\partial\Omega$, respectively.

First, we would like to show that the model equations (3.9)-(3.11) conserve energy.

Lemma 3.21. The energy

$$\mathcal{E} := \int_\Omega (|E^r|^2 + |E^z|^2 + |B^\theta|^2)\, r dr dz, \tag{3.13}$$

is conserved for the solution (E^z, E^r, B^θ) of (3.9)-(3.11) with the PEC boundary condition (3.12).

Proof. Multiplying (3.9)-(3.11) by E^r, E^z, B^θ, respectively, integrating over domain Ω under cylindrical coordinate system, and then adding the results together, we obtain

$$\begin{aligned}
&\frac{1}{2}\frac{d}{dt}\left[\int_\Omega (|E^r|^2 + |E^z|^2 + |B^\theta|^2)\, r dr dz\right] \\
&\qquad = -\int_\Omega E^r \frac{\partial B^\theta}{\partial z} r dr dz + \int_\Omega (E^z B^\theta + r E^z \frac{\partial B^\theta}{\partial r}) dr dz \\
&\qquad\qquad + \int_\Omega (B^\theta \frac{\partial E^z}{\partial r} - B^\theta \frac{\partial E^r}{\partial z}) r dr dz \\
&\qquad = -\int_\Omega \frac{\partial (E^r B^\theta)}{\partial z} r dr dz + \int_\Omega \frac{\partial (E^z B^\theta)}{\partial r} r dr dz + \int_\Omega E^z B^\theta dr dz \\
&\qquad = \int_{\partial\Omega} (-n_z E^r + n_r E^z) B^\theta r d\boldsymbol{r} - \int_\Omega E^z B^\theta dr dz + \int_\Omega E^z B^\theta dr dz \\
&\qquad = 0,
\end{aligned}$$

where we used integration by parts in the second last step, and the PEC boundary condition (3.12) in the last step. □

3.3 The DG method

To apply a nodal discontinuous Galerkin method discretization Hesthaven and Warburton (2008), it can be helpful to informally write equations (3.9)-(3.11) in conservation form Blank et al. (2013):

$$\partial_t \boldsymbol{u} + \nabla \cdot \boldsymbol{F}(\boldsymbol{u}) = \frac{1}{r}\boldsymbol{C}\boldsymbol{u}, \tag{3.14}$$

where $\boldsymbol{u} = \begin{bmatrix} E^z \\ E^r \\ B^\theta \end{bmatrix}$, $\nabla = \begin{bmatrix} \frac{\partial}{\partial z} \\ \frac{\partial}{\partial r} \end{bmatrix}$, $\boldsymbol{F}(\boldsymbol{u}) = \begin{bmatrix} 0 & -B^\theta \\ B^\theta & 0 \\ E^r & -E^z \end{bmatrix}$, and $\boldsymbol{C} = \begin{bmatrix} 0 & 0 & 1 \\ 0 & 0 & 0 \\ 0 & 0 & 0 \end{bmatrix}$.

Like other finite element methods Li and Huang (2013), the computational domain, Ω, is triangulated by a collection of K elements $\mathbf{D}^k$ that only overlap on their boundaries, $\partial\mathbf{D}^k$, such that $\Omega = \bigcup_{k=1}^{K} \mathbf{D}^k$. Since the boundaries of the elements overlap, there are no longer unique solutions at the boundary of every element. The solution chosen at the boundaries of each element is derived by the numerical flux, $\boldsymbol{F}^*$, whose calculation is shown later. The finite element space is then given by:

$$V_h := \{\boldsymbol{u}_h^k \in L^\infty(\Omega) : \boldsymbol{u}_h^k|_{\mathbf{D}^k} \in P^N(\mathbf{D}^k), k = 1, ..., K\}, \tag{3.15}$$

where $P^N(\mathbf{D}^k)$ are locally defined 3-tuple polynomials of order N with two independent variables.

The local approximation to $\boldsymbol{u}$, $\boldsymbol{u}_h^k(\boldsymbol{r}, t) = (E_h^z, E_h^r, B_h^\theta)^T \in (V_h)^3$ can then be expressed using Lagrange interpolation:

$$\boldsymbol{r} \in \mathbf{D}^k : \boldsymbol{u}_h^k(\boldsymbol{r}, t) = \sum_{i=1}^{N_p} \boldsymbol{u}_h^k(\boldsymbol{r}_i, t)\ell_i^k(\boldsymbol{r}) \tag{3.16}$$

where $\ell_i^k(\boldsymbol{r})$ is the 2-D Lagrange polynomial defined at grid point $\boldsymbol{r}_i = (z_i, r_i)$ on the element $\mathbf{D}^k$, and $N_p = \frac{(N+1)(N+2)}{2}$ is the number of grid points.

The residual $\boldsymbol{R}_h := \partial_t \boldsymbol{u}_h + \nabla \cdot \boldsymbol{F}(\boldsymbol{u}_h) - \frac{1}{r}\boldsymbol{C}\boldsymbol{u}_h$ is then required to be orthogonal to all test functions $\varphi_h \in V_h$, which results in the following requirement Blank et al. (2013):

$$\int_{\mathbf{D}^k} \boldsymbol{R}_h \cdot \varphi_h r d\boldsymbol{r} = -\int_{\partial \mathbf{D}^k} (\boldsymbol{F}(\boldsymbol{u}_h^k) - \boldsymbol{F}^*(\boldsymbol{u}_h))\hat{\boldsymbol{n}} \cdot \varphi_h r d\boldsymbol{r}, \tag{3.17}$$

where $\boldsymbol{F}^*$ is the numerical flux that is introduced to assist coupling between neighboring elements, and the test functions have been chosen such that $\varphi_h = \ell_i^k$. Note that here the integral is computed in cylindrical coordinates, requiring the integrand to be multiplied by r. Because of this, the implementation of the scheme becomes considerably different from the Cartesian coordinate problem from this point on. One example showing the big difference can be seen in Machorro's work on the discontinuous Galerkin method for solving 1-D spherical neutron transport equation Machorro (2007).

Following the same procedure originally outlined in Hesthaven and Warburton (2008) and extended to cylindrical coordinate in Blank et al. (2013), the general 3-D numerical flux is calculated by taking the Rankine-Huginoit conditions to be

$$(\boldsymbol{F}_E - \boldsymbol{F}_E^*)\hat{\boldsymbol{n}}_3 = -\frac{1}{2}\hat{\boldsymbol{n}}_3 \times ([[\boldsymbol{B}]] - \alpha \hat{\boldsymbol{n}}_3 \times [[\boldsymbol{E}]]), \tag{3.18}$$

$$(\boldsymbol{F}_B - \boldsymbol{F}_B^*)\hat{\boldsymbol{n}}_3 = \frac{1}{2}\hat{\boldsymbol{n}}_3 \times ([[\boldsymbol{E}]] + \alpha \hat{\boldsymbol{n}}_3 \times [[\boldsymbol{B}]]), \tag{3.19}$$

where $\hat{\boldsymbol{n}}_3$ is the 3-D normal unit vector to the current interface between elements. Here, α can be taken to be any value between 0 and 1, with $\alpha = 0$ resulting in a nondissipative central flux and $\alpha = 1$ resulting in the classic upwind flux. The notation $[[\boldsymbol{E}]]$ is defined as the jump across an element face, which is $[[\boldsymbol{E}]] = \boldsymbol{E}^- - \boldsymbol{E}^+$, where $\boldsymbol{E}^-$ and $\boldsymbol{E}^+$ denote the $\boldsymbol{E}$ values from the underlying element and its

neighboring element, respectively.

Converting equations (3.18) and (3.19) into two dimensional cylindrical coordinates, we let $\boldsymbol{E} = (E^z, E^r, 0)'$, $\boldsymbol{B} = (0, 0, B^\theta)'$, and $\hat{\boldsymbol{n}}_3 = (n_z, n_r, 0)'$ in equations (3.18) and (3.19). Note that because $\hat{\boldsymbol{n}}_3$ is a unit vector we now have that $n_z^2 + n_r^2 = 1$. Equation (3.18) then gives us:

$$\begin{aligned}(\boldsymbol{F}_E - \boldsymbol{F}_E^*)\hat{\boldsymbol{n}}_3 &= -\frac{1}{2}\begin{pmatrix} n_r[[B^\theta]] \\ -n_z[[B^\theta]] \\ 0 \end{pmatrix} + \frac{\alpha}{2}\begin{pmatrix} n_r(n_z[[E^r]] - n_r[[E^z]]) \\ -n_z(n_z[[E^r]] - n_r[[E^z]]) \\ 0 \end{pmatrix} \\ &= \frac{1}{2}\begin{pmatrix} -n_r[[B^\theta]] + \alpha n_z(n_r[[E^r]] + n_z[[E^z]]) - \alpha[[E^z]](n_r^2 + n_z^2) \\ n_z[[B^\theta]] + \alpha n_r(n_r[[E^r]] + n_z[[E^z]]) - \alpha[[E^r]](n_r^2 + n_z^2) \\ 0 \end{pmatrix}.\end{aligned} \tag{3.20}$$

Taking the z and r components of this gives us:

$$[(\boldsymbol{F}_E - \boldsymbol{F}_E^*)\hat{\boldsymbol{n}}_3]_z = \frac{1}{2}\left(-n_r[[B^\theta]] + \alpha(n_z[[\hat{\boldsymbol{n}} \cdot \hat{\boldsymbol{E}}]] - [[E^z]])\right), \tag{3.21}$$

$$[(\boldsymbol{F}_E - \boldsymbol{F}_E^*)\hat{\boldsymbol{n}}_3]_r = \frac{1}{2}\left(n_z[[B^\theta]] + \alpha(n_r[[\hat{\boldsymbol{n}} \cdot \hat{\boldsymbol{E}}]] - [[E^r]])\right). \tag{3.22}$$

Equation (3.19) then gives us:

$$(\boldsymbol{F}_B - \boldsymbol{F}_B^*)\hat{\boldsymbol{n}}_3 = \frac{1}{2}\begin{pmatrix} 0 \\ 0 \\ n_z[[E^r]] - n_r[[E^z]] \end{pmatrix} + \frac{\alpha}{2}\begin{pmatrix} 0 \\ 0 \\ -[[B^\theta]](n_z^2 + n_r^2) \end{pmatrix}. \tag{3.23}$$

So taking only the θ component of this flux gives us:

$$[(\boldsymbol{F}_B - \boldsymbol{F}_B^*)\hat{\boldsymbol{n}}_3]_\theta = \frac{1}{2}\left(n_z[[E^r]] - n_r[[E^z]] - \alpha[[B^\theta]]\right). \tag{3.24}$$

Combining these results together gives us the following fluxes used in the implementation of our DG scheme:

$$\begin{aligned}(\boldsymbol{F} - \boldsymbol{F}^*)\hat{\boldsymbol{n}} &= \begin{pmatrix} [(\boldsymbol{F}_E - \boldsymbol{F}_E^*)\hat{\boldsymbol{n}}_3]_z \\ [(\boldsymbol{F}_E - \boldsymbol{F}_E^*)\hat{\boldsymbol{n}}_3]_r \\ [(\boldsymbol{F}_B - \boldsymbol{F}_B^*)\hat{\boldsymbol{n}}_3]_\theta \end{pmatrix} \\ &= \frac{1}{2}\begin{pmatrix} -n_r[[B^\theta]] + \alpha(n_z[[\hat{\boldsymbol{n}} \cdot \hat{\boldsymbol{E}}]] - [[E^z]]) \\ n_z[[B^\theta]] + \alpha(n_r[[\hat{\boldsymbol{n}} \cdot \hat{\boldsymbol{E}}]] - [[E^r]]) \\ n_z[[E^r]] - n_r[[E^z]] - \alpha[[B^\theta]] \end{pmatrix}.\end{aligned} \tag{3.25}$$

Substituting this into (3.17) gives the following semi-discrete scheme: For any test functions $u_h, v_h, w_h \in V_h$, find $(E_h^z, E_h^r, B_h^\theta)$ such that,

$$\begin{aligned}
\int_{D^k} \frac{dE_h^z}{dt} u_h r dr dz &= \int_{D^k} (\frac{1}{r} B_h^\theta + \frac{\partial B_h^\theta}{\partial r}) u_h r dr dz \\
&\quad + \frac{1}{2} \int_{\partial D^k} \left\{ -n_r [[B_h^\theta]] + \alpha (n_z [[\hat{\boldsymbol{n}} \cdot \hat{\boldsymbol{E}}_h]] - [[E_h^z]]) \right\} u_h r d\boldsymbol{r}, \quad (3.26) \\
\int_{D^k} \frac{dE_h^r}{dt} v_h r dr dz &= - \int_{D^k} \frac{\partial B_h^\theta}{\partial z} v_h r dr dz \\
&\quad + \frac{1}{2} \int_{\partial D^k} \left\{ n_z [[B_h^\theta]] + \alpha (n_r [[\hat{\boldsymbol{n}} \cdot \hat{\boldsymbol{E}}_h]] - [[E_h^r]]) \right\} v_h r d\boldsymbol{r}, \quad (3.27) \\
\int_{D^k} \frac{dB_h^\theta}{dt} w_h r dr dz &= \int_{D^k} (\frac{\partial E_h^z}{\partial r} - \frac{\partial E_h^r}{\partial z}) w_h r dr dz \\
&\quad + \frac{1}{2} \int_{\partial D^k} \left\{ n_z [[E_h^r]] - n_r [[E_h^z]] - \alpha [[B_h^\theta]] \right\} w_h r d\boldsymbol{r}. \quad (3.28)
\end{aligned}$$

To discretize in time, we use the low-storage five-stage fourth-order explicit Runge-Kutta method as Hesthaven and Warburton (2008).

First, we would like to show that the numerical scheme (3.26)-(3.28) is stable.

Lemma 3.31. Denote the energy

$$\mathcal{E}_h(t) := \int_\Omega (|E_h^r|^2 + |E_h^z|^2 + |B_h^\theta|^2)\ r dr dz. \quad (3.29)$$

Then the solution $(E_h^r, E_h^z, B_h^\theta))$ of (3.26)-(3.28) satisfy the following stability: For any $t \geq 0$,

$$\mathcal{E}_h(t) \leq \mathcal{E}_h(0).$$

Proof. Choosing $u_h = E_h^z, v_h = E_h^r, w_h = B_h^\theta$ in (3.26)-(3.28), respectively, summing up the results, and integrating by parts, we obtain the LHS (Left Hand Side) and RHS (Right Hand Side) terms:

$$LHS := \frac{d}{dt} \int_{D^k} \frac{1}{2} (|E_h^r|^2 + |E_h^z|^2 + |B_h^\theta|^2)\ r dr dz, \quad (3.30)$$

and

$$
\begin{aligned}
RHS &:= \int_{D^k} \frac{\partial (rB_h^\theta)}{\partial r} E_h^z dr dz - \int_{D^k} \frac{\partial B_h^\theta}{\partial z} E_h^r r dr dz \\
&\quad + \frac{1}{2} \int_{\partial D^k} \left\{ -n_r [[B_h^\theta]] + \alpha (n_z [[\hat{\boldsymbol{n}} \cdot \boldsymbol{E}_h]] - [[E_h^z]]) \right\} E_h^z r d\boldsymbol{r} \\
&\quad + \frac{1}{2} \int_{\partial D^k} \left\{ n_z [[B_h^\theta]] + \alpha (n_r [[\hat{\boldsymbol{n}} \cdot \boldsymbol{E}_h]] - [[E_h^r]]) \right\} E_h^r r d\boldsymbol{r} \\
&\quad + \int_{D^k} (\frac{\partial E_h^z}{\partial r} - \frac{\partial E_h^r}{\partial z}) B_h^\theta r dr dz \\
&\quad + \frac{1}{2} \int_{\partial D^k} \left\{ n_z [[E_h^r]] - n_r [[E_h^z]] - \alpha [[B_h^\theta]] \right\} B_h^\theta r d\boldsymbol{r} \\
&= \int_{\partial D^k} n_r \cdot r B_h^\theta \cdot E_h^z dz - \int_{\partial D^k} n_z \cdot B_h^\theta \cdot E_h^r r dr \\
&\quad + \frac{1}{2} \int_{\partial D^k} \left\{ -n_r [[B_h^\theta]] + \alpha (n_z [[\hat{\boldsymbol{n}} \cdot \boldsymbol{E}_h]] - [[E_h^z]]) \right\} E_h^z r d\boldsymbol{r} \\
&\quad + \frac{1}{2} \int_{\partial D^k} \left\{ n_z [[B_h^\theta]] + \alpha (n_r [[\hat{\boldsymbol{n}} \cdot \boldsymbol{E}_h]] - [[E_h^r]]) \right\} E_h^r r d\boldsymbol{r} \\
&\quad + \frac{1}{2} \int_{\partial D^k} \left\{ n_z [[E_h^r]] - n_r [[E_h^z]] - \alpha [[B_h^\theta]] \right\} B_h^\theta r d\boldsymbol{r}, \qquad (3.31)
\end{aligned}
$$

where all volume integrals cancel out after integration by parts.

Recalling that $\hat{\boldsymbol{n}} \cdot \boldsymbol{E}_h = n_z E_h^z + n_r E_h^r$, and summing up the contributions of all elements D^k, we have

$$
\begin{aligned}
RHS_1 &:= \sum_{k=1}^{K} \frac{1}{2} \int_{\partial D^k} \alpha (n_z [[\hat{\boldsymbol{n}} \cdot \boldsymbol{E}_h]] - [[E_h^z]]) E_h^z r d\boldsymbol{r} \\
&\quad + \frac{1}{2} \int_{\partial D^k} \alpha (n_r [[\hat{\boldsymbol{n}} \cdot \boldsymbol{E}_h]] - [[E_h^r]]) E_h^r r d\boldsymbol{r} \\
&= \sum_{k=1}^{K} \frac{\alpha}{2} \int_{\partial D^k} \left([[\hat{\boldsymbol{n}} \cdot \boldsymbol{E}_h]] \hat{\boldsymbol{n}} \cdot \boldsymbol{E}_h - [[E_h^z]] E_h^z - [[E_h^r]] E_h^r \right) r d\boldsymbol{r} \\
&= \frac{\alpha}{2} \sum_{i=1}^{Nfaces} \int_{\partial D^i} \left([[\hat{\boldsymbol{n}} \cdot \boldsymbol{E}_h]]^2 - [[E_h^z]]^2 - [[E_h^r]]^2 \right) r d\boldsymbol{r} \\
&= \frac{\alpha}{2} \sum_{i=1}^{Nfaces} \int_{\partial D^i} \left((n_r [[E_h^r]] + n_z [[E_h^z]])^2 - (n_r^2 + n_z^2) [[E_h^z]]^2 \right. \\
&\quad \left. - (n_r^2 + n_z^2) [[E_h^r]]^2 \right) r d\boldsymbol{r}
\end{aligned}
$$

$$= \frac{\alpha}{2}\sum_{i=1}^{Nfaces}\int_{\partial D^i} -\left(n_r[[E_h^z]]-n_z[[E_h^r]]\right)^2 r d\boldsymbol{r}, \tag{3.32}$$

where we used the fact that $n_r^2+n_z^2=1$ and the notation $Nfaces$ for the total number of element faces (counted once per element face) in the mesh.

Similarly, by summing up the contributions of those terms involving B_h^θ in (3.30) over all elements, we obtain

$$\begin{aligned}
RHS_2 &:= \sum_{k=1}^{K}\frac{1}{2}\int_{\partial D^k}\left\{-[[B_h^\theta]]n_r E_h^z+[[B_h^\theta]]n_z E_h^r+n_z[[E_h^r]])B_h^\theta-n_r[[E_h^z]]B_h^\theta\right\} r d\boldsymbol{r}\\
&\quad+\sum_{k=1}^{K}\int_{\partial D^k}(B_h^\theta\cdot n_r E_h^z-B_h^\theta\cdot n_z E_h^r) r d\boldsymbol{r}-\sum_{k=1}^{K}\frac{\alpha}{2}\int_{\partial D^k}[[B_h^\theta]]B_h^\theta r d\boldsymbol{r}\\
&= \sum_{k=1}^{K}\frac{1}{2}\int_{\partial D^k}\left\{-[[B_h^\theta]](n_r E_h^z-n_z E_h^r)+[[n_z E_h^r-n_r E_h^z]]B_h^\theta\right\} r d\boldsymbol{r}\\
&\quad+\sum_{i=1}^{Nfaces}\int_{\partial D^i}[[B_h^\theta(n_r E_h^z-n_z E_h^r)]] r d\boldsymbol{r}-\sum_{i=1}^{Nfaces}\frac{\alpha}{2}\int_{\partial D^i}[[B_h^\theta]]^2 r d\boldsymbol{r}\\
&= \sum_{i=1}^{Nfaces}\int_{\partial D^i}-[[B_h^\theta]][[n_r E_h^z-n_z E_h^r]] r d\boldsymbol{r}\\
&\quad+\sum_{i=1}^{Nfaces}\int_{\partial D^i}[[B_h^\theta(n_r E_h^z-n_z E_h^r)]] r d\boldsymbol{r}-\sum_{i=1}^{Nfaces}\frac{\alpha}{2}\int_{\partial D^i}[[B_h^\theta]]^2 r d\boldsymbol{r}\\
&= -\frac{\alpha}{2}\sum_{i=1}^{Nfaces}\int_{\partial D^i}[[B_h^\theta]]^2 r d\boldsymbol{r}.
\end{aligned}\tag{3.33}$$

Summing up (3.30) and (3.31) over all elements D^k, and using the estimates (3.32) and (3.33), we obtain

$$\frac{d\mathcal{E}_h(t)}{dt}=-\alpha\sum_{i=1}^{Nfaces}\int_{\partial D^i}\left\{(n_r[[\boldsymbol{E}_h^z]]-n_z[[E_h^r]])^2+[[B_h^\theta]]^2\right\} r d\boldsymbol{r}\le 0,$$

which concludes the proof. □

Finally, we present the error analysis for the semi-discrete scheme. Let us intro-

duce the weighted L^2 projection operator Π_h on each element D^k:

$$\int_{D^k} (\Pi_h u - u) w_h r dr dz = 0 \quad \forall\ w_h \in P^N(D^k). \tag{3.34}$$

Furthermore, we denote $L^2_r(\Omega)$ for the weighted Lebesgue space of all measurable function u defined in Ω for which $||u||^2_{L^2_r(\Omega)} := \int_\Omega |u|^2 r dr dz < \infty$. Thanks for those pioneering work Belhachmi et al. (2006), all the standard approximation results have been proved to be true in the corresponding weighted spaces, e.g.,

$$\begin{aligned} &||\Pi_h u - u||_{L^2_r(\Omega)} + h||\nabla(\Pi_h u - u)||_{L^2_r(\Omega)} + h^{1/2}||\Pi_h u - u||_{L^2_r(\partial\Omega)} \\ &\quad \le C h^{N+1} |u|_{H^{N+1}_r(\Omega)}, \end{aligned} \tag{3.35}$$

where we denote the weighted Sobolev semi-norm $|u|_{H^l_r(\Omega)} = (\sum_{k=0}^{l} ||\frac{\partial^l u}{\partial r^k \partial z^{l-k}}||_{L^2_r(\Omega)})^{1/2}$.

Theorem 3.31. Let (E^r, E^z, B^θ) and $(E^r_h, E^z_h, B^\theta_h)$ be the solutions of (3.9)-(3.11) and (3.26)-(3.28), respectively. Then for any $t > 0$ we have

$$\begin{aligned} &(||E^r - E^r_h||_{L^2_r(\Omega)} + ||E^z - E^z_h||_{L^2_r(\Omega)} + ||B^\theta - B^\theta_h||_{L^2_r(\Omega)})(t) \\ \le\ & C(||\Pi_h E^r - E^r_h||_{L^2_r(\Omega)} + ||\Pi_h E^z - E^z_h||_{L^2_r(\Omega)} + ||\Pi_h B^\theta - B^\theta_h||_{L^2_r(\Omega)})(0) + Ch^N. \end{aligned}$$

Proof. Using the projection definition to the governing equations (3.9)-(3.11), we have: For any $u_v, v_h, w_h \in V_h$,

$$\int_{D^k} \frac{d}{dt}(\Pi_h E^z) u_h r dr dz = \int_{D^k} \Pi_h (\frac{1}{r} B^\theta_h + \frac{\partial B^\theta_h}{\partial r}) u_h r dr dz \tag{3.36}$$

$$\int_{D^k} \frac{d}{dt}(\Pi_h E^r) v_h r dr dz = -\int_{D^k} \Pi_h (\frac{\partial B^\theta_h}{\partial z}) v_h r dr dz \tag{3.37}$$

$$\int_{D^k} \frac{d}{dt}(\Pi_h B^\theta) w_h r dr dz = \int_{D^k} \Pi_h (\frac{\partial E^z_h}{\partial r} - \frac{\partial E^r_h}{\partial z}) w_h r dr dz. \tag{3.38}$$

Denote $\frac{\partial}{\partial \tilde{r}} = \frac{1}{r}\frac{\partial}{\partial r}$. Subtracting (3.26) from (3.36) and using the definition of projection

operator Π_h, we can obtain the error equation for E^z:

$$
\begin{aligned}
&\int_{D^k} \frac{d}{dt}(\Pi_h E^z - E_h^z) u_h r dr dz \\
&= \int_{D^k} \left[\Pi_h (\frac{\partial}{\partial \tilde{r}}(r(\Pi_h B^\theta - B_h^\theta))) + \Pi_h (\frac{\partial}{\partial \tilde{r}}(r(B^\theta - \Pi_h B^\theta))) \right] u_h r dr dz \\
&\quad -\frac{1}{2}\int_{\partial D^k} \left\{ -n_r [[B_h^\theta - \Pi_h B^\theta]] + \alpha (n_z [[\hat{\boldsymbol{n}} \cdot (\boldsymbol{E}_h - \Pi_h \boldsymbol{E})]] - [[E_h^z - \Pi_h E^z]]) \right\} u_h r d\boldsymbol{r} \\
&\quad -\frac{1}{2}\int_{\partial D^k} \left\{ -n_r [[\Pi_h B^\theta]] + \alpha (n_z [[\hat{\boldsymbol{n}} \cdot \Pi_h \boldsymbol{E}]] - [[\Pi_h E^z]]) \right\} u_h r d\boldsymbol{r} \\
&= \int_{D^k} \Pi_h (\frac{\partial}{\partial \tilde{r}}(r(\Pi_h B^\theta - B_h^\theta))) u_h r dr dz \qquad (3.39) \\
&\quad +\frac{1}{2}\int_{\partial D^k} \left\{ -n_r [[\Pi_h B^\theta - B_h^\theta]] + \alpha (n_z [[\hat{\boldsymbol{n}} \cdot (\Pi_h \boldsymbol{E} - \boldsymbol{E}_h)]] - [[\Pi_h E^z - E_h^z]]) \right\} u_h r d\boldsymbol{r} \\
&\quad +(S_{E^z}, u_h)_{D^k},
\end{aligned}
$$

where the local truncation error

$$
\begin{aligned}
(S_{E^z}, u_h)_{D^k} &= \int_{D^k} \Pi_h (\frac{\partial}{\partial \tilde{r}}(r(B^\theta - \Pi_h B^\theta))) u_h r dr dz \qquad (3.40) \\
&\quad -\frac{1}{2}\int_{\partial D^k} \left\{ -n_r [[\Pi_h B^\theta]] + \alpha (n_z [[\hat{\boldsymbol{n}} \cdot \Pi_h \boldsymbol{E}]] - [[\Pi_h E^z]]) \right\} u_h r d\boldsymbol{r}.
\end{aligned}
$$

Similarly, subtracting (3.27) from (3.37), we can obtain the error equation for E^r:

$$
\begin{aligned}
&\int_{D^k} \frac{d}{dt}(\Pi_h E^r - E_h^r) v_h r dr dz \\
&= -\int_{D^k} \left[\Pi_h \frac{\partial}{\partial z}(\Pi_h B^\theta - B_h^\theta) + \Pi_h \frac{\partial}{\partial z}(B^\theta - \Pi_h B^\theta) \right] v_h r dr dz \\
&\quad -\frac{1}{2}\int_{\partial D^k} \left\{ n_z [[B_h^\theta - \Pi_h B^\theta]] + \alpha (n_r [[\hat{\boldsymbol{n}} \cdot (\boldsymbol{E}_h - \Pi_h \boldsymbol{E})]] - [[E_h^r - \Pi_h E^r]]) \right\} v_h r d\boldsymbol{r} \\
&\quad -\frac{1}{2}\int_{\partial D^k} \left\{ n_z [[\Pi_h B^\theta]] + \alpha (n_r [[\hat{\boldsymbol{n}} \cdot \Pi_h \boldsymbol{E}]] - [[\Pi_h E^r]]) \right\} v_h r d\boldsymbol{r} \\
&= -\int_{D^k} \Pi_h \frac{\partial}{\partial z}(\Pi_h B^\theta - B_h^\theta) v_h r dr dz \qquad (3.41) \\
&\quad +\frac{1}{2}\int_{\partial D^k} \left\{ n_z [[\Pi_h B^\theta - B_h^\theta]] + \alpha (n_r [[\hat{\boldsymbol{n}} \cdot (\Pi_h \boldsymbol{E} - \boldsymbol{E}_h)]] - [[\Pi_h E^r - E_h^r]]) \right\} v_h r d\boldsymbol{r} \\
&\quad +(S_{E^r}, v_h)_{D^k},
\end{aligned}
$$

where the local truncation error

$$
\begin{aligned}
(S_{E^r}, v_h)_{D^k} &= -\int_{D^k} \Pi_h \frac{\partial}{\partial z}(B^\theta - \Pi_h B^\theta) v_h r dr dz \\
&\quad -\frac{1}{2}\int_{\partial D^k} \left\{ n_z [[\Pi_h B^\theta]] + \alpha (n_r [[\hat{\boldsymbol{n}} \cdot \Pi_h \boldsymbol{E}]] - [[\Pi_h E^r]]) \right\} v_h r d\boldsymbol{r}.
\end{aligned} \tag{3.42}
$$

By the same argument, we can obtain the error equation for B^θ:

$$
\begin{aligned}
&\int_{D^k} \frac{d}{dt}(\Pi_h B^\theta - B_h^\theta) w_h r dr dz \\
&= \int_{D^k} \left[\Pi_h (\frac{\partial}{\partial r}(\Pi_h E^z - E_h^z)) + \Pi_h (\frac{\partial}{\partial r}(E^z - \Pi_h E^z)) \right] w_h r dr dz \\
&\quad - \int_{D^k} \left[\Pi_h (\frac{\partial}{\partial z}(\Pi_h E^r - E_h^r)) + \Pi_h (\frac{\partial}{\partial z}(E^r - \Pi_h E^r)) \right] w_h r dr dz \\
&\quad + \frac{1}{2}\int_{\partial D^k} \left\{ n_z [[\Pi_h E^r - E_h^r]] - n_r [[\Pi_h E^z - E_h^z]] - \alpha [[\Pi_h B^\theta - B_h^\theta]] \right\} w_h r d\boldsymbol{r} \\
&\quad - \frac{1}{2}\int_{\partial D^k} \left\{ n_z [[\Pi_h E^r]] - n_r [[\Pi_h E^z]] - \alpha [[\Pi_h B^\theta]] \right\} w_h r d\boldsymbol{r} \\
&= \int_{D^k} \left[\Pi_h (\frac{\partial}{\partial r}(\Pi_h E^z - E_h^z)) - \Pi_h (\frac{\partial}{\partial z}(\Pi_h E^r - E_h^r)) \right] w_h r dr dz \\
&\quad + \frac{1}{2}\int_{\partial D^k} \left\{ n_z [[\Pi_h E^r - E_h^r]] - n_r [[\Pi_h E^z - E_h^z]] - \alpha [[\Pi_h B^\theta - B_h^\theta]] \right\} w_h r d\boldsymbol{r} \\
&\quad + (S_{B^\theta}, w_h)_{D^k},
\end{aligned} \tag{3.43}
$$

where

$$
\begin{aligned}
(S_{B^\theta}, w_h)_{D^k} &= \int_{D^k} \left[\Pi_h (\frac{\partial}{\partial r}(E^z - \Pi_h E^z)) - \Pi_h (\frac{\partial}{\partial z}(E^r - \Pi_h E^r)) \right] w_h r dr dz \\
&\quad - \frac{1}{2}\int_{\partial D^k} \left\{ n_z [[\Pi_h E^r]] - n_r [[\Pi_h E^z]] - \alpha [[\Pi_h B^\theta]] \right\} w_h r d\boldsymbol{r}.
\end{aligned} \tag{3.44}
$$

Choosing $v_h = \Pi_h E^r - E_h^r, u_h = \Pi_h E^z - E_h^z$ and $w_h = \Pi_h B^\theta - B_h^\theta$ in (3.39), (3.41) and (3.43), respectively, then adding the results together, and following the stability analysis, we have

$$
\frac{1}{2}\frac{d}{dt}(||\Pi_h E^r - E_h^r||^2_{L_r^2(\Omega)} + ||\Pi_h E^z - E_h^z||^2_{L_r^2(\Omega)} + ||\Pi_h B^\theta - B_h^\theta||^2_{L_r^2(\Omega)})
$$

$$
\begin{aligned}
= \quad & -\alpha \sum_{i=1}^{Nfaces} \int_{\partial D^k} \left\{ (n_r[[\Pi_h E^z - E_h^z]] - n_z[[\Pi_h E^r - E_h^r]])^2 + [[\Pi_h B^\theta - B_h^\theta]]^2 \right\} r d\boldsymbol{r} \\
& + \sum_{k=1}^{K} \left[(S_{E^r}, \Pi_h E^r - E_h^r)_{D^k} + (S_{E^z}, \Pi_h E^z - E_h^z)_{D^k} \right. \\
& \left. + (S_{B^\theta}, \Pi_h B^\theta - B_h^\theta)_{D^k} \right]. \qquad (3.45)
\end{aligned}
$$

By the definition (3.41), we have

$$
\begin{aligned}
(S_{E^r}, \Pi_h E^r - E_h^r)_{D^k} \quad = \quad & -\int_{D^k} \Pi_h (\frac{\partial}{\partial z}(B^\theta - \Pi_h B^\theta)) \cdot (\Pi_h E^r - E_h^r) r dr dz \\
& -\frac{1}{2} \int_{\partial D^k} \left\{ n_z [[\Pi_h B^\theta]] \right. \\
& \left. + \alpha (n_r [[\hat{\boldsymbol{n}} \cdot \Pi_h \boldsymbol{E}]] - [[\Pi_h E^r]]) \right\} (\Pi_h E^r - E_h^r) r d\boldsymbol{r} \\
:= \quad & \sum_{i=1}^{2} Err_i. \qquad (3.46)
\end{aligned}
$$

By the Cauchy-Schwarz inequality and the projection property (3.35), we have

$$
\begin{aligned}
Err_1 \quad = \quad & -\int_{D^k} (\frac{\partial}{\partial z}(B^\theta - \Pi_h B^\theta)) \cdot (\Pi_h E^r - E_h^r) r dr dz \\
\leq \quad & C h^N |B^\theta|_{H_r^{N+1}(D^k)} ||\Pi_h E^r - E_h^r||_{L_r^2(D^k)}. \qquad (3.47)
\end{aligned}
$$

Similarly, by the trace inequality with weighted inner product $\int_\Omega (\cdot, \cdot) r dr dz$, we have

$$
\begin{aligned}
Err_2 \quad = \quad & -\frac{1}{2} \int_{\partial D^k} \left\{ n_z [[\Pi_h B^\theta - B^\theta]] \right. \\
& \left. + \alpha (n_r [[\hat{\boldsymbol{n}} \cdot (\Pi_h \boldsymbol{E} - \boldsymbol{E})]] - [[\Pi_h E^r - E^r]]) \right\} (\Pi_h E^r - E_h^r) r d\boldsymbol{r} \\
\leq \quad & C h^N (|B^\theta|_{H_r^{N+1}(\Omega)} + |E^r|_{H_r^{N+1}(D^k)} \\
& + |E^z|_{H_r^{N+1}(D^k)} ||) \Pi_h E^r - E_h^r||_{L_r^2(D^k)}. \qquad (3.48)
\end{aligned}
$$

Substituting (3.47) and (3.48) into (3.46), we obtain

$$
\sum_{k=1}^{K} (S_{E^r}, \Pi_h E^r - E_h^r)_{D^k} \leq C h^N ||\Pi_h E^r - E_h^r||_{L_r^2(\Omega)}. \qquad (3.49)
$$

By the same technique, we can prove that

$$\sum_{k=1}^{K}(S_{E^z}, \Pi_h E^z - E_h^z)_{D^k} \leq Ch^N ||\Pi_h E^z - E_h^z||_{L_r^2(\Omega)}. \tag{3.50}$$

and

$$\sum_{k=1}^{K}(S_{B^\theta}, \Pi_h B^\theta - B_h^\theta)_{D^k} \leq Ch^N ||\Pi_h B^\theta - B_h^\theta||_{L_r^2(\Omega)}. \tag{3.51}$$

Substituting the estimates (3.49)-(3.51) into (3.45), dropping the negative term on the right hand side of (3.45), then using the Gronwall inequality, the triangle inequality and the estimate (3.35), we conclude the proof. □

Theorem 3.3.1 shows that we can have the following error estimate

$$(||E^r - E_h^r||_{L_r^2(\Omega)} + ||E^z - E_h^z||_{L_r^2(\Omega)} + ||B^\theta - B_h^\theta||_{L_r^2(\Omega)})(t) \leq Ch^N,$$

under the standard initial approximation

$$E_h^r(0) = \Pi_h E^r(0), \quad E_h^z(0) = \Pi_h E^z(0), \quad B_h^\theta(0) = \Pi_h B^\theta(0).$$

This is confirmed by our numerical results presented in the next section.

3.4 Numerical results

Convergence rate test for the DG method

Here we consider solving the 2-D rotationally symmetric Maxwell's equations (3.9)-(3.11) with source terms f_1, f_2, f_3 added to the right hand side of (3.9)-(3.11),

respectively. More specifically we pick the source functions to be:

$$f_1 = (1-\pi)\cos(\pi r)\sin(\pi z)\cos(t) \tag{3.52}$$

$$f_2 = (1+\pi)\sin(\pi r)\cos(\pi z)\cos(t) - \frac{1}{r}\cos(\pi r)\cos(\pi z)\cos(t) \tag{3.53}$$

$$f_3 = \cos(\pi r)\cos(\pi z)\sin(t) \tag{3.54}$$

such that the analytic solution to the system of equations is:

$$E^r = \cos(\pi r)\sin(\pi z)\sin(t) \tag{3.55}$$

$$E^z = \sin(\pi r)\cos(\pi z)\sin(t) \tag{3.56}$$

$$B^\theta = \cos(\pi r)\cos(\pi z)\cos(t). \tag{3.57}$$

All simulations were ran for 1000 time steps with a constant time step of $\tau = 0.0001$ and up to a final time of $T = 0.1$ on a domain of $(r, z) \in [0, 1] \times [0, 1]$. For the boundary we imposed the PEC boundary condition (3.12). To test convergence rate of our scheme, we calculated the sum of the L_r^2 errors of each solution component by solving the problem on a series of uniformly refined meshes. The coarsest mesh has a mesh size of $h = 0.01$ shown in Fig. 3.1.

The obtained convergence rates for the L^2 error

$$||e_h||_{L_r^2} := ||E_h^r - E^r||_{L_r^2(\Omega)} + ||E_h^z - E^z||_{L_r^2(\Omega)} + ||B_h^\theta - B^\theta||_{L_r^2(\Omega)}$$

and for the L^∞ error

$$||e_h||_{L^\infty} := ||E_h^r - E^r||_{L^\infty(\Omega)} + ||E_h^z - E^z||_{L^\infty(\Omega)} + ||B_h^\theta - B^\theta||_{L^\infty(\Omega)}$$

are presented in Tables 3.1 and 3.2, respectively. Table 3.1 showes clearly $O(h^N)$ convergence rate in the L_r^2 norm, which is consistent with our theoretical analysis.

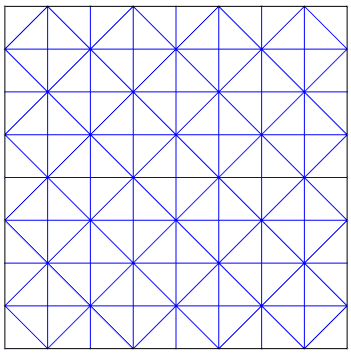

Figure 3.1. The exemplary coarse mesh used in the error convergence analysis.

The numerical results in Table 3.2 show $O(h^N)$ convergence rate in the L^∞ norm, though its rigorous proof is still open.

Table 3.1. The L_r^2 error convergence rates for e_h obtained with basis functions of order $N = 1$ to 4.

N	e_h	$e_{h/2}$	Rates	$e_{h/4}$	Rates	$e_{h/8}$	Rates
1	3.1915E-03	1.3789E-03	1.2107	6.6663E-04	1.0485	3.3308E-04	1.0010
2	4.4756E-05	8.6212E-06	2.3761	1.9635E-06	2.1344	4.7913E-07	2.0349
3	5.4792E-07	5.9657E-08	3.1992	7.1527E-09	3.0601	8.7891E-10	3.0246
4	4.1907E-09	2.2624E-10	4.2112	1.3373E-11	4.0804	8.2221E-13	4.0236

Comparison between the DG method and the FDTD method

Because there is not a known exact solution for corrugated domains, the solution of the DG method was compared with the (much simpler to implement) FDTD method in order to verify results of the DG method. Because of the limitation of the FDTD method, we used a square corrugation to test the DG method against the FDTD

Table 3.2. The L^∞ error convergence rates for e_h obtained with basis functions of order $N = 1$ to 4.

N	e_h	$e_{h/2}$	Rates	$e_{h/4}$	Rates	$e_{h/8}$	Rates
1	7.6057E-03	3.1592E-03	1.2675	1.4549E-03	1.1186	6.9724E-04	1.0612
2	1.6566E-04	2.9603E-05	2.4844	6.0339E-06	2.2946	1.3729E-06	2.1358
3	5.4792E-07	8.3520E-07	3.0825	1.0080E-07	3.0506	1.2390E-08	3.0243
4	7.0750E-06	2.1158E-09	4.3458	1.1399E-10	4.2142	6.5732E-12	4.1162

method. In the following simulation both methods were run on a domain with 2 corrugations; each 1 unit wide and 0.1 units deep. In order to get a better visual result for comparison a much narrower pulse defined by $f(t) = \frac{1}{r}\exp(\frac{-(t-.3)^2}{2(.1)^2})$ was used.

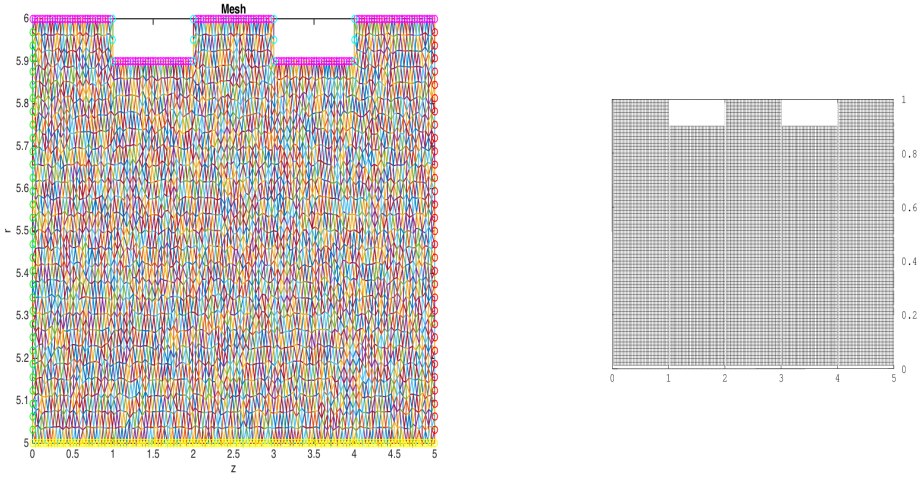

Figure 3.2. The meshes used in the DG and FDTD methods. Both domains are the same, their images just have different aspect ratios.

To make the results comparable, not only was the same domain used, but also similar time steps and mesh sizes. For the DG simulation a polynomial order of $N = 1$, and a mesh size of approximately $h = 10^{-2}$ were used. The time step was

automatically calculated to be $\Delta t = 0.0026$ based on the mesh size to avoid violating the CFL condition. For the FDTD simulation the parameters used were: a mesh size of $\Delta z = 0.0250 \times \Delta r = 0.0125$ with a time step of $\Delta t = 0.0031$. Plots of some snapshots of E^r at different times are put in Fig. 3.3 side-by-side for a clear comparison of the FDTD method verses the DG method. Fig. 3.3 shows that our solutions obtained by these two different methods are indistinguishable by eyes.

Modeling of corrugated cables by the DG method

To make sure that our code worked correctly, we carried out many tests for various corrugated domains with different meshes, time step sizes, and wave sources. The corrugated domains used in these examples are related to the dimensions of RF-19 corrugated coaxial cable which was provided by NSTec. The below results were obtained by using the Gaussian wave source:

$$u(0, r, t) = \frac{1}{r} \exp\left(-\frac{(t - 5\sigma)^2}{2(\sigma)^2}\right)$$

where $\sigma = 2.5$ mean$(h(z))$, and $h(z)$ is the function describing the height of the cable from the central axis.

The first simulation is done for a "sawtooth" corrugation, since our DG method can discretize this corrugated domain exactly by triangular elements. Snapshots of E^r are plotted in Figure 3.4.

To see the effects of corrugated cables on the signal propagation, we finally simulated both an un-corrugated cable (see Fig. 3.6l (Right Column)), and a corrugated cable (see Fig. 3.6l (Left Column)) described by function $h(z) = 7 + \cos(\frac{2\pi z}{7})$ (based

on the RF-19 cable parameters) under almost the same conditions. Snapshots of E^r are plotted in Figure 11, which shows that the corrugated cable has limited effects on the signal propagation.

3.5 Conclusions

In this chapter we focused on solving the two-dimensional (2-D) time-dependent Maxwell's equations in both Cartesian and cylindrical coordinate systems. Since no experimental data was available to compare, we simulated the pulse propagation by using both the FDTD and DG methods. Both our FDTD and DG implementations have been rigorously tested to ensure they work correctly from a numerical analysis point of view. Many cases with different wave sources, different corrugated domains, various mesh sizes and different basis functions for the DG methods have simulated.

Our study found that the corrugated coaxial cable has effects on the pulse propagation in the cable depending on the depth of the corrugation and its periodicity. Of course, many challenges still remain, for example, how to implement simulations for a very long distance (over 1000 feet long), and how to model real 3-D corrugated coaxial cables. These challenges will inspire our continuous investigation in this subject.

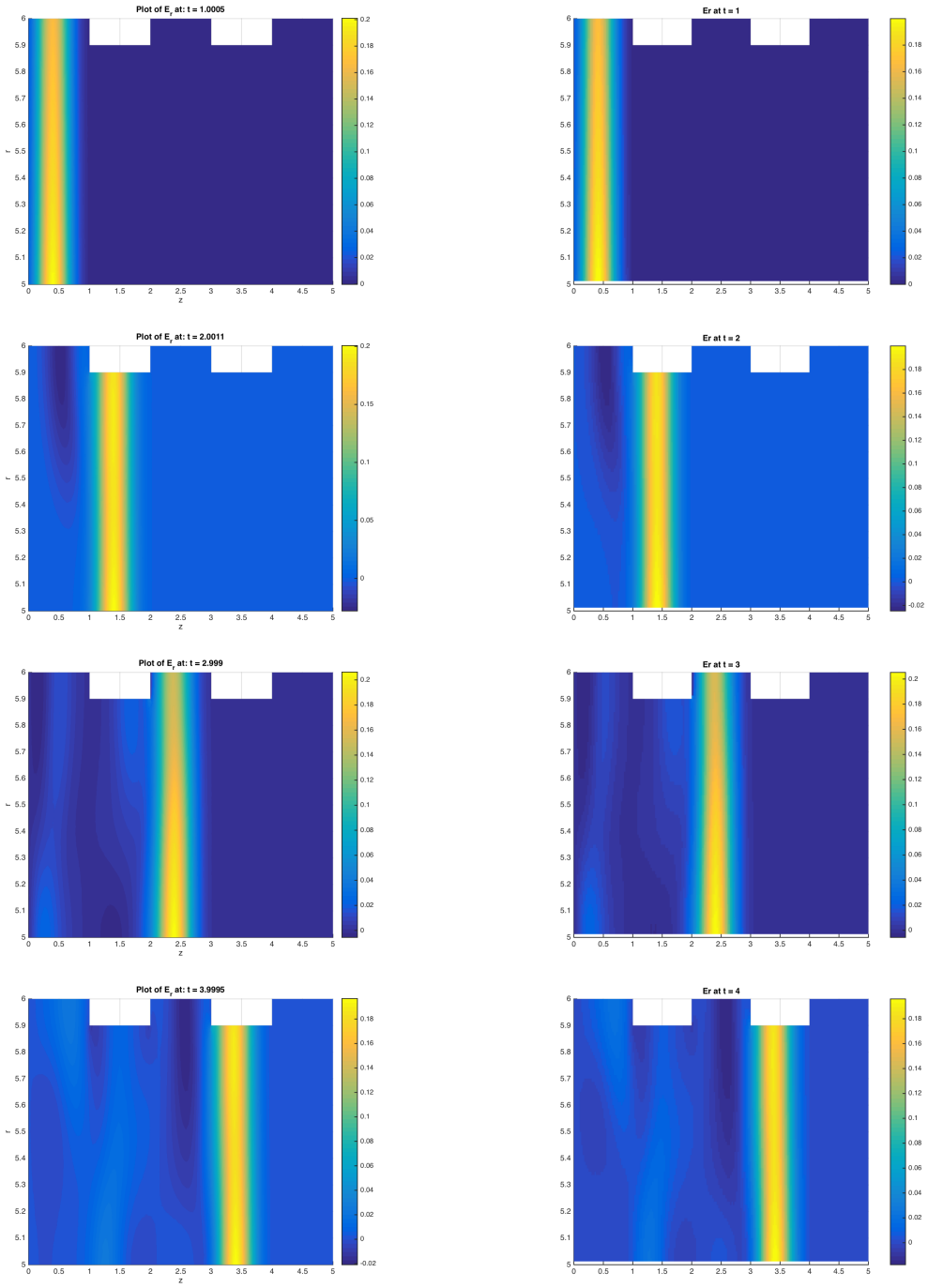

Figure 3.3. (Left) DG method at $t = 1, 2, 3, 4$; (Right) FDTD method at $t = 1, 2, 3, 4$.

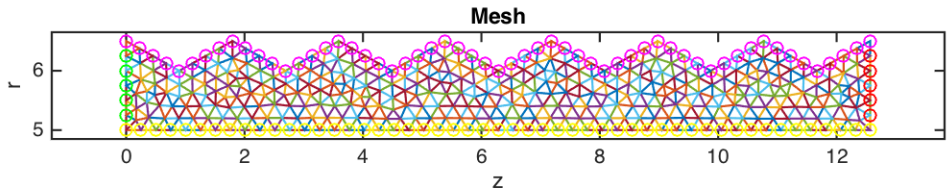

(a) Mesh with color labeled boundaries generated using measurements from images of RF-19 cable.

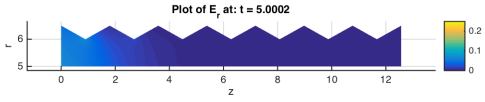

(b) $t = 5$.

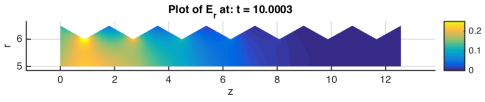

(c) $t = 10$.

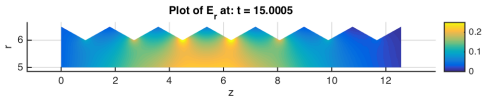

(d) $t = 15$.

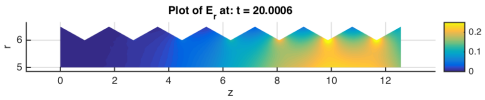

(e) $t = 20$.

Figure 3.4. Mesh and snapshots of E^r for a "sawtooth" corrugation. Maximum element size of 0.251, and polynomial basis function of order $N = 10$.

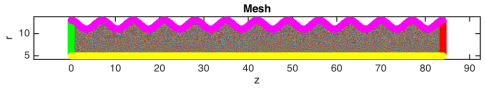

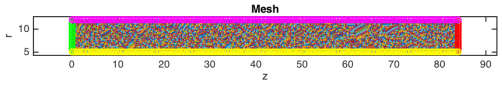

Figure 3.5. Corrugated and non-corrugated meshes with color labeled boundaries generated using measurements from images of RF-19 cable.

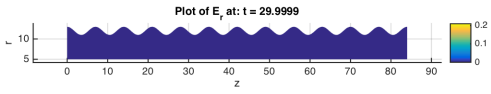

(a) $t = 30$.

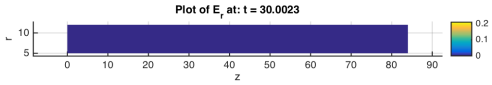

(b) $t = 30$.

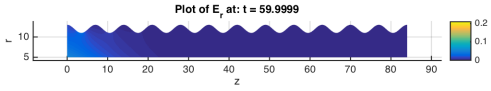

(c) $t = 60$.

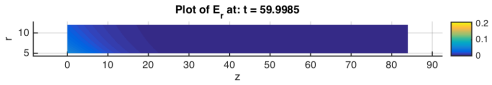

(d) $t = 60$.

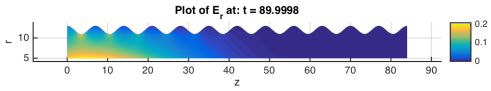

(e) $t = 90$.

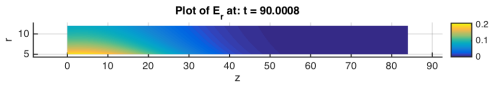

(f) $t = 90$.

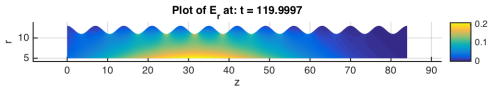

(g) $t = 120$.

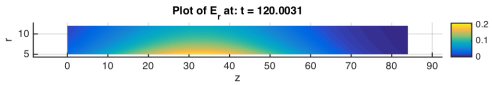

(h) $t = 120$.

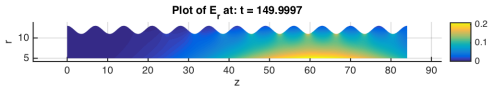

(i) $t = 150$.

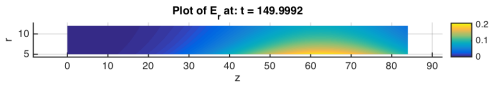

(j) $t = 150$.

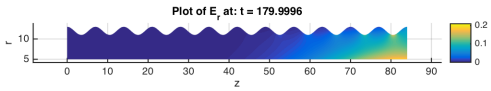

(k) $t = 180$.

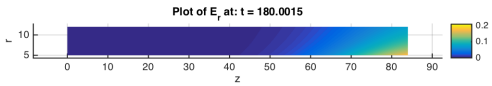

(l) $t = 180$.

Figure 3.6. Mesh and snapshots of E^r for a corrugation function of $h(z) = 7 + \cos(\frac{2\pi z}{7})$ which models the RF-19 cable, compared to mesh and snapshots of E^r for a non-corrugated version of the RF-19 cable side by side. Maximum element size of 0.38, minimum element size of 0.06, and polynomial order of $N = 3$.

CHAPTER 4

A WEAK GALERKIN FOR THE TIME-DEPENDENT MAXWELL'S EQUATIONS

4.1 Introduction

In Mu *et al.* extension of the WG method to the time-harmonic Maxwell's equations Mu et al. (2015a), optimal order convergence was proved in various norms. Three dimensional numerical results show that WG method is capable of solving Maxwell's equations. Inspired by their 2015 paper, here we develop the WG method to solve the time-dependent Maxwell's equations. We like to remark that there are many excellent works on DG methods for solving Maxwell's equations in free space Fezoui et al. (2005); Grote et al. (2007) and in dispersive media Demkowicz and Li (2013); Li and Hesthaven (2014); Li et al. (2012); Lu et al. (2004); Scheid and Lanteri (2013); Wang et al. (2010, 2015). More details and references on DG methods for Maxwell's equations can be found in books Hesthaven and Warburton (2008) and (Li and Huang, 2013, Ch.4).

Under the assumptions that ϵ and μ are constants, and σ and ρ are zero, we can solve for the electric field $\mathbf{E}$ from (1.2) and (1.1) to get:

$$\frac{1}{\mu\epsilon}\nabla\times(\nabla\times\mathbf{E})+\frac{\partial^2\mathbf{E}}{\partial t^2}=0,\quad \nabla\cdot\mathbf{E}=0. \tag{4.1}$$

This leads to the model problem in $d = 2, 3$ dimensions:

$$\begin{aligned} \frac{1}{\mu\epsilon}\nabla \times (\nabla \times \mathbf{u}) + \frac{\partial^2 \mathbf{u}}{\partial t^2} &= \boldsymbol{f} \quad \text{in } \Omega \times [0, T], \\ \mathbf{u} \times \boldsymbol{n}_\Omega &= \boldsymbol{\phi} \quad \text{on } \partial\Omega, \end{aligned} \tag{4.2}$$

where we discard the divergence free condition since the solution is naturally divergence free if the given initial field is divergence free. Here, $\boldsymbol{n}_\Omega$ is taken to be the outwards normal unit vector to the boundary of the domain $\partial\Omega$. To generalize the problem an arbitrary source term, $\boldsymbol{f} \in [H(div; \Omega)]^d$ (where $\nabla \cdot \boldsymbol{f} = 0$ in Ω), and a Dirichlet boundary condition, $\boldsymbol{\phi} \in [L^2(\partial\Omega)]^d$, were added. Additionally, if $\boldsymbol{\phi}$ is taken to be $\mathbf{0}$, then we arrive at the standard perfect electric conductor (PEC) boundary conditions. Here and below the physical domain Ω is a bounded Lipschitz polyhedral domain in R^d with connected boundary $\partial\Omega$.

This chapter is organized as follows. In Section 4.2 we introduce the concept of a weak curl, along with other definitions necessary for the weak Galerkin scheme. In Section 4.3 the semi-discrete scheme is defined, and stability and error analysis are provided. In Section 4.4 a 2nd order fully-discrete scheme is proposed, and stability and error analysis are provided. Section 4.5 then provides an example implementation of the scheme in 2-D with the lowest order element. Then Section 4.6 provides numerical results from the implementation that confirm the error analysis provided in earlier sections. Finally, Section 4.7 concludes the chapter. The research presented in this chapter was submitted to be published as Shields et al. (view) where I was the leading author and Jichun Li and Eric Machorro were contributing authors.

4.2 Preliminaries and Notations

The Weak Curl

The concept of a weak curl was discussed in Mu et al. (2015a), however, it is presented here for completeness. Let K be any polyhedral domain in $\mathbb{R}^d$ with boundary ∂K. A weak function on K refers to a function defined by the ordered pair: $\mathbf{v} = \{\mathbf{v}_0, \mathbf{v}_b\}$ such that $\mathbf{v}_0 \in [L^2(K)]^d$ and $\mathbf{v}_b \in [L^2(\partial K)]^d$. The first component $\mathbf{v}_0$ can be understood as the value of $\mathbf{v}$ in K, and the second component $\mathbf{v}_b$ represents $\mathbf{v}$ on the boundary of K. We denote the space of weak functions on K as:

$$\mathcal{V}(K) := \{\mathbf{v} = \{\mathbf{v}_0, \mathbf{v}_b\} : \mathbf{v}_0 \in [L^2(K)]^d, \mathbf{v}_b \times \boldsymbol{n}_K \in [L^2(\partial K)]^d\} \tag{4.3}$$

And we denote $\boldsymbol{n}_K$ to be the outward unit normal vector to ∂K.

Definition 1: Weak curl For any $\mathbf{v} \in \mathcal{V}(K)$, the weak curl of $\mathbf{v}$ is defined as a continuous linear functional $\nabla_w \times \mathbf{v} \in [H^1(K)]^d$ whose action on each $\boldsymbol{\varphi} \in [H^1(K)]^d$ is given by

$$(\nabla_w \times \mathbf{v}, \boldsymbol{\varphi})_K := (\mathbf{v}_0, \nabla \times \boldsymbol{\varphi})_K - \langle \mathbf{v}_b \times \boldsymbol{n}_K, \boldsymbol{\varphi} \rangle_{\partial K} \tag{4.4}$$

where $(\cdot, \cdot)_K$ is the L^2 inner product on K and $\langle \cdot, \cdot \rangle_{\partial K}$ is the L^2 inner product on ∂K.

The Weak Formulation

The space $H(curl; \Omega)$ is defined as the set of vector-valued functions on Ω which, together with their curl, are square integrable, i.e.:

$$H(curl; \Omega) = \{\mathbf{v} : \mathbf{v} \in [L^2(\Omega)]^d, \nabla \times \mathbf{v} \in [L^2(\Omega)]^d\}.$$

Additionally, we define the subspace of $H(curl;\Omega)$ as follows:

$$H_0(curl;\Omega) = \{\mathbf{v} \in H(curl;\Omega) : \mathbf{v} \times \boldsymbol{n}_\Omega = \mathbf{0} \quad \text{on } \partial\Omega\}.$$

With the above definitions and letting $\nu = \frac{1}{\mu\epsilon}$, we consider the weak formulation for (4.2): Find $\mathbf{u} \in H(curl;\Omega)$ such that $\mathbf{u} \times \boldsymbol{n}_\Omega = \boldsymbol{\phi}$ on $\partial\Omega$ and

$$(\nu\nabla \times \mathbf{u}, \nabla \times \mathbf{v})_\Omega + \left(\frac{\partial^2 \mathbf{u}}{\partial t^2}, \mathbf{v}\right)_\Omega = (\boldsymbol{f}, \mathbf{v})_\Omega, \quad \forall \mathbf{v} \in H_0(curl;\Omega). \tag{4.5}$$

The Weak Galerkin Finite Element Spaces

Let $\mathcal{K}_h$ be the partition of the domain Ω with mesh size h. Denote the set of all faces of elements of $\mathcal{K}_h$ to be $\mathcal{E}_h$ and let $\mathcal{E}_h^0 = \mathcal{E}_h \setminus \partial\Omega$ be the set of all interior faces.

Definition 2: Discrete weak curl The discrete weak curl operator, denoted by $\nabla_{w,k-1}\times$, is definited as the unique polynomial $(\nabla_{w,k-1} \times \mathbf{v}) \in [P_{k-1}(K)]^d$ that satisfies:

$$(\nabla_{w,k-1} \times \mathbf{v}, \boldsymbol{\varphi})_K := (\mathbf{v}_0, \nabla \times \boldsymbol{\varphi})_K - \langle \mathbf{v}_b \times \boldsymbol{n}_K, \boldsymbol{\varphi}\rangle_{\partial K}, \quad \forall\, \boldsymbol{\varphi} \in [P_{k-1}(K)]^d. \tag{4.6}$$

Without confusion, below we simply denote $\nabla_{w,k-1}\times$ as $\nabla_w \times$.

Similar to what was found in Mu et al. (2015a); Wang and Ye (2014), let $d = 3$ and K be any polyhedral element in $\mathcal{K}_h$ with boundary ∂K (a similar argument can be done for the $d = 2$ case). For each face $e \subset \partial K$, let $\mathbf{t}_1$ and $\mathbf{t}_2$ be two assigned unit vectors on the face e, and let $\boldsymbol{n}_K$ be the unit normal vector to e such that $\mathbf{t}_1$, $\mathbf{t}_2$, and $\boldsymbol{n}_K$ are all orthogonal to each other for $\mathbf{v}_b \in [L^2(\partial K)]^3$. Thus, we have $\mathbf{v}_b|_e = v_1\mathbf{t}_1 + v_2\mathbf{t}_2 + v_n\boldsymbol{n}_K$ for some constants v_1, v_2, v_n. Define $\overline{\mathbf{v}}_b = v_1\mathbf{t}_1 + v_2\mathbf{t}_2$ as the

projection of $\mathbf{v}_b$ in the tangential plane. It is clear that $\overline{\mathbf{v}}_b \times \boldsymbol{n}_K = \mathbf{v}_b \times \boldsymbol{n}_K$. Since the weak curl only uses $\mathbf{v}_b \times \boldsymbol{n}_K$, it is advantageous to use the value of $\overline{\mathbf{v}}_b$ instead of $\mathbf{v}_b$ to reduce the number of unknowns. Therefore, throughout the rest of this chapter we will let $\mathbf{v}_b = \overline{\mathbf{v}}_b$. This will be quite useful in the definition of the numerical scheme in subsequent sections.

Let $e \in \mathcal{E}_h$, and let $\mathbf{t}_1$ and $\mathbf{t}_2$ be two linearly independent tangential unit vectors on e. For $k \geq 1$, define WG finite element spaces associated with $\mathcal{K}_h$ as:

$$V_h = \left\{ \mathbf{v}_h = \{\mathbf{v}_{0h}, \mathbf{v}_{bh}\} : \mathbf{v}_{0h}|_K \in [P_k(K)]^d, \mathbf{v}_{bh} = v_1\mathbf{t}_1 + v_2\mathbf{t}_2, \right.$$
$$\left. v_1, v_2 \in P_k(e), e \subset \partial K \right\}, \tag{4.7}$$

and $V_h^0 = \{\mathbf{v}_h \in V_h : \mathbf{v}_{bh} \times \boldsymbol{n}_\Omega = \mathbf{0} \text{ on } \partial\Omega\}$.

Note that due to the definition of $\mathbf{v}_h = \{\mathbf{v}_{0h}, \mathbf{v}_{bh}\} \in V_h$, $\mathbf{v}_{0h}$ and $\mathbf{v}_{bh}$ do not have any continuity constraints. In fact, $\mathbf{v}_{0h}$ in neighboring elements do not have any continuity enforced between them. However, as in Mu et al. (2015a), we enforce tangential continuity between $\mathbf{v}_{bh}$'s that share the same face:

$$\mathbf{v}_{bh}|_{K_1} \times \boldsymbol{n}_{K_1} = -\mathbf{v}_{bh}|_{K_2} \times \boldsymbol{n}_{K_2} \tag{4.8}$$

Here $\boldsymbol{n}_{K_1} = -\boldsymbol{n}_{K_2}$ is the normal vector to the shared face of elements K_1 and K_2.

We are then able to define a stability term which will be used later:

$$s(\mathbf{v}, \mathbf{w}) := \sum_{K \in \mathcal{K}_h} h_K^{-1} \langle (\mathbf{v}_0 - \mathbf{v}_b) \times \mathbf{n}, (\mathbf{w}_0 - \mathbf{w}_b) \times \mathbf{n} \rangle_{\partial K} \tag{4.9}$$

where h_K denotes the diameter of element K, defined by: $h_K := diam(K)$.

In addition, as in Mu et al. (2015a) the following semi-norm is defined for weak functions in the finite element space, $\mathbf{v}_h = \{\mathbf{v}_{0h}, \mathbf{v}_{bh}\} \in V_h$:

$$|\mathbf{v}_h|_{1,h} := \left(\sum_{K \in \mathcal{K}_h} h_K^{-1} ||(\mathbf{v}_{0h} - \mathbf{v}_{bh}) \times \boldsymbol{n}_K||^2_{L^2(\partial K)} \right)^{1/2} = (s(\mathbf{v}_h, \mathbf{v}_h))^{1/2} \tag{4.10}$$

For simplicity and convenience the following notation is used throughout the rest of the chapter. The standard L^2 norm over an element K, $||\cdot||_{L^2(K)}$, is written as $||\cdot||_K$, and the induced standard L^2 norm over its boundary, $||\cdot||_{L^2(\partial K)}$, is written as $||\cdot||_{\partial K}$. Additionally, the L^2 norm over the entire domain, $||\cdot||_{L^2(\Omega)}$ is just denoted as $||\cdot||$.

4.3 The Semi-discrete Scheme

Semi-discrete Weak Galerkin Algorithm. Find $\mathbf{u}_h = \{\mathbf{u}_{0h}, \mathbf{u}_{bh}\} \in V_h$ satisfying $\mathbf{u}_{bh} \times \boldsymbol{n}_\Omega = Q_b \boldsymbol{\phi}$ on $\partial\Omega$ and

$$(\nu \nabla_w \times \mathbf{u}_h, \nabla_w \times \mathbf{v}_h)_\Omega + \left(\frac{\partial^2 \mathbf{u}_{0h}}{\partial t^2}, \mathbf{v}_{0h} \right)_\Omega + s\left(\frac{\partial \mathbf{u}_h}{\partial t}, \mathbf{v}_h \right) = (\boldsymbol{f}, \mathbf{v}_{0h})_\Omega \qquad \forall \mathbf{v}_h \in V_h^0, \tag{4.11}$$

where $Q_b \boldsymbol{\phi} \in [P_k(\partial K \cap \partial\Omega)]^d$ is the standard L^2 projection of the boundary value $\boldsymbol{\phi}$ on each boundary segment.

Stability of the semi-discrete scheme

Theorem 4.31. For any $\tau \in (0, T]$,

$$\frac{\nu}{2} ||\nabla_w \times \mathbf{u}_h(\tau)||^2 + \frac{1}{2} \left|\left| \frac{\partial \mathbf{u}_{0h}}{\partial t}(\tau) \right|\right|^2 + \int_0^\tau \left| \frac{\partial \mathbf{u}_h}{\partial t} \right|^2_{1,h} dt \leq C \left[\frac{\nu}{2} ||\nabla_w \times \mathbf{u}_h(0)||^2 + \frac{1}{2} \left|\left| \frac{\partial \mathbf{u}_{0h}}{\partial t}(0) \right|\right|^2 + \int_0^\tau ||\boldsymbol{f}||^2 dt \right], \tag{4.12}$$

where the constant $C = \exp(\tau)$ is independent of time t and the mesh size h. Hence, the semi-discrete weak Galerkin scheme (4.11) is unconditionally stable.

Proof. Let $\mathbf{v}_h = \{\partial_t \mathbf{u}_0, \partial_t \mathbf{u}_b\}$ in (4.11) to get

$$\left(\nu \nabla_w \times \mathbf{u}_h, \nabla_w \times \frac{\partial \mathbf{u}_h}{\partial t}\right)_\Omega + \left(\frac{\partial^2 \mathbf{u}_{0h}}{\partial t^2}, \frac{\partial \mathbf{u}_{0h}}{\partial t}\right)_\Omega + s\left(\frac{\partial \mathbf{u}_h}{\partial t}, \frac{\partial \mathbf{u}_h}{\partial t}\right) = \left(\boldsymbol{f}, \frac{\partial \mathbf{u}_{0h}}{\partial t}\right)_\Omega. \tag{4.13}$$

This can be rewritten as

$$\frac{\nu}{2}\frac{\partial}{\partial t}||\nabla_w \times \mathbf{u}_h||^2 + \frac{1}{2}\frac{\partial}{\partial t}\left|\left|\frac{\partial \mathbf{u}_{0h}}{\partial t}\right|\right|^2 + \left|\frac{\partial \mathbf{u}_h}{\partial t}\right|_{1,h}^2 = \left(\boldsymbol{f}, \frac{\partial \mathbf{u}_{0h}}{\partial t}\right)_\Omega. \tag{4.14}$$

We then integrate both sides over time from 0 to τ to arrive at

$$\begin{aligned}\frac{\nu}{2}(||\nabla_w \times \mathbf{u}_h(\tau)||^2 - ||\nabla_w \times \mathbf{u}_h(0)||^2) + \frac{1}{2}\left(\left|\left|\frac{\partial \mathbf{u}_{0h}}{\partial t}(\tau)\right|\right|^2 - \left|\left|\frac{\partial \mathbf{u}_{0h}}{\partial t}(0)\right|\right|^2\right) \\ + \int_0^\tau \left|\frac{\partial \mathbf{u}_h}{\partial t}\right|_{1,h}^2 dt = \int_0^\tau \left(\boldsymbol{f}, \frac{\partial \mathbf{u}_{0h}}{\partial t}\right)_\Omega dt.\end{aligned} \tag{4.15}$$

Then, using Young's inequality along with the Cauchy-Schwarz inequality gives us

$$\begin{aligned}\frac{\nu}{2}(||\nabla_w \times \mathbf{u}_h(\tau)||^2 - ||\nabla_w \times \mathbf{u}_h(0)||^2) + \frac{1}{2}\left(\left|\left|\frac{\partial \mathbf{u}_{0h}}{\partial t}(\tau)\right|\right|^2 - \left|\left|\frac{\partial \mathbf{u}_{0h}}{\partial t}(0)\right|\right|^2\right) \\ + \int_0^\tau \left|\frac{\partial \mathbf{u}_h}{\partial t}\right|_{1,h}^2 dt \leq \frac{1}{2}\int_0^\tau ||\boldsymbol{f}||^2 dt + \frac{1}{2}\int_0^\tau \left|\left|\frac{\partial \mathbf{u}_{0h}}{\partial t}\right|\right|^2 dt.\end{aligned} \tag{4.16}$$

Finally, rearranging terms and using Grönwall's inequality concludes the proof. □

Error analysis for the semi-discrete scheme

For each element $K \in \mathcal{K}_h$, and each face $e \subset \partial K$, denote $\mathbf{Q}_0$ to be the L^2 projection onto $[P_k(K)]^d$ and let Q_b be the L^2 projection onto $P_k(e)$. Then the following projection onto the finite element space V_h is defined to be:

$$\mathbf{Q}_h \mathbf{v} = \{\mathbf{Q}_0 \mathbf{v}, Q_b \mathbf{v} = Q_b(v_1)\mathbf{t}_1 + Q_b(v_2)\mathbf{t}_2\},$$

where $\mathbf{t}_1$, and $\mathbf{t}_2$ are two linearly independent unit tangential vectors on the face. In addition, $\mathbb{Q}_h$ is defined to be the local L^2 projection onto $[P_{k-1}(K)]^d$. The following property of the projection operator and the weak curl was proved in Mu et al. (2015a), but is included here for the sake of completion.

Lemma 4.31.

$$\nabla_w \times (\mathbf{Q}_h \mathbf{u}) = \mathbb{Q}_h(\nabla \times \mathbf{u}) \tag{4.17}$$

Proof. Using the definition of weak curl, integration by parts, and the definition of $\mathbf{Q}_h$ and $\mathbb{Q}_h$, we have: For any $w \in [P_{k-1}(K)]^d$,

$$\begin{aligned}(\nabla_w \times (\mathbf{Q}_h u), \mathbf{w})_K &= (\mathbf{Q}_0 \mathbf{u}, \nabla \times \mathbf{w})_K - \langle (Q_b \mathbf{u}) \times \mathbf{n}, \mathbf{w} \rangle_{\partial K} \\ &= (\mathbf{u}, \nabla \times \mathbf{w})_K - \langle \mathbf{u} \times \mathbf{n}, \mathbf{w} \rangle_{\partial K} \\ &= (\nabla \times \mathbf{u}, \mathbf{w})_K = (\mathbb{Q}_h(\nabla \times \mathbf{u}), \mathbf{w})_K,\end{aligned}$$

which concludes the proof. □

Define the error function at time t as follows:

$$\boldsymbol{\varepsilon}_h = \{\boldsymbol{\varepsilon}_0, \boldsymbol{\varepsilon}_b\} = \{\mathbf{Q}_0 \mathbf{u}(t) - \mathbf{u}_{0h}(t), Q_b \mathbf{u}(t) - \mathbf{u}_{bh}(t)\} \tag{4.18}$$

For simplicity and clarity in the proof, PEC boundary conditions are assumed. However, this result can extend to the more general Dirichlet boundary condition presented in the initial problem.

Lemma 4.32. Let $\mathbf{u}_h$ be the semi-discrete WG finite element solution arising from (4.11) with the PEC boundary condition $\boldsymbol{\phi} = \mathbf{0}$, and $\boldsymbol{\varepsilon}_h$ be the error between the semi-discrete WG finite element solution and the L^2 projection of the exact solution

as defined in (4.18). Then the following error equation is satisfied:

$$(\nu\nabla_w \times \boldsymbol{\varepsilon}_h, \nabla_w \times \mathbf{v}_h)_\Omega + \left(\frac{\partial^2 \boldsymbol{\varepsilon}_0}{\partial t^2}, \mathbf{v}_0\right)_\Omega + s\left(\frac{\partial \boldsymbol{\varepsilon}_h}{\partial t}, \mathbf{v}_h\right) = l(\mathbf{u}, \mathbf{v}_h) + s\left(\frac{\partial \mathbf{Q}_h \mathbf{u}}{\partial t}, \mathbf{v}_h\right), \tag{4.19}$$

where

$$l(\mathbf{u}, \mathbf{v}_h) = \sum_{K \in \mathcal{K}} \langle (I - \mathbb{Q}_h)\nabla \times \mathbf{u}, \nu(\mathbf{v}_{bh} - \mathbf{v}_{0h}) \times \boldsymbol{n}_K \rangle_{\partial K}.$$

Proof. Using Lemma 4.31, the definition of $\mathbf{Q}_h$, the definition of weak curl, and integration by parts, we have

$$\begin{aligned}
(\nu\nabla_w \times (\mathbf{Q}_h \mathbf{u}), \nabla_w \times \mathbf{v}_h)_K &= (\nu\mathbb{Q}_h(\nabla \times \mathbf{u}), \nabla_w \times \mathbf{v}_h)_K \\
&= (\mathbf{v}_{0h}, \nabla \times (\nu\mathbb{Q}(\nabla \times \mathbf{u})))_K - \langle \mathbf{v}_{bh} \times \boldsymbol{n}_K, \nu\mathbb{Q}_h(\nabla \times \mathbf{u}) \rangle_{\partial K} \\
&= (\nabla \times \mathbf{v}_{0h}, \nu\mathbb{Q}(\nabla \times \mathbf{u}))_K \\
&\qquad - \langle (\mathbf{v}_{bh} - \mathbf{v}_{0h}) \times \boldsymbol{n}_K, \nu\mathbb{Q}_h(\nabla \times \mathbf{u}) \rangle_{\partial K} \\
&= (\nu\nabla \times \mathbf{u}, \nabla \times \mathbf{v}_{0h})_K \\
&\qquad - \langle \mathbb{Q}_h(\nabla \times \mathbf{u}), \nu(\mathbf{v}_{bh} - \mathbf{v}_{0h}) \times \boldsymbol{n}_K \rangle_{\partial K}.
\end{aligned} \tag{4.20}$$

Using the definition of $\mathbf{Q}_h$ again, and summing over all elements,

$$\left(\frac{\partial^2 \mathbf{u}}{\partial t^2}, \mathbf{v}_{0h}\right)_\Omega = \left(\mathbf{Q}_0 \frac{\partial^2 \mathbf{u}}{\partial t^2}, \mathbf{v}_{0h}\right)_\Omega = \left(\frac{\partial^2 \mathbf{Q}_0 \mathbf{u}}{\partial t^2}, \mathbf{v}_{0h}\right)_\Omega. \tag{4.21}$$

We then multiply the governing equation (4.2) by $\mathbf{v}_{0h}$ and integrate over the domain to get

$$(\nabla \times (\nu\nabla \times \mathbf{u}), \mathbf{v}_{0h})_\Omega + \left(\frac{\partial^2 \mathbf{u}}{\partial t^2}, \mathbf{v}_{0h}\right)_\Omega = (\boldsymbol{f}, \mathbf{v}_{0h})_\Omega. \tag{4.22}$$

If we use the continuity condition, (4.8), we can see that all integrals of the interior edges cancel. This in addition with the PEC boundary condition $\boldsymbol{\phi} = \mathbf{0}$ gives:

$$\sum_{K \in \mathcal{K}_h} \langle \mathbf{v}_{bh} \times \boldsymbol{n}_K, \nu \nabla \times \mathbf{u} \rangle_{\partial K} = 0.$$

Hence, through integration by parts we have

$$(\nabla \times (\nu \nabla \times \mathbf{u}), \mathbf{v}_{0h}) =$$

$$\sum_{K \in \mathcal{K}_h} (\nu \nabla \times \mathbf{u}, \nabla \times \mathbf{v}_{0h}) - \sum_{K \in \mathcal{K}_h} \langle \nu(\mathbf{v}_{bh} - \mathbf{v}_{0h}) \times \boldsymbol{n}_K, \nabla \times \mathbf{u} \rangle_{\partial K}. \tag{4.23}$$

Observe from that by summing (4.20) over all elements

$$(\nu \nabla \times \mathbf{u}, \nabla \times \mathbf{v}_{0h})_\Omega = (\nu \nabla_w \times (\mathbf{Q}_h \mathbf{u}), \nabla_w \times \mathbf{v}_h)_\Omega$$

$$+ \sum_{K \in \mathcal{K}} \langle \mathbb{Q}_h(\nabla \times \mathbf{u}), \nu(\mathbf{v}_{bh} - \mathbf{v}_{0h}) \times \boldsymbol{n}_K \rangle_{\partial K}. \tag{4.24}$$

Therefore, combining (4.24) and (4.23) we get

$$(\nabla \times (\nu \nabla \times \mathbf{u}), \mathbf{v}_{0h}) = (\nu \nabla_w \times (\mathbf{Q}_h \mathbf{u}), \nabla_w \times \mathbf{v}_h)$$

$$- \sum_{K \in \mathcal{K}_h} \langle (I - \mathbb{Q}_h) \nabla \times \mathbf{u}, \nu(\mathbf{v}_{bh} - \mathbf{v}_{0h}) \times \boldsymbol{n}_K \rangle_{\partial K}. \tag{4.25}$$

Plugging (4.25) and (4.21) into (4.22), adding $s\left(\frac{\partial \mathbf{Q}_h \mathbf{u}}{\partial t}, \mathbf{v}_h\right)$, and subtracting the scheme (4.11) then gives the desired result:

$$(\nu \nabla_w \times \boldsymbol{\varepsilon}_h, \nabla_w \times \mathbf{v}_h) + \left(\frac{\partial^2 \boldsymbol{\varepsilon}_0}{\partial t^2}, \mathbf{v}_{0h}\right) + s\left(\frac{\partial \boldsymbol{\varepsilon}_h}{\partial t}, \mathbf{v}_h\right)$$

$$= l(\mathbf{u}, \mathbf{v}_h) + s\left(\frac{\partial \mathbf{Q}_h \mathbf{u}}{\partial t}, \mathbf{v}_h\right). \tag{4.26}$$

□

The following lemma provides a spatial error bound for the scheme. Its proof can be found in Mu et al. (2015a).

Lemma 4.33. Let $\mathbf{w} \in [H^{p+1}(\Omega)]^d$ and $v_h \in V_h$ with $\frac{1}{2} < p \leq k$. Then we have

$$|s(\mathbf{Q}_h\mathbf{w}, \mathbf{v}_h)| \leq Ch^p||\mathbf{w}||_{p+1}|\mathbf{v}_h|_{1,h}, \tag{4.27}$$

$$|l(\mathbf{w}, \mathbf{v}_h)| \leq Ch^p||\mathbf{w}||_{p+1}|\mathbf{v}_h|_{1,h}. \tag{4.28}$$

With this, we are now ready to present the error bound for the weak Galerkin semi-discrete scheme.

Theorem 4.32. The semi-discrete weak Galerkin scheme (4.11) with PEC boundary condition, $\boldsymbol{\phi} = \mathbf{0}$, satisfies the following error estimate: For any $\tau \in (0, T]$,

$$\begin{aligned}\nu||\nabla_w \times \boldsymbol{\varepsilon}_h(\tau)||^2 + \left|\left|\frac{\partial \boldsymbol{\varepsilon}_0(\tau)}{\partial t}\right|\right|^2 + \int_0^\tau \left|\frac{\partial \boldsymbol{\varepsilon}_h}{\partial t}\right|_{1,h}^2 dt \\ \leq \nu\,||\nabla_w \times \boldsymbol{\varepsilon}_h(0)||^2 + \left|\left|\frac{\partial \boldsymbol{\varepsilon}_0(0)}{\partial t}\right|\right|^2 \\ + Ch^{2p}\int_0^\tau \left(||\mathbf{u}||_{p+1}^2 + \left|\left|\frac{\partial \mathbf{u}}{\partial t}\right|\right|_{p+1}^2\right) dt\end{aligned} \tag{4.29}$$

where the constant $C > 0$ is independent of time t and the mesh size h. In conclusion, assuming no initial errors, the semi-discrete weak Galerkin scheme's error is of order $O(h^p)$ in the energy norm.

Proof. If we let $\mathbf{v}_h = \{\partial_t \boldsymbol{\varepsilon}_0, \partial_t \boldsymbol{\varepsilon}_b\}$ in Lemma 4.32, we get

$$\frac{\nu}{2}\frac{\partial}{\partial t}||\nabla_w \times \boldsymbol{\varepsilon}_h||^2 + \frac{1}{2}\frac{\partial}{\partial t}\left|\left|\frac{\partial \boldsymbol{\varepsilon}_0}{\partial t}\right|\right|^2 + \left|\frac{\partial \boldsymbol{\varepsilon}_h}{\partial t}\right|_{1,h}^2 = l\left(\mathbf{u}, \frac{\partial \boldsymbol{\varepsilon}_h}{\partial t}\right) + s\left(\frac{\partial \mathbf{Q}_h\mathbf{u}}{\partial t}, \frac{\partial \boldsymbol{\varepsilon}_h}{\partial t}\right). \tag{4.30}$$

We then apply Lemma 4.33, to obtain

$$\begin{aligned}\frac{\nu}{2}\frac{\partial}{\partial t}||\nabla_w \times \boldsymbol{\varepsilon}_h||^2 + \frac{1}{2}\frac{\partial}{\partial t}\left|\left|\frac{\partial \boldsymbol{\varepsilon}_0}{\partial t}\right|\right|^2 + \left|\frac{\partial \boldsymbol{\varepsilon}_h}{\partial t}\right|_{1,h}^2 \\ \leq Ch^p\left(||\mathbf{u}||_{p+1} + \left|\left|\frac{\partial \mathbf{u}}{\partial t}\right|\right|_{p+1}\right)\left|\frac{\partial \boldsymbol{\varepsilon}_h}{\partial t}\right|_{1,h}.\end{aligned} \tag{4.31}$$

By Young's inequality, and rearranging terms we see that

$$\frac{\nu}{2}\frac{\partial}{\partial t}\left|\left|\nabla_w \times \boldsymbol{\varepsilon}_h\right|\right|^2 + \frac{1}{2}\frac{\partial}{\partial t}\left|\left|\frac{\partial \boldsymbol{\varepsilon}_0}{\partial t}\right|\right|^2 + \frac{1}{2}\left|\frac{\partial \boldsymbol{\varepsilon}_h}{\partial t}\right|_{1,h}^2 \leq \frac{1}{2}Ch^{2p}\left(||\mathbf{u}||_{p+1}^2 + \left|\left|\frac{\partial \mathbf{u}}{\partial t}\right|\right|_{p+1}^2\right). \tag{4.32}$$

Integration from $t = 0$ to τ completes the proof. □

4.4 The Fully-discrete Scheme

To discretize (4.11) further in time, we divide $[0, T]$ by $N + 1$ uniformly spaced points $t^j, j = 0, \cdots, N$, where the time step size $\Delta t = T/N$. Define $\mathbf{u}_h^n = \mathbf{u}_h(t^n)$ as the value of $\mathbf{u}_h$ at t^n. We propose the following fully-discrete scheme.

Fully-discrete Weak Galerkin Algorithm. Find $\mathbf{u}_h^{n+1} = \{\mathbf{u}_{0h}^{n+1}, \mathbf{u}_{bh}^{n+1}\} \in V_h$ satisfying $\mathbf{u}_{bh}^{n+1} \times \boldsymbol{n}_\Omega = Q_b\boldsymbol{\phi}^{n+1}$ on $\partial\Omega$ and

$$\left(\nu\nabla_w \times \frac{\mathbf{u}_h^{n+1} + \mathbf{u}_h^{n-1}}{2}, \nabla_w \times \mathbf{v}_h\right)_\Omega + \left(\frac{\mathbf{u}_{0h}^{n+1} - 2\mathbf{u}_{0h}^n + \mathbf{u}_{0h}^{n-1}}{\Delta t^2}, \mathbf{v}_{0h}\right)_\Omega + s\left(\frac{\mathbf{u}_h^{n+1} - \mathbf{u}_h^{n-1}}{2\Delta t}, \mathbf{v}_h\right) = (\boldsymbol{f}^n, \mathbf{v}_{0h})_\Omega \quad \forall \mathbf{v}_h \in V_h^0, \tag{4.33}$$

where $Q_b\boldsymbol{\phi}^{n+1}$ is an approximation of the boundary value $\boldsymbol{\phi}(t^{n+1})$ in the polynomial space $[P_k(\partial K \cap \partial\Omega)]^d$, defined in Section 4.3

Stability of the implicit, fully-discrete scheme

Theorem 4.41. Under the assumption that $\Delta t < 1$, the following stability result holds for our fully-discrete weak Galerkin finite element scheme (4.33):

$$\begin{aligned}
&\nu(||\nabla_w \times \mathbf{u}_h^N||^2 + ||\nabla_w \times \mathbf{u}_h^{N-1}||^2) + \frac{1}{2}\left|\left|\frac{\mathbf{u}_{0h}^N - \mathbf{u}_{0h}^{N-1}}{\Delta t}\right|\right|^2 \\
&\qquad + 2\Delta t \sum_{n=1}^{N-1} \left|\frac{\mathbf{u}_h^{n+1} - \mathbf{u}_h^{n-1}}{2\Delta t}\right|_{1,h}^2 \\
&\leq C \exp(N \cdot \Delta t) \left[\nu(||\nabla_w \times \mathbf{u}_h^1||^2 + ||\nabla_w \times \mathbf{u}_h^0||^2) + \left|\left|\frac{\mathbf{u}_{0h}^1 - \mathbf{u}_{0h}^0}{\Delta t}\right|\right|^2 \right. \\
&\qquad \left. + \Delta t \sum_{n=1}^{N-1} ||\boldsymbol{f}^n||^2\right]. \qquad (4.34)
\end{aligned}$$

where the constant C is independent of the mesh size h and time step size Δt. In conclusion, the scheme is unconditionally stable.

Proof. We begin by letting $\mathbf{v}_h = \mathbf{u}_h^{n+1} - \mathbf{u}_h^{n-1}$ in (4.33) to get

$$\begin{aligned}
&\left(\nu \nabla_w \times \frac{\mathbf{u}_h^{n+1} + \mathbf{u}_h^{n-1}}{2}, \nabla_w \times (\mathbf{u}_h^{n+1} - \mathbf{u}_h^{n-1})\right) \\
&\qquad + \left(\frac{\mathbf{u}_{0h}^{n+1} - 2\mathbf{u}_{0h}^n + \mathbf{u}_{0h}^{n-1}}{\Delta t^2}, \mathbf{u}_{0h}^{n+1} - \mathbf{u}_0^{n-1}\right) \\
&\qquad + s\left(\frac{\mathbf{u}_h^{n+1} - \mathbf{u}_h^{n-1}}{2\Delta t}, \mathbf{u}_h^{n+1} - \mathbf{u}_h^{n-1}\right) = (\boldsymbol{f}^n, \mathbf{u}_{0h}^{n+1} - \mathbf{u}_{0h}^{n-1}), \qquad (4.35)
\end{aligned}$$

which can be rewritten as follows:

$$\begin{aligned}
&\frac{\nu}{2}(||\nabla_w \times \mathbf{u}_h^{n+1}||^2 - ||\nabla_w \times \mathbf{u}_h^{n-1})||^2) + \left|\left|\frac{\mathbf{u}_{0h}^{n+1} - \mathbf{u}_{0h}^n}{\Delta t}\right|\right|^2 - \left|\left|\frac{\mathbf{u}_{0h}^n - \mathbf{u}_{0h}^{n-1}}{\Delta t}\right|\right|^2 \\
&\qquad + 2\Delta t \left|\frac{\mathbf{u}_h^{n+1} - \mathbf{u}_h^{n-1}}{2\Delta t}\right|_{1,h}^2 = (\boldsymbol{f}^n, \mathbf{u}_{0h}^{n+1} - \mathbf{u}_{0h}^{n-1}). \qquad (4.36)
\end{aligned}$$

Applying the Cauchy-Schwarz, and Young's inequalities to the right hand side, we have

$$(\boldsymbol{f}^n, \mathbf{u}_{0h}^{n+1} - \mathbf{u}_{0h}^{n-1}) \leq 2\Delta t ||\boldsymbol{f}^n||^2 + \frac{\Delta t}{8}\left|\left|\frac{\mathbf{u}_{0h}^{n+1} - \mathbf{u}_{0h}^{n-1}}{\Delta t}\right|\right|^2$$

$$\leq 2\Delta t||\boldsymbol{f}^n||^2 + \frac{\Delta t}{4}\left(\left|\left|\frac{\mathbf{u}_{0h}^{n+1}-\mathbf{u}_{0h}^{n}}{\Delta t}\right|\right|^2 + \left|\left|\frac{\mathbf{u}_{0h}^{n}-\mathbf{u}_{0h}^{n-1}}{\Delta t}\right|\right|^2\right). \quad (4.37)$$

If we substitute this into (4.36) and sum the result from $n = 1$ to $n = N-1$ we get that

$$\begin{aligned}\frac{\nu}{2}(||\nabla_w \times \mathbf{u}_h^N||^2 + ||\nabla_w \times \mathbf{u}_h^{N-1}||^2 - ||\nabla_w \times \mathbf{u}_h^1||^2 - ||\nabla_w \times \mathbf{u}_h^0||^2) + \left|\left|\frac{\mathbf{u}_{0h}^{N}-\mathbf{u}_{0h}^{N-1}}{\Delta t}\right|\right|^2 \\ - \left|\left|\frac{\mathbf{u}_{0h}^{1}-\mathbf{u}_{0h}^{0}}{\Delta t}\right|\right|^2 + 2\Delta t\sum_{n=1}^{N-1}\left|\frac{\mathbf{u}_h^{n+1}-\mathbf{u}_h^{n-1}}{2\Delta t}\right|_{1,h}^2 \\ \leq 2\Delta t\sum_{n=1}^{N-1}||\boldsymbol{f}^n||^2 + \frac{\Delta t}{4}\sum_{n=1}^{N-1}\left(\left|\left|\frac{\mathbf{u}_{0h}^{n+1}-\mathbf{u}_{0h}^{n}}{\Delta t}\right|\right|^2 + \left|\left|\frac{\mathbf{u}_{0h}^{n}-\mathbf{u}_{0h}^{n-1}}{\Delta t}\right|\right|^2\right) \\ \leq 2\Delta t\sum_{n=1}^{N-1}||\boldsymbol{f}^n||^2 + \frac{\Delta t}{2}\sum_{n=0}^{N-1}\left|\left|\frac{\mathbf{u}_{0h}^{n+1}-\mathbf{u}_{0h}^{n}}{\Delta t}\right|\right|^2. \quad (4.38)\end{aligned}$$

Assuming that $\frac{\Delta t}{2} < \frac{1}{2}$, we can subtract $\frac{\Delta t}{2}\left|\left|\frac{\mathbf{u}_{0h}^{N}-\mathbf{u}_{0h}^{N-1}}{\Delta t}\right|\right|^2$ from both sides to get

$$\begin{aligned}\frac{\nu}{2}(||\nabla_w \times \mathbf{u}_h^N||^2 + ||\nabla_w \times \mathbf{u}_h^{N-1}||^2 - ||\nabla_w \times \mathbf{u}_h^1||^2 - ||\nabla_w \times \mathbf{u}_h^0)||^2) \\ + \frac{1}{2}\left|\left|\frac{\mathbf{u}_{0h}^{N}-\mathbf{u}_{0h}^{N-1}}{\Delta t}\right|\right|^2 - \left|\left|\frac{\mathbf{u}_{0h}^{1}-\mathbf{u}_{0h}^{0}}{\Delta t}\right|\right|^2 + 2\Delta t\sum_{n=1}^{N-1}\left|\frac{\mathbf{u}_h^{n+1}-\mathbf{u}_h^{n-1}}{2\Delta t}\right|_{1,h}^2 \\ \leq 2\Delta t\sum_{n=1}^{N-1}||\boldsymbol{f}^n||^2 + \frac{\Delta t}{2}\sum_{n=0}^{N-2}\left|\left|\frac{\mathbf{u}_{0h}^{n+1}-\mathbf{u}_{0h}^{n}}{\Delta t}\right|\right|^2. \quad (4.39)\end{aligned}$$

The proof is complete by applying the discrete Grönwall's inequality to the above inequality. □

Error analysis for the fully-discrete scheme

Define the error function at time step n to be

$$\boldsymbol{\varepsilon}_h^n = \{\boldsymbol{\varepsilon}_0^n, \boldsymbol{\varepsilon}_b^n\} = \{\mathbf{Q}_0\mathbf{u}(t^n) - \mathbf{u}_{0h}^n, Q_b\mathbf{u}(t^n) - \mathbf{u}_{bh}^n\}. \quad (4.40)$$

The following error equations then hold for the fully-discrete WG scheme.

Lemma 4.41. Let $\mathbf{u}_h^{n+1}$ be the fully-discrete WG finite element solution arising from (4.33) with PEC boundary condition $\boldsymbol{\phi} = \mathbf{0}$, and $\boldsymbol{\varepsilon}_h^n$ be the error as defined in (4.40). Then the following error equation is satisfied:

$$\begin{aligned}
&\left(\nu\nabla_w \times \frac{\boldsymbol{\varepsilon}_h^{n+1} + \boldsymbol{\varepsilon}_h^{n-1}}{2}, \nabla_w \times \mathbf{v}_h\right) + \left(\frac{\boldsymbol{\varepsilon}_0^{n+1} - 2\boldsymbol{\varepsilon}_0^n + \boldsymbol{\varepsilon}_0^{n-1}}{\Delta t^2}, \mathbf{v}_{0h}\right) \\
&\quad + s\left(\frac{\boldsymbol{\varepsilon}_h^{n+1} - \boldsymbol{\varepsilon}_h^{n-1}}{2\Delta t}, \mathbf{v}_h\right) \\
&= l(\mathbf{u}(t^n), \mathbf{v}_h) + s\left(\frac{\mathbf{Q}_h\mathbf{u}(t^{n+1}) - \mathbf{Q}_h\mathbf{u}(t^{n-1})}{2\Delta t}, \mathbf{v}_h\right) \\
&\quad + \left(\frac{\mathbf{Q}_0\mathbf{u}(t^{n+1}) - 2\mathbf{Q}_0\mathbf{u}(t^n) + \mathbf{Q}_0\mathbf{u}(t^{n-1})}{\Delta t^2} - \frac{\partial^2\mathbf{Q}_0\mathbf{u}}{\partial t^2}(t^n), \mathbf{v}_{0h}\right) \\
&\quad + \left(\nu\nabla_w \times \left(\frac{\mathbf{Q}_h\mathbf{u}(t^{n+1}) + \mathbf{Q}_h\mathbf{u}(t^{n-1})}{2} - \mathbf{Q}_h\mathbf{u}(t^n)\right), \nabla_w \times \mathbf{v}_h\right).
\end{aligned}$$

Proof. Evaluating (4.21), (4.22), and (4.25) at $t = t^n$ results in the following 3 equations:

$$\left(\frac{\partial^2\mathbf{u}}{\partial t^2}(t^n), \mathbf{v}_{0h}\right)_\Omega = \left(\mathbf{Q}_0\frac{\partial^2\mathbf{u}}{\partial t^2}(t^n), \mathbf{v}_{0h}\right)_\Omega = \left(\frac{\partial^2\mathbf{Q}_0\mathbf{u}}{\partial t^2}(t^n), \mathbf{v}_{0h}\right)_\Omega, \tag{4.41}$$

$$(\nabla \times (\nu\nabla \times \mathbf{u}(t^n)), \mathbf{v}_{0h})_\Omega + \left(\frac{\partial^2\mathbf{u}}{\partial t^2}(t^n), \mathbf{v}_{0h}\right)_\Omega = (\boldsymbol{f}^n, \mathbf{v}_{0h})_\Omega, \tag{4.42}$$

and

$$\begin{aligned}
(\nabla \times (\nu\nabla \times \mathbf{u}(t^n)), \mathbf{v}_{0h})_\Omega &= (\nu\nabla_w \times (\mathbf{Q}_h\mathbf{u}(t^n)), \nabla_w \times \mathbf{v}_h)_\Omega \\
&\quad - \sum_{K\in\mathcal{K}_h} \langle (I - \mathbb{Q}_h)\nabla \times \mathbf{u}(t^n), \nu(\mathbf{v}_{bh} - \mathbf{v}_{0h}) \times \boldsymbol{n}_K\rangle_{\partial K}.
\end{aligned} \tag{4.43}$$

If we add a stabilization term, $s\left(\frac{\mathbf{Q}_h\mathbf{u}(t^{n+1}) - \mathbf{Q}_h\mathbf{u}(t^{n-1})}{2\Delta t}, \mathbf{v}_h\right)$, to both sides of (4.42), plug in (4.43) and (4.41), and subtract the scheme (4.33), we obtain

$$(\nu\nabla_w \times (\mathbf{Q}_h\mathbf{u}(t^n)), \nabla_w \times \mathbf{v}_h)_\Omega - \left(\nu\nabla_w \times \frac{\mathbf{u}_h^{n+1} + \mathbf{u}_h^{n-1}}{2}, \nabla_w \times \mathbf{v}_h\right)_\Omega$$

$$+\left(\frac{\partial^2 \mathbf{Q}_0\mathbf{u}}{\partial t^2}(t^n),\mathbf{v}_{0h}\right)_\Omega-\left(\frac{\mathbf{u}_{0h}^{n+1}-2\mathbf{u}_{0h}^{n}+\mathbf{u}_{0h}^{n-1}}{\Delta t^2},\mathbf{v}_{0h}\right)_\Omega+s\left(\frac{\boldsymbol{\varepsilon}_h^{n+1}-\boldsymbol{\varepsilon}_h^{n-1}}{2\Delta t},\mathbf{v}_h\right)$$
$$=l(\mathbf{u}(t^n),\mathbf{v}_h)+s\left(\frac{\mathbf{Q}_h\mathbf{u}(t^{n+1})-\mathbf{Q}_h\mathbf{u}(t^{n-1})}{2\Delta t},\mathbf{v}_h\right), \tag{4.44}$$

by definition of $l(\cdot,\cdot)$ in lemma 4.32.

Adding $\left(\frac{\mathbf{Q}_0\mathbf{u}(t^{n+1})-2\mathbf{Q}_0\mathbf{u}(t^n)+\mathbf{Q}_0\mathbf{u}(t^{n-1})}{\Delta t^2},\mathbf{v}_{0h}\right)_\Omega$ to both sides of (4.44), and rearranging terms gives us

$$\begin{aligned}&(\nu\nabla_w\times(\mathbf{Q}_h\mathbf{u}(t^n)),\nabla_w\times\mathbf{v}_h)_\Omega-\left(\nu\nabla_w\times\frac{\mathbf{u}_h^{n+1}+\mathbf{u}_h^{n-1}}{2},\nabla_w\times\mathbf{v}_h\right)_\Omega\\&\quad+\left(\frac{\boldsymbol{\varepsilon}_0^{n+1}-2\boldsymbol{\varepsilon}_0^{n}+\boldsymbol{\varepsilon}_0^{n-1}}{\Delta t^2},\mathbf{v}_{0h}\right)_\Omega+s\left(\frac{\boldsymbol{\varepsilon}_h^{n+1}-\boldsymbol{\varepsilon}_h^{n-1}}{2\Delta t},\mathbf{v}_h\right)\\&=l(\mathbf{u}(t^n),\mathbf{v}_h)+s\left(\frac{\mathbf{Q}_h\mathbf{u}(t^{n+1})-\mathbf{Q}_h\mathbf{u}(t^{n-1})}{2\Delta t},\mathbf{v}_h\right)\\&\quad+\left(\frac{\mathbf{Q}_0\mathbf{u}(t^{n+1})-2\mathbf{Q}_0\mathbf{u}(t^n)+\mathbf{Q}_0\mathbf{u}(t^{n-1})}{\Delta t^2}-\frac{\partial^2\mathbf{Q}_0\mathbf{u}(t^n)}{\partial t^2},\mathbf{v}_{0h}\right)_\Omega.\end{aligned} \tag{4.45}$$

Finally, we add $\left(\nu\nabla_w\times\frac{\mathbf{Q}_h\mathbf{u}(t^{n+1})+\mathbf{Q}_h\mathbf{u}(t^{n-1})}{2},\nabla_w\times\mathbf{v}_h\right)_\Omega$ to both sides, and rearrange some terms to arrive at the desired result. □

The following lemma will be used to provide a time error estimate for the fully-discrete weak Galerkin scheme. Its proof is a straightforward consequence of Taylor's remainder theorem, and so it will not be included here.

Lemma 4.42. For any $1\le n\le N-1$,

$$\left|\left|\frac{\mathbf{u}(t^{n+1})-2\mathbf{u}(t^n)+\mathbf{u}(t^{n-1})}{\Delta t^2}-\frac{\partial^2\mathbf{u}}{\partial t^2}(t^n)\right|\right|^2\le\frac{\Delta t^3}{126}\int_{t^{n-1}}^{t^{n+1}}\left|\left|\frac{\partial^4\mathbf{u}}{\partial t^4}\right|\right|^2dt, \tag{4.46}$$

and

$$\left|\left|\frac{\mathbf{u}(t^{n+1})+\mathbf{u}(t^{n-1})}{2}-\mathbf{u}(t^n)\right|\right|^2\le\frac{\Delta t^3}{6}\int_{t^{n-1}}^{t^{n+1}}\left|\left|\frac{\partial^2\mathbf{u}}{\partial t^2}\right|\right|^2dt. \tag{4.47}$$

With these results, we are now ready for the error estimate for the fully-discrete weak Galerkin scheme.

Theorem 4.42. For $\Delta t < 1$, the fully-discrete weak Galerkin scheme (4.33) with PEC boundary condition, $\boldsymbol{\phi} = \mathbf{0}$, satisfies the following error estimate:

$$\begin{aligned}
&\frac{\nu}{2}(||\nabla_w \times \boldsymbol{\varepsilon}_h^m||^2 + ||\nabla_w \times \boldsymbol{\varepsilon}_h^{m-1}||^2) + \frac{1}{2}\left|\left|\frac{\boldsymbol{\varepsilon}_0^m - \boldsymbol{\varepsilon}_0^{m-1}}{\Delta t}\right|\right|^2 + \Delta t \sum_{n=1}^{m-1}\left|\frac{\boldsymbol{\varepsilon}_h^{n+1} - \boldsymbol{\varepsilon}_h^{n-1}}{2\Delta t}\right|_{1,h}^2 \\
&\qquad \leq C\exp(T)[\frac{\nu}{2}(||\nabla_w \times \boldsymbol{\varepsilon}_h^1||^2 + ||\nabla_w \times \boldsymbol{\varepsilon}_h^0||^2) + \left|\left|\frac{\boldsymbol{\varepsilon}_0^1 - \boldsymbol{\varepsilon}_0^0}{\Delta t}\right|\right|^2 \\
&\qquad\quad + \Delta t^4\left(\int_0^T \left|\left|\frac{\partial^4 \mathbf{u}}{\partial t^4}\right|\right|^2 dt + \int_0^T \left|\left|\nabla \times \nu\nabla \times \frac{\partial^2 \mathbf{u}}{\partial t^2}\right|\right|^2 dt\right) \\
&\qquad\quad + h^{2p}\Delta t \sum_{n=1}^{m-1}\left(||\mathbf{u}(t^n)||_{p+1} + \left|\left|\frac{\mathbf{u}(t^{n+1}) - \mathbf{u}(t^{n-1})}{2\Delta t}\right|\right|_{p+1}\right)^2],
\end{aligned}$$

where, $m \geq 2$, and the constant $C > 0$ is independent of the time step Δt and the mesh size h. In conclusion, assuming there are no initial errors, the fully-discrete weak Galerkin scheme's error is of order $O(\Delta t^2 + h^p)$ in the energy norm.

Proof. Letting $\mathbf{v}_h = \boldsymbol{\varepsilon}_h^{n+1} - \boldsymbol{\varepsilon}_h^{n-1}$ in Lemma 4.41, and applying Lemma 4.33, we have

$$\begin{aligned}
&\frac{\nu}{2}\left|\left|\nabla_w \times \boldsymbol{\varepsilon}_h^{n+1}\right|\right|^2 - \frac{\nu}{2}\left|\left|\nabla_w \times \boldsymbol{\varepsilon}_h^{n-1}\right|\right|^2 + \left|\left|\frac{\boldsymbol{\varepsilon}_0^{n+1} - \boldsymbol{\varepsilon}_0^n}{\Delta t}\right|\right|^2 - \left|\left|\frac{\boldsymbol{\varepsilon}_0^n - \boldsymbol{\varepsilon}_0^{n-1}}{\Delta t}\right|\right|^2 \\
&\qquad + 2\Delta t\left|\frac{\boldsymbol{\varepsilon}_h^{n+1} - \boldsymbol{\varepsilon}_h^{n-1}}{2\Delta t}\right|_{1,h}^2 \\
&\leq Ch^p\left|\left|\mathbf{u}(t^n)\right|\right|_{p+1}\left|\boldsymbol{\varepsilon}_h^{n+1} - \boldsymbol{\varepsilon}_h^{n-1}\right|_{1,h} \\
&\qquad + Ch^p\left|\left|\frac{\mathbf{u}(t^{n+1}) - \mathbf{u}(t^{n-1})}{2\Delta t}\right|\right|_{p+1}\left|\boldsymbol{\varepsilon}_h^{n+1} - \boldsymbol{\varepsilon}_h^{n-1}\right|_{1,h} \\
&\qquad + \left(\frac{\mathbf{Q}_0\mathbf{u}(t^{n+1}) - 2\mathbf{Q}_0\mathbf{u}(t^n) + \mathbf{Q}_0\mathbf{u}(t^{n-1})}{\Delta t^2} - \frac{\partial^2 \mathbf{Q}_0\mathbf{u}}{\partial t^2}(t^n), \boldsymbol{\varepsilon}_0^{n+1} - \boldsymbol{\varepsilon}_0^{n-1}\right)_\Omega \\
&\qquad + \left(\nu\nabla_w \times \left(\frac{\mathbf{Q}_h\mathbf{u}(t^{n+1}) + \mathbf{Q}_h\mathbf{u}(t^{n-1})}{2} - \mathbf{Q}_h\mathbf{u}(t^n)\right), \nabla_w \times (\boldsymbol{\varepsilon}_h^{n+1} - \boldsymbol{\varepsilon}_h^{n-1})\right)_\Omega.
\end{aligned} \tag{4.48}$$

Then, if we apply Lemma 4.31, Young's inequality and the definition of the $\mathbf{Q}_0$ and

$\mathbb{Q}_h$ projections, we get

$$\begin{aligned}
&\frac{\nu}{2}\left|\left|\nabla_w \times \boldsymbol{\varepsilon}_h^{n+1}\right|\right|^2 - \frac{\nu}{2}\left|\left|\nabla_w \times \boldsymbol{\varepsilon}_h^{n-1}\right|\right|^2 + \left|\left|\frac{\boldsymbol{\varepsilon}_0^{n+1}-\boldsymbol{\varepsilon}_0^{n}}{\Delta t}\right|\right|^2 - \left|\left|\frac{\boldsymbol{\varepsilon}_0^{n}-\boldsymbol{\varepsilon}_0^{n-1}}{\Delta t}\right|\right|^2 \\
&\qquad + 2\Delta t\left|\frac{\boldsymbol{\varepsilon}_h^{n+1}-\boldsymbol{\varepsilon}_h^{n-1}}{2\Delta t}\right|_{1,h}^2 \\
&\leq Ch^{2p}\Delta t\left(\left|\left|\mathbf{u}(t^n)\right|\right|_{p+1} + \left|\left|\frac{\mathbf{u}(t^{n+1})-\mathbf{u}(t^{n-1})}{2\Delta t}\right|\right|_{p+1}\right)^2 + \Delta t\left|\frac{\boldsymbol{\varepsilon}_h^{n+1}-\boldsymbol{\varepsilon}_h^{n-1}}{2\Delta t}\right|_{1,h}^2 \\
&\qquad + \left(\frac{\mathbf{u}(t^{n+1})-2\mathbf{u}(t^n)+\mathbf{u}(t^{n-1})}{\Delta t^2} - \frac{\partial^2 \mathbf{u}}{\partial t^2}(t^n), \boldsymbol{\varepsilon}_0^{n+1}-\boldsymbol{\varepsilon}_0^{n-1}\right)_\Omega \\
&\qquad + \left(\nu\nabla\times\left(\frac{\mathbf{u}(t^{n+1})+\mathbf{u}(t^{n-1})}{2} - \mathbf{u}(t^n)\right), \nabla_w \times (\boldsymbol{\varepsilon}_h^{n+1}-\boldsymbol{\varepsilon}_h^{n-1})\right)_\Omega . \qquad (4.49)
\end{aligned}$$

Using the definition of the weak curl operator, the fact that all boundary integrals cancel out due to the unique boundary definition, and the PEC boundary condition gives us

$$\begin{aligned}
&\frac{\nu}{2}\left|\left|\nabla_w \times \boldsymbol{\varepsilon}_h^{n+1}\right|\right|^2 - \frac{\nu}{2}\left|\left|\nabla_w \times \boldsymbol{\varepsilon}_h^{n-1}\right|\right|^2 + \left|\left|\frac{\boldsymbol{\varepsilon}_0^{n+1}-\boldsymbol{\varepsilon}_0^{n}}{\Delta t}\right|\right|^2 - \left|\left|\frac{\boldsymbol{\varepsilon}_0^{n}-\boldsymbol{\varepsilon}_0^{n-1}}{\Delta t}\right|\right|^2 \\
&\qquad + 2\Delta t\left|\frac{\boldsymbol{\varepsilon}_h^{n+1}-\boldsymbol{\varepsilon}_h^{n-1}}{2\Delta t}\right|_{1,h}^2 \\
&\leq Ch^{2p}\Delta t\left(\left|\left|\mathbf{u}(t^n)\right|\right|_{p+1} + \left|\left|\frac{\mathbf{u}(t^{n+1})-\mathbf{u}(t^{n-1})}{2\Delta t}\right|\right|_{p+1}\right)^2 + \Delta t\left|\frac{\boldsymbol{\varepsilon}_h^{n+1}-\boldsymbol{\varepsilon}_h^{n-1}}{2\Delta t}\right|_{1,h}^2 \\
&\qquad + \left(\frac{\mathbf{u}(t^{n+1})-2\mathbf{u}(t^n)+\mathbf{u}(t^{n-1})}{\Delta t^2} - \frac{\partial^2 \mathbf{u}}{\partial t^2}(t^n), \boldsymbol{\varepsilon}_0^{n+1}-\boldsymbol{\varepsilon}_0^{n-1}\right)_\Omega \\
&\qquad + \left(\nabla\times\nu\nabla\times\left(\frac{\mathbf{u}(t^{n+1})+\mathbf{u}(t^{n-1})}{2} - \mathbf{u}(t^n)\right), \boldsymbol{\varepsilon}_0^{n+1}-\boldsymbol{\varepsilon}_0^{n-1}\right)_\Omega . \qquad (4.50)
\end{aligned}$$

Applying the Cauchy-Schwarz and Young's inequalities and rearranging terms, we further have

$$\begin{aligned}
&\frac{\nu}{2}\left|\left|\nabla_w \times \boldsymbol{\varepsilon}_h^{n+1}\right|\right|^2 - \frac{\nu}{2}\left|\left|\nabla_w \times \boldsymbol{\varepsilon}_h^{n-1}\right|\right|^2 + \left|\left|\frac{\boldsymbol{\varepsilon}_0^{n+1}-\boldsymbol{\varepsilon}_0^{n}}{\Delta t}\right|\right|^2 - \left|\left|\frac{\boldsymbol{\varepsilon}_0^{n}-\boldsymbol{\varepsilon}_0^{n-1}}{\Delta t}\right|\right|^2 \\
&\qquad + \Delta t\left|\frac{\boldsymbol{\varepsilon}_h^{n+1}-\boldsymbol{\varepsilon}_h^{n-1}}{2\Delta t}\right|_{1,h}^2
\end{aligned}$$

$$
\begin{aligned}
&\leq Ch^{2p}\Delta t\left(||\mathbf{u}(t^n)||_{p+1}+\left|\left|\frac{\mathbf{u}(t^{n+1})-\mathbf{u}(t^{n-1})}{2\Delta t}\right|\right|_{p+1}\right)^2\\
&\quad+4\Delta t\left|\left|\frac{\mathbf{u}(t^{n+1})-2\mathbf{u}(t^n)+\mathbf{u}(t^{n-1})}{\Delta t^2}-\frac{\partial^2\mathbf{u}}{\partial t^2}(t^n)\right|\right|^2+\frac{\Delta t}{16}\left|\left|\frac{\boldsymbol{\varepsilon}_0^{n+1}-\boldsymbol{\varepsilon}_0^{n-1}}{\Delta t}\right|\right|^2\\
&\quad+4\Delta t\left|\left|\nabla\times\nu\nabla\times\left(\frac{\mathbf{u}(t^{n+1})+\mathbf{u}(t^{n-1})}{2}-\mathbf{u}(t^n)\right)\right|\right|^2+\frac{\Delta t}{16}\left|\left|\frac{\boldsymbol{\varepsilon}_0^{n+1}-\boldsymbol{\varepsilon}_0^{n-1}}{\Delta t}\right|\right|^2\\
&\leq Ch^{2p}\Delta t\left(||\mathbf{u}(t^n)||_{p+1}+\left|\left|\frac{\mathbf{u}(t^{n+1})-\mathbf{u}(t^{n-1})}{2\Delta t}\right|\right|_{p+1}\right)^2+\frac{\Delta t}{4}\left|\left|\frac{\boldsymbol{\varepsilon}_0^{n+1}-\boldsymbol{\varepsilon}_0^{n}}{\Delta t}\right|\right|^2\\
&\quad+4\Delta t\left|\left|\frac{\mathbf{u}(t^{n+1})-2\mathbf{u}(t^n)+\mathbf{u}(t^{n-1})}{\Delta t^2}-\frac{\partial^2\mathbf{u}}{\partial t^2}(t^n)\right|\right|^2+\frac{\Delta t}{4}\left|\left|\frac{\boldsymbol{\varepsilon}_0^{n}-\boldsymbol{\varepsilon}_0^{n-1}}{\Delta t}\right|\right|^2\\
&\quad+4\Delta t\left|\left|\nabla\times\nu\nabla\times\left(\frac{\mathbf{u}(t^{n+1})+\mathbf{u}(t^{n-1})}{2}-\mathbf{u}(t^n)\right)\right|\right|^2. \qquad (4.51)
\end{aligned}
$$

If we sum the resulting terms from $n=1$ to $m-1$, we obtain

$$
\begin{aligned}
&\frac{\nu}{2}\left(\left|\left|\nabla_w\times\boldsymbol{\varepsilon}_h^m\right|\right|^2+\left|\left|\nabla_w\times\boldsymbol{\varepsilon}_h^{m-1}\right|\right|^2-\left|\left|\nabla_w\times\boldsymbol{\varepsilon}_h^1\right|\right|^2-\left|\left|\nabla_w\times\boldsymbol{\varepsilon}_h^0\right|\right|^2\right)\\
&\qquad+\left|\left|\frac{\boldsymbol{\varepsilon}_0^m-\boldsymbol{\varepsilon}_0^{m-1}}{\Delta t}\right|\right|^2-\left|\left|\frac{\boldsymbol{\varepsilon}_0^1-\boldsymbol{\varepsilon}_0^0}{\Delta t}\right|\right|^2+\Delta t\sum_{n=1}^{m-1}\left|\frac{\boldsymbol{\varepsilon}_h^{n+1}-\boldsymbol{\varepsilon}_h^{n-1}}{2\Delta t}\right|_{1,h}^2\\
&\leq Ch^{2p}\Delta t\sum_{n=1}^{m-1}\left(||\mathbf{u}(t^n)||_{p+1}+\left|\left|\frac{\mathbf{u}(t^{n+1})-\mathbf{u}(t^{n-1})}{2\Delta t}\right|\right|_{p+1}\right)^2\\
&\qquad+4\Delta t\sum_{n=1}^{m-1}\left|\left|\nabla\times\nu\nabla\times\left(\frac{\mathbf{u}(t^{n+1})+\mathbf{u}(t^{n-1})}{2}-\mathbf{u}(t^n)\right)\right|\right|^2\\
&\qquad+4\Delta t\sum_{n=1}^{m-1}\left|\left|\frac{\mathbf{u}(t^{n+1})-2\mathbf{u}(t^n)+\mathbf{u}(t^{n-1})}{\Delta t^2}-\frac{\partial^2\mathbf{u}}{\partial t^2}(t^n)\right|\right|^2\\
&\qquad+\frac{\Delta t}{2}\sum_{n=0}^{m-1}\left|\left|\frac{\boldsymbol{\varepsilon}_0^{n+1}-\boldsymbol{\varepsilon}_0^{n}}{\Delta t}\right|\right|^2. \qquad (4.52)
\end{aligned}
$$

Under the assumption of $\frac{\Delta t}{2}<\frac{1}{2}$, we can subtract $\frac{\Delta t}{2}\left|\left|\frac{\boldsymbol{\varepsilon}_0^m-\boldsymbol{\varepsilon}_0^{m-1}}{\Delta t}\right|\right|^2$ from both sides to obtain

$$
\begin{aligned}
&\frac{\nu}{2}\left(\left|\left|\nabla_w\times\boldsymbol{\varepsilon}_h^m\right|\right|^2+\left|\left|\nabla_w\times\boldsymbol{\varepsilon}_h^{m-1}\right|\right|^2-\left|\left|\nabla_w\times\boldsymbol{\varepsilon}_h^1\right|\right|^2-\left|\left|\nabla_w\times\boldsymbol{\varepsilon}_h^0\right|\right|^2\right)\\
&\qquad+\frac{1}{2}\left|\left|\frac{\boldsymbol{\varepsilon}_0^m-\boldsymbol{\varepsilon}_0^{m-1}}{\Delta t}\right|\right|^2-\left|\left|\frac{\boldsymbol{\varepsilon}_0^1-\boldsymbol{\varepsilon}_0^0}{\Delta t}\right|\right|^2+\Delta t\sum_{n=1}^{m-1}\left|\frac{\boldsymbol{\varepsilon}_h^{n+1}-\boldsymbol{\varepsilon}_h^{n-1}}{2\Delta t}\right|_{1,h}^2
\end{aligned}
$$

$$\leq Ch^{2p}\Delta t\sum_{n=1}^{m-1}\left(||\mathbf{u}(t^n)||_{p+1}+\left|\left|\frac{\mathbf{u}(t^{n+1})-\mathbf{u}(t^{n-1})}{2\Delta t}\right|\right|_{p+1}\right)^2$$
$$+4\Delta t\sum_{n=1}^{m-1}\left|\left|\nabla\times\nu\nabla\times\left(\frac{\mathbf{u}(t^{n+1})+\mathbf{u}(t^{n-1})}{2}-\mathbf{u}(t^n)\right)\right|\right|^2$$
$$+4\Delta t\sum_{n=1}^{m-1}\left|\left|\frac{\mathbf{u}(t^{n+1})-2\mathbf{u}(t^n)+\mathbf{u}(t^{n-1})}{\Delta t^2}-\frac{\partial^2\mathbf{u}(t^n)}{\partial t^2}\right|\right|^2$$
$$+\frac{\Delta t}{2}\sum_{n=0}^{m-2}\left|\left|\frac{\boldsymbol{\varepsilon}_0^{n+1}-\boldsymbol{\varepsilon}_0^n}{\Delta t}\right|\right|^2. \tag{4.53}$$

Then, after applying the discrete Grönwall's inequality and Lemmas 4.4.2 and 4.4.2,

$$\frac{\nu}{2}\left(\left|\left|\nabla_w\times\boldsymbol{\varepsilon}_h^m\right|\right|^2+\left|\left|\nabla_w\times\boldsymbol{\varepsilon}_h^{m-1}\right|\right|^2\right)+\frac{1}{2}\left|\left|\frac{\boldsymbol{\varepsilon}_0^m-\boldsymbol{\varepsilon}_0^{m-1}}{\Delta t}\right|\right|^2+\Delta t\sum_{n=1}^{m-1}\left|\frac{\boldsymbol{\varepsilon}_h^{n+1}-\boldsymbol{\varepsilon}_h^{n-1}}{2\Delta t}\right|_{1,h}^2$$
$$\leq C\exp(T)[\frac{\nu}{2}(||\nabla_w\times\boldsymbol{\varepsilon}_h^1||^2+||\nabla_w\times\boldsymbol{\varepsilon}_h^0||^2)+\left|\left|\frac{\boldsymbol{\varepsilon}_0^1-\boldsymbol{\varepsilon}_0^0}{\Delta t}\right|\right|^2$$
$$+h^{2p}\Delta t\sum_{n=1}^{m-1}\left(||\mathbf{u}(t^n)||_{p+1}+\left|\left|\frac{\mathbf{u}(t^{n+1})-\mathbf{u}(t^{n-1})}{2\Delta t}\right|\right|_{p+1}\right)^2$$
$$+\Delta t^4\left(\int_0^T\left|\left|\frac{\partial^4\mathbf{u}}{\partial t^4}\right|\right|^2dt+\int_0^T\left|\left|\nabla\times\nu\nabla\times\frac{\partial^2\mathbf{u}}{\partial t^2}\right|\right|^2dt\right)], \tag{4.54}$$

which concludes the proof. □

4.5 Implementation of the WG method

Choosing the finite element space and respective basis functions

Even though we have proved the convergence and stability results for 3-D, we can extend the theoretical analysis directly to 2-D by using a 2-D version of the curl operator. Though practical problems are in 3-D, for simplicity, we currently focus on a 2-D implementation of the scheme. Hence the numerical results for this chapter are done in 2-D only.

The test and trial spaces that we chose for our implementation are of the lowest order in order to simplify calculations and to show how to implement the method more clearly. Thus, our finite element spaces that we used are composed of linear elements, which give an order of accuracy of $O(h)$ in the energy norm according to our error analysis. Denote $\mathcal{E}_h$ to be the set of all element edges in the domain, and $\boldsymbol{\tau}_i$ to be the tangential vector for each element edge $e_i \subset \partial K$. Our finite element spaces are defined as follows. Given a triangulation, $\mathcal{T}_h$, of the domain Ω, for each $K \in \mathcal{T}_h$:

$$V_0(K) = \{\boldsymbol{v}_0 : \boldsymbol{v}_0|_K \in [P_1(K)]^2\} \tag{4.55}$$

$$V_b(K) = \{\boldsymbol{v}_b : \boldsymbol{v}_b|_K = \sum_{i=1}^{3}(v_{1,i} + v_{2,i}s)\boldsymbol{\tau}_i, \text{ and } v_{1,i}, v_{2,i} \in P_0(e_i), e_i \subset \partial K\} \tag{4.56}$$

The total finite element space is then formally defined as follows:

$$V_h = \{\boldsymbol{v}_h = \{\boldsymbol{v}_0, \boldsymbol{v}_b\} : \boldsymbol{v}_0|_K \in V_0, \boldsymbol{v}_b|_K \in V_b, \forall K \in \mathcal{T}_h\} \tag{4.57}$$

In addition to these two spaces used in the creation of our finite element space, a third space is needed for the construction of the discrete weak curl operator on each element K. By the definition of the discrete weak curl operator, the space used must be one degree less than the spaces used to approximate the solution, i.e. $P_0(K)$.

After the spaces are chosen, a suitable basis must be chosen as well. The following bases were used in this specific implementation due to their simplicity:

$$\begin{aligned} V_0(K) &= \text{span}\{\boldsymbol{\phi}_{0,i} : i = 1...(N_0 = 6)\} \\ &= \text{span}\left\{\begin{pmatrix}1\\0\end{pmatrix}, \begin{pmatrix}x\\0\end{pmatrix}, \begin{pmatrix}y\\0\end{pmatrix}, \begin{pmatrix}0\\1\end{pmatrix}, \begin{pmatrix}0\\x\end{pmatrix}, \begin{pmatrix}0\\y\end{pmatrix}\right\}, \qquad (x, y) \in K \end{aligned} \tag{4.58}$$

$$\begin{aligned} V_b(K) &= \text{span}\{\boldsymbol{\phi}_{b,i} : i = 1...(N_b = 6)\} \\ &= \text{span}\{\boldsymbol{\tau}_1, s\boldsymbol{\tau}_1, \boldsymbol{\tau}_2, s\boldsymbol{\tau}_2, \boldsymbol{\tau}_3, s\boldsymbol{\tau}_3\}, \qquad s \in [0, |e_i|] \end{aligned} \tag{4.59}$$

$$P_0(K) = \text{span}\{\chi_i : i = 1...(N_v = 1)\} = \text{span}\{1\} \tag{4.60}$$

Note that $\boldsymbol{\phi}_{b1}$ and $\boldsymbol{\phi}_{b2}$ are only defined on e_1, and likewise for the other 2 pairs of basis functions.

Construction of the linear system

Given the basis functions, we can represent the numerical solution $\boldsymbol{u}_h$ as:

$$\boldsymbol{u}_h|_K = \left\{ \sum_{i=1}^{N_0} u_{0,i}\boldsymbol{\varphi}_{0,i}, \sum_{i=1}^{N_b} u_{b,i}\boldsymbol{\varphi}_{b,i} \right\}$$

We substitute this into the fully-discrete scheme, then let our test functions be each basis function:

$$\boldsymbol{v}_h = \boldsymbol{\varphi}_{j,h} = \{\boldsymbol{\varphi}_{0,j}, \boldsymbol{\varphi}_{b,j}\}, \quad j = 1...(N_0 + N_b)$$

where we have $\boldsymbol{\varphi}_{b,j} = 0$ for $j = 1...N_0$, and $\boldsymbol{\varphi}_{0,j} = 0$ for $j = N_0 + 1, ..., N_0 + N_b$.

This gives us the following linear system for our fully discrete scheme on each K:

$$\begin{aligned} C_K \left(\frac{\vec{u}_h^{n+1} + \vec{u}_h^{n-1}}{2} \right) + M_K \left(\frac{\vec{u}_0^{n+1} - 2\vec{u}_0^{n} + \vec{u}_0^{n-1}}{\Delta t^2} \right) \\ + S_K \left(\frac{\vec{u}_h^{n+1} - \vec{u}_h^{n-1}}{2\Delta t} \right) = b_k \end{aligned} \tag{4.61}$$

where $\vec{u}_h^n = [u_{0,1}...u_{0,N_0}, u_{b,1}...u_{b,N_b}]^T$. Or, if we solve for the $(n+1)$th time step:

$$\begin{aligned} \vec{u}_h^{n+1} = &\left(\frac{1}{2}C_K + \frac{1}{\Delta t^2}M_K + \frac{1}{2\Delta t}S_K \right)^{-1} 2M_K \vec{u}_h^n \\ &- \left(\frac{1}{2}C_K + \frac{1}{\Delta t^2}M_K + \frac{1}{2\Delta t}S_K \right)^{-1} \left(\frac{1}{2}C_K + \frac{1}{\Delta t^2}M_K - \frac{1}{2\Delta t}S_K \right) \vec{u}_h^{n-1} \\ &+ \left(\frac{1}{2}C_K + \frac{1}{\Delta t^2}M_K + \frac{1}{2\Delta t}S_K \right)^{-1} b_K \end{aligned} \tag{4.62}$$

where C_K, M_K, and S_K are the curl, mass and stability matrices respectively, and

$$[b_K] = \begin{bmatrix} (\boldsymbol{f}^n, \boldsymbol{\varphi}_{0,j})_K \\ \mathbf{0}_{N_b \times 1} \end{bmatrix}$$

Note that since this is discretized with a second order finite difference scheme in time, we need two initial conditions, $\vec{u}_h^0$ and $\vec{u}_0^1$. To implement this we must find the projection of our initial condition at the first two time steps onto our interior and boundary finite element spaces.

Constructing the matrices

Following the steps outlined in Mu et al. (2013) we see that each of the 3 matrices can be written in the form:

$$C_K = \begin{bmatrix} C_{0,0} & C_{0,b} \\ C_{b,0} & C_{b,b} \end{bmatrix} \tag{4.63}$$

Following the paper once again we arrive at the following analogous definitions for the 4 blocks of the curl matrix:

$$\begin{aligned} C_{0,0} &= Z_K^t D_K^{-t} A_K D_K^{-1} Z_K, \quad C_{0,b} = -Z_K^t D_K^{-t} A_K D_K^{-1} T_K, \\ C_{b,0} &= -T_K^t D_K^{-t} A_K D_K^{-1} Z_K, \quad C_{b,b} = T_K^t D_K^{-t} A_K D_K^{-1} T_K. \end{aligned} \tag{4.64}$$

where Z_K, T_K, D_K, and A_K are defined as:

$$\begin{aligned} [Z_K]_{i,j} &= \int_K (\nabla \times \chi_i) \cdot \boldsymbol{\varphi}_{0,j} dA, && i = 1...N_v, j = 1...N_0, \\ [T_K]_{i,j} &= \int_{\partial K} \chi_i \cdot \boldsymbol{\varphi}_{b,j} \times \boldsymbol{n}_K dS, && i = 1...N_v, j = 1...N_b, \\ [D_K]_{i,j} &= \int_K \chi_i \cdot \chi_j dA, && i, j = 1...N_v, \\ [A_K]_{i,j} &= \int_K \nu \chi_i \cdot \chi_j dA, && i, j = 1...N_v. \end{aligned} \tag{4.65}$$

Using the basis functions chosen earlier, we have the following values for Z_K, T_K,

D_K, and A_K:

$$Z_K = [0\ 0\ 0\ 0\ 0\ 0], \quad T_K = \left[|e_1| \ \ \frac{1}{2}|e_1|^2 \ \ |e_2| \ \ \frac{1}{2}\,|e_2|^2 \ \ |e_3| \ \ \frac{1}{2}|e_3|^2\right],$$
$$D_K = |K|, \quad A_K = \nu|K|. \tag{4.66}$$

Using these values and the formulas from (4.64), we have:

$$C_{0,0} = C_{0,b} = C_{b,0} = \mathbf{0}_{6\times 6}$$

and

$$C_{b,b} = \frac{1}{|K|}\begin{bmatrix} |e_1|^2 & \frac{1}{2}|e_1|^3 & |e_1||e_2| & \frac{1}{2}|e_1||e_2|^2 & |e_1||e_3| & \frac{1}{2}|e_1||e_3|^2 \\ \frac{1}{2}|e_1|^3 & \frac{1}{4}|e_1|^4 & \frac{1}{2}|e_1|^2|e_2| & \frac{1}{4}|e_1|^2|e_2|^2 & \frac{1}{2}|e_1|^2|e_3| & \frac{1}{4}|e_1|^2|e_3|^2 \\ |e_1||e_2| & \frac{1}{2}|e_1|^2|e_2| & |e_2|^2 & \frac{1}{2}|e_2|^3 & |e_2||e_3| & \frac{1}{2}|e_2||e_3|^2 \\ \frac{1}{2}|e_1||e_2|^2 & \frac{1}{4}|e_1|^2|e_2|^2 & \frac{1}{2}|e_2|^3 & \frac{1}{4}|e_2|^4 & \frac{1}{2}|e_2|^2|e_3| & \frac{1}{4}|e_2|^2|e_3|^2 \\ |e_1||e_3| & \frac{1}{2}|e_1|^2|e_3| & |e_2||e_3| & \frac{1}{2}|e_2|^2|e_3| & |e_3|^2 & \frac{1}{2}|e_3|^3 \\ \frac{1}{2}|e_1||e_3|^2 & \frac{1}{4}|e_1|^2|e_3|^2 & \frac{1}{2}|e_2||e_3|^2 & \frac{1}{4}|e_2|^2|e_3|^2 & \frac{1}{2}|e_3|^3 & \frac{1}{4}|e_3|^4 \end{bmatrix},$$

which completes the construction of the curl matrix.

The mass matrix can then be computed in a similar blockwise fashion:

$$M_K = \begin{bmatrix} M_{0,0} & M_{0,b} \\ M_{b,0} & M_{b,b} \end{bmatrix}$$

where

$$M_{0,b} = M_{b,0} = M_{b,b} = \mathbf{0}_{6\times 6}$$

from the lack of boundary term in the scheme and

$$[M_{0,0}]_{i,j} = \int_K \boldsymbol{\varphi}_{0,i} \cdot \boldsymbol{\varphi}_{0,j} dA, \qquad i,j = 1...N_0.$$

Computing $M_{0,0}$ with our chosen basis functions yields the nonzero entries to be:

$$[M_{0,0}]_{1,1} = [M_{0,0}]_{4,4} = 1,$$

$$[M_{0,0}]_{2,1} = [M_{0,0}]_{1,2} = [M_{0,0}]_{5,4} = [M_{0,0}]_{4,5} = \frac{1}{3}(x_1 + x_2 + x_3),$$

$$[M_{0,0}]_{3,1} = [M_{0,0}]_{1,3} = [M_{0,0}]_{6,4} = [M_{0,0}]_{4,6} = \frac{1}{3}(y_1 + y_2 + y_3),$$

$$[M_{0,0}]_{2,2} = [M_{0,0}]_{5,5} = \frac{1}{6}(x_1^2 + (x_1 + x_2)(x_2 + x_3) + x_3^2),$$

$$[M_{0,0}]_{2,3} = [M_{0,0}]_{3,2} = [M_{0,0}]_{6,5} = [M_{0,0}]_{5,6} = \frac{1}{12}(x_1(2y_1 + y_2 + y_3) + x_2(y_1 + 2y_2 + y_3) + x_3(y_1 + y_2 + 2y_3)),$$

$$[M_{0,0}]_{3,3} = [M_{0,0}]_{6,6} = \frac{1}{6}(y_1^2 + (y_1 + y_2)(y_2 + y_3) + y_3^2),$$

which completes the construction of the mass matrix.

To compute the stability matrix we must first compute the L^2-projection onto the boundary of each element of the interior basis functions. To do this we first use the fact that the L^2-projection of the interior basis function Q_b must be a linear combination of the boundary basis functions, i.e.

$$Q_b \boldsymbol{\varphi}_{0,i} = \sum_{j=1}^{N_b} c_{i,j} \boldsymbol{\varphi}_{b,j} \qquad \text{for } i = 1...N_0.$$

Additionally, by definition of L^2-projection we have:

$$\langle Q_b \boldsymbol{\varphi}_{0,i}, \boldsymbol{\varphi}_{b,j} \rangle_{\partial K} = \langle \boldsymbol{\varphi}_{0,i}, \boldsymbol{\varphi}_{b,j} \rangle_{\partial K} \qquad \text{for } j = 1...N_b.$$

Using both of these definitions on the first edge of the triangle we can get a system of linear equations for c_1 and c_2:

$$Q_b \boldsymbol{\varphi}_{0,i}|_{e_1} = c_{i,1} \boldsymbol{\varphi}_{b,1} + c_{i,2} \boldsymbol{\varphi}_{b,2},$$

$$\langle c_{i,1} \boldsymbol{\varphi}_{b,1} + c_{i,2} \boldsymbol{\varphi}_{b,2}, \boldsymbol{\varphi}_{b,1} \rangle_{\partial K} = \langle \boldsymbol{\varphi}_{0,i}, \boldsymbol{\varphi}_{b,1} \rangle_{\partial K},$$

$$\langle c_{i,1}\boldsymbol{\varphi}_{b,1} + c_{i,2}\boldsymbol{\varphi}_{b,2}, \boldsymbol{\varphi}_{b,2}\rangle_{\partial K} = \langle \boldsymbol{\varphi}_{0,i}, \boldsymbol{\varphi}_{b,2}\rangle_{\partial K}.$$

We can then rewrite this as the following linear system:

$$\begin{bmatrix} \langle \boldsymbol{\varphi}_{b,1}, \boldsymbol{\varphi}_{b,1}\rangle_{\partial K} & \langle \boldsymbol{\varphi}_{b,1}, \boldsymbol{\varphi}_{b,2}\rangle_{\partial K} \\ \langle \boldsymbol{\varphi}_{b,2}, \boldsymbol{\varphi}_{b,1}\rangle_{\partial K} & \langle \boldsymbol{\varphi}_{b,2}, \boldsymbol{\varphi}_{b,2}\rangle_{\partial K} \end{bmatrix} \begin{bmatrix} c_{i,1} \\ c_{i,2} \end{bmatrix} = \begin{bmatrix} \langle \boldsymbol{\varphi}_{0,i}, \boldsymbol{\varphi}_{b,1}\rangle_{\partial K} \\ \langle \boldsymbol{\varphi}_{0,i}, \boldsymbol{\varphi}_{b,2}\rangle_{\partial K} \end{bmatrix}.$$

A similar process can be used for the other 2 edges to find $c_{i,3}, c_{i,4}, c_{i,5}$ and $c_{i,6}$:

$$\begin{bmatrix} \langle \boldsymbol{\varphi}_{b,3}, \boldsymbol{\varphi}_{b,3}\rangle_{\partial K} & \langle \boldsymbol{\varphi}_{b,3}, \boldsymbol{\varphi}_{b,4}\rangle_{\partial K} \\ \langle \boldsymbol{\varphi}_{b,4}, \boldsymbol{\varphi}_{b,3}\rangle_{\partial K} & \langle \boldsymbol{\varphi}_{b,4}, \boldsymbol{\varphi}_{b,4}\rangle_{\partial K} \end{bmatrix} \begin{bmatrix} c_{i,3} \\ c_{i,4} \end{bmatrix} = \begin{bmatrix} \langle \boldsymbol{\varphi}_{0,i}, \boldsymbol{\varphi}_{b,3}\rangle_{\partial K} \\ \langle \boldsymbol{\varphi}_{0,i}, \boldsymbol{\varphi}_{b,4}\rangle_{\partial K} \end{bmatrix},$$

$$\begin{bmatrix} \langle \boldsymbol{\varphi}_{b,5}, \boldsymbol{\varphi}_{b,5}\rangle_{\partial K} & \langle \boldsymbol{\varphi}_{b,5}, \boldsymbol{\varphi}_{b,6}\rangle_{\partial K} \\ \langle \boldsymbol{\varphi}_{b,6}, \boldsymbol{\varphi}_{b,5}\rangle_{\partial K} & \langle \boldsymbol{\varphi}_{b,6}, \boldsymbol{\varphi}_{b,6}\rangle_{\partial K} \end{bmatrix} \begin{bmatrix} c_{i,5} \\ c_{i,6} \end{bmatrix} = \begin{bmatrix} \langle \boldsymbol{\varphi}_{0,i}, \boldsymbol{\varphi}_{b,5}\rangle_{\partial K} \\ \langle \boldsymbol{\varphi}_{0,i}, \boldsymbol{\varphi}_{b,6}\rangle_{\partial K} \end{bmatrix}.$$

Combining these into a block matrix system, and computing the components directly, we get 6 linear systems to solve for our 6 interior basis functions:

$$\begin{bmatrix} |e_1| & \frac{|e_1|^2}{2} & 0 & 0 & 0 & 0 \\ \frac{|e_1|^2}{2} & \frac{|e_1|^3}{3} & 0 & 0 & 0 & 0 \\ 0 & 0 & |e_2| & \frac{|e_2|^2}{2} & 0 & 0 \\ 0 & 0 & \frac{|e_2|^2}{2} & \frac{|e_2|^3}{3} & 0 & 0 \\ 0 & 0 & 0 & 0 & |e_3| & \frac{|e_3|^2}{2} \\ 0 & 0 & 0 & 0 & \frac{|e_3|^2}{2} & \frac{|e_3|^3}{3} \end{bmatrix} \begin{bmatrix} c_{i,1} \\ c_{i,2} \\ c_{i,3} \\ c_{i,4} \\ c_{i,5} \\ c_{i,6} \end{bmatrix} = \begin{bmatrix} \langle \boldsymbol{\varphi}_{0,i}, \boldsymbol{\varphi}_{b,1}\rangle_{\partial K} \\ \langle \boldsymbol{\varphi}_{0,i}, \boldsymbol{\varphi}_{b,2}\rangle_{\partial K} \\ \langle \boldsymbol{\varphi}_{0,i}, \boldsymbol{\varphi}_{b,3}\rangle_{\partial K} \\ \langle \boldsymbol{\varphi}_{0,i}, \boldsymbol{\varphi}_{b,4}\rangle_{\partial K} \\ \langle \boldsymbol{\varphi}_{0,i}, \boldsymbol{\varphi}_{b,5}\rangle_{\partial K} \\ \langle \boldsymbol{\varphi}_{0,i}, \boldsymbol{\varphi}_{b,6}\rangle_{\partial K} \end{bmatrix}.$$

Here, the 6 right hand side vectors for the 6 interior basis functions cannot be directly calculated by hand for an arbitrary element. Because the right hand side vectors are computed using boundary integrals, we must consider the neighboring elements since tangential continuity is enforced along the boundary elements. In order to keep consistency with the direction of integration, if we have two elements with a shared boundary, the boundary integrals must be integrated in opposite directions. To enforce this, we must choose one of the two elements, and replace the basis function $s\tau_i$ with $(|e_i| - s)\boldsymbol{\tau}_i$. Since the choice of the element here is somewhat arbitrary (albeit it must still be a consistent choice throughout the whole domain) it is not easy to list a generalized formula for the right hand side vectors for each element.

Once we have solved for the $c_{i,j}$, and therefore found the L^2-projection, we can then use them to compute the boundary integrals used for the entries in the stability matrix. Starting with the definition of the stabilizing term on each element we have:

$$\begin{aligned}
s(\boldsymbol{u}_h, \boldsymbol{\varphi}_{h,j})|_K &= h_K^{-1}\langle (Q_b\boldsymbol{u}_0 - \boldsymbol{u}_b) \times \boldsymbol{n}_K, (Q_b\boldsymbol{\varphi}_{0,j} - \boldsymbol{\varphi}_{b,j}) \times \boldsymbol{n}_K\rangle_{\partial K} \\
&= h_K^{-1}(\langle Q_b\boldsymbol{u}_0 \cdot \boldsymbol{\tau}_K, Q_b\boldsymbol{\varphi}_{0,j} \cdot \boldsymbol{\tau}_K\rangle_{\partial K} - \langle Q_b\boldsymbol{u}_0 \cdot \boldsymbol{\tau}_K, \boldsymbol{\varphi}_{b,j} \cdot \boldsymbol{\tau}_K\rangle_{\partial K} \\
&\quad - \langle \boldsymbol{u}_b \cdot \boldsymbol{\tau}_K, Q_b\boldsymbol{\varphi}_{0,j} \cdot \boldsymbol{\tau}_K\rangle_{\partial K} + \langle u_b \cdot \boldsymbol{\tau}_K, \boldsymbol{\varphi}_{b,j} \cdot \boldsymbol{\tau}_K\rangle_{\partial K}) \\
&= h_K^{-1} \sum_{i=1}^{N_0} u_{0,i}(\langle Q_b\boldsymbol{\varphi}_{0,i} \cdot \boldsymbol{\tau}_K, Q_b\boldsymbol{\varphi}_{0,j} \cdot \boldsymbol{\tau}_K\rangle_{\partial K} - \langle Q_b\boldsymbol{\varphi}_{0,i} \cdot \boldsymbol{\tau}_K, \boldsymbol{\varphi}_{b,j} \cdot \boldsymbol{\tau}_K\rangle_{\partial K}) \\
&\quad + h_K^{-1} \sum_{i=1}^{N_b} u_{b,i}(-\langle \boldsymbol{\varphi}_{b,i} \cdot \boldsymbol{\tau}_K, Q_b\boldsymbol{\varphi}_{0,j} \cdot \boldsymbol{\tau}_K\rangle_{\partial K} + \langle \boldsymbol{\varphi}_{b,i} \cdot \boldsymbol{\tau}_K, \boldsymbol{\varphi}_{b,j} \cdot \boldsymbol{\tau}_K\rangle_{\partial K})
\end{aligned}$$

where $\boldsymbol{\tau}_K$ is the tangential unit vector to ∂K. This finally gives us:

$$S_K = h_K^{-1} \begin{bmatrix} S_{0,0} & S_{0,b} \\ S_{b,0} & S_{b,b} \end{bmatrix}$$

where

$$\begin{aligned}
[S_{0,0}]_{i,j} &= \int_{\partial K} Q_b\boldsymbol{\varphi}_{0,i} \cdot \boldsymbol{\tau}_K \cdot Q_b\boldsymbol{\varphi}_{0,j} \cdot \boldsymbol{\tau}_K dS, \\
[S_{0,b}]_{i,j} &= -\int_{\partial K} Q_b\boldsymbol{\varphi}_{0,i} \cdot \boldsymbol{\tau}_K \cdot \boldsymbol{\varphi}_{b,j} \cdot \boldsymbol{\tau}_K dS, \\
[S_{b,0}]_{i,j} &= -\int_{\partial K} \boldsymbol{\varphi}_{b,i} \cdot \boldsymbol{\tau}_K \cdot Q_b\boldsymbol{\varphi}_{0,j} \cdot \boldsymbol{\tau}_K dS, \\
[S_{b,b}]_{i,j} &= \int_{\partial K} \boldsymbol{\varphi}_{b,i} \cdot \boldsymbol{\tau}_K \cdot \boldsymbol{\varphi}_{b,j} \cdot \boldsymbol{\tau}_K dS.
\end{aligned} \tag{4.67}$$

It should be noted that $S_{0,b} = S_{b,0}^T$, and $S_{0,0}$ and $S_{b,b}$ are symmetric, therefore making S_K symmetric.. Now using the L^2-projection to compute $S_{0,0}$ we have:

$$[S_{0,0}]_{i,j} = \int_{\partial K} Q_b\phi_{0,i} \cdot \tau \cdot Q_b\phi_{0,j} \cdot \tau dS$$

$$
\begin{aligned}
&= \int_{edge1} (c_{i,1}\phi_{b,1} + c_{i,2}\phi_{b,2}) \cdot \tau_1 \cdot (c_{j,1}\phi_{b,1} + c_{j,2}\phi_{b,2}) \cdot \tau_1 dS \\
&\qquad + \int_{edge2} (c_{i,3}\phi_{b,3} + c_{i,4}\phi_{b,4}) \cdot \tau_2 \cdot (c_{j,3}\phi_{b,3} + c_{j,4}\phi_{b,4}) \cdot \tau_2 dS \\
&\qquad + \int_{edge3} (c_{i,5}\phi_{b,5} + c_{i,6}\phi_{b,6}) \cdot \tau_3 \cdot (c_{j,5}\phi_{b,5} + c_{j,6}\phi_{b,6}) \cdot \tau_3 dS \\
&= \int_{edge1} (c_{i,1} + c_{i,2}s) \cdot (c_{j,1} + c_{j,2}s) ds + \int_{edge2} (c_{i,3} + c_{i,4}s) \cdot (c_{j,3} + c_{j,4}s) ds \\
&\qquad + \int_{edge3} (c_{i,5} + c_{i,6}s) \cdot (c_{j,5} + c_{j,6}s) ds \\
&= \frac{1}{6}|e_1|(3c_{i,1}(2c_{j,1} + c_{j,2}|e_1|) + c_{i,2}|e_1|(3c_{j,1} + 2c_{j,2}|e_1|)) \\
&\qquad + \frac{1}{6}|e_2|(3c_{i,3}(2c_{j,3} + c_{j,4}|e_2|) + c_{i,4}|e_2|(3c_{j,3} + 2c_{j,4}|e_2|)) \\
&\qquad + \frac{1}{6}|e_3|(3c_{i,5}(2c_{j,5} + c_{j,6}|e_3|) + c_{i,6}|e_3|(3c_{j,5} + 2c_{j,6}|e_3|)). \qquad (4.68)
\end{aligned}
$$

Likewise for $S_{0,b}$ and $S_{b,0} = S_{0,b}^T$:

$$
\begin{aligned}
[S_{0,b}]_{i,1} &= -\int_{\partial K} Q_b \phi_{0,i} \cdot \tau \cdot \phi_{b,1} \cdot \tau dS = -\int_{edge1} (c_{i,1}\phi_{b,1} + c_{i,2}\phi_{b,2}) \cdot \tau_1 \cdot \phi_{b,1} \cdot \tau_1 dS \\
&= -\int_{edge1} (c_{i,1} + c_{i,2}s) ds = -c_{i,1}|e_1| - \frac{1}{2}c_{i,2}|e_1|^2, \qquad (4.69)
\end{aligned}
$$

$$
\begin{aligned}
[S_{0,b}]_{i,2} &= -\int_{\partial K} Q_b \phi_{0,i} \cdot \tau \cdot \phi_{b,2} \cdot \tau dS = -\int_{edge1} (c_{i,1}\phi_{b,1} + c_{i,2}\phi_{b,2}) \cdot \tau_1 \cdot \phi_{b,2} \cdot \tau_1 dS \\
&= -\int_{edge1} (c_{i,1}s + c_{i,2}s^2) ds = -\frac{1}{2}c_{i,1}|e_1|^2 - \frac{1}{3}c_{i,2}|e_1|^3, \qquad (4.70)
\end{aligned}
$$

$$
\begin{aligned}
[S_{0,b}]_{i,3} &= -\int_{\partial K} Q_b \phi_{0,i} \cdot \tau \cdot \phi_{b,3} \cdot \tau dS = -\int_{edge2} (c_{i,3}\phi_{b,3} + c_{i,4}\phi_{b,4}) \cdot \tau_2 \cdot \phi_{b,3} \cdot \tau_2 dS \\
&= -\int_{edge2} (c_{i,3} + c_{i,4}s) ds = -c_{i,3}|e_2| - \frac{1}{2}c_{i,4}|e_2|^2 \qquad (4.71)
\end{aligned}
$$

$$
\begin{aligned}
[S_{0,b}]_{i,4} &= -\int_{\partial K} Q_b \phi_{0,i} \cdot \tau \cdot \phi_{b,4} \cdot \tau dS = -\int_{edge2} (c_{i,3}\phi_{b,3} + c_{i,4}\phi_{b,4}) \cdot \tau_2 \cdot \phi_{b,4} \cdot \tau_2 dS \\
&= -\int_{edge2} (c_{i,3}s + c_{i,4}s^2) ds = -\frac{1}{2}c_{i,3}|e_2|^2 - \frac{1}{3}c_{i,4}|e_2|^3, \qquad (4.72)
\end{aligned}
$$

$$
\begin{aligned}
[S_{0,b}]_{i,5} &= -\int_{\partial K} Q_b \phi_{0,i} \cdot \tau \cdot \phi_{b,5} \cdot \tau dS = -\int_{edge3} (c_{i,5}\phi_{b,5} + c_{i,6}\phi_{b,6}) \cdot \tau_3 \cdot \phi_{b,5} \cdot \tau_3 dS \\
&= -\int_{edge3} (c_{i,5} + c_{i,6}s) ds = -c_{i,5}|e_3| - \frac{1}{2}c_{i,6}|e_3|^2, \qquad (4.73)
\end{aligned}
$$

$$[S_{0,b}]_{i,6} = -\int_{\partial K} Q_b \phi_{0,i} \cdot \tau \cdot \phi_{b,6} \cdot \tau dS = -\int_{edge3} (c_{i,5}\phi_{b,5} + c_{i,6}\phi_{b,6}) \cdot \tau_3 \cdot \phi_{b,6} \cdot \tau_3 dS$$
$$= -\int_{edge3} (c_{i,5}s + c_{i,6}s^2) ds = -\frac{1}{2}c_{i,5}|e_3|^2 - \frac{1}{3}c_{i,6}|e_3|^3. \tag{4.74}$$

Finally, $S_{b,b}$ can be directly calculated to be:

$$S_{b,b} = \begin{bmatrix} |e_1| & \frac{|e_1|^2}{2} & 0 & 0 & 0 & 0 \\ \frac{|e_1|^2}{2} & \frac{|e_1|^3}{3} & 0 & 0 & 0 & 0 \\ 0 & 0 & |e_2| & \frac{|e_2|^2}{2} & 0 & 0 \\ 0 & 0 & \frac{|e_2|^2}{2} & \frac{|e_2|^3}{3} & 0 & 0 \\ 0 & 0 & 0 & 0 & |e_3| & \frac{|e_3|^2}{2} \\ 0 & 0 & 0 & 0 & \frac{|e_3|^2}{2} & \frac{|e_3|^3}{3} \end{bmatrix}.$$

Assembling the global matrices

Once we have the local matrices defined and constructed on every element we must assemble them into the global matrix. Tangential continuity is only enforced on the element boundaries. Expanding $\boldsymbol{u}_b$ in terms of its basis functions on each element edge, in 2D problems, we have:

$$(u_{b,i}\boldsymbol{\varphi}_{b,i} + u_{b,i+1}\boldsymbol{\varphi}_{b,i+1}) \cdot \boldsymbol{\tau} = (u_{b,j}\boldsymbol{\varphi}_{b,j} + u_{b,j+1}\boldsymbol{\varphi}_{b,j+1}) \cdot \boldsymbol{\tau},$$

$$(u_{b,i}\boldsymbol{\tau}_i + u_{b,i+1}s\boldsymbol{\tau}_i) \cdot \boldsymbol{\tau} = (u_{b,j}\boldsymbol{\tau}_j + u_{b,j+1}s\boldsymbol{\tau}_j) \cdot \boldsymbol{\tau},$$

where $\boldsymbol{\tau}_i$ is the tangential vector for the shared edge of element K_1 and $\boldsymbol{\tau}_j$ is the tangential vector for the shared edge of element K_2. Since the two vectors share the same edge, but point in opposite directions we have from our current definitions: $\boldsymbol{\tau}_i = -\boldsymbol{\tau}_j = \boldsymbol{\tau}$. This gives us:

$$u_{b,i} + su_{b,i+1} = -(u_{b,j} + su_{b,j+1}),$$

that is, the $u_{b,i}$ are equal to the negative of each other across each element edge. This means that instead of enforcing equality across the element edges to ensure continuity,

we must enforce the two values to be opposite signs at a shared edge.

4.6 Numerical results

Following the steps provided above for the implementation of the scheme, we have provided convergence results for our scheme that agree with the proved results in a previous section. The convergence results that have been proven show the convergence of a so-called weak curl norm, defined by: $||u_h||_{wc}^2 = ||\nabla_w \times u_h||_{L^2}^2 + ||u_0||_{L^2}^2$, to be $O(h^p + \Delta t^2)$. In addition to showing the convergence of the weak curl norm of the scheme, we have also provided the convergence results for the L^2 and L^∞ norms. Although these results imply that the L^2 and L^∞ norms are an order higher in space, with a rate of convergence of $O(h^{p+1} + \Delta t^2)$, this has yet to be proven.

To test the convergence rate of the spatial error we consider the following 2D version of (4.2):

$$\frac{1}{\mu\epsilon}\nabla \times (\nabla \times \boldsymbol{u}) + \frac{\partial^2 \boldsymbol{u}}{\partial t^2} = \boldsymbol{f} \quad \text{in } \Omega \times [0,T] \tag{4.75}$$

$$\boldsymbol{u} \times \boldsymbol{n} = \phi \quad \text{on } \partial\Omega \tag{4.76}$$

where $\epsilon = \mu = 1, \phi = 0, \boldsymbol{f} = \begin{bmatrix} \pi^2 \cos(\pi x)\sin(\pi y)t^2 \\ -\pi^2 \sin(\pi x)\cos(\pi y)t^2 \end{bmatrix}, \Omega = [0,1] \times [0,1]$, and $\boldsymbol{u} = \begin{bmatrix} u_x \\ u_y \end{bmatrix}$.

Along with the necessary initial conditions, these assumptions give the exact solution:

$$\boldsymbol{u} = \begin{bmatrix} u_x \\ u_y \end{bmatrix} = \begin{bmatrix} \cos(\pi x)\sin(\pi y)t^2 \\ -\sin(\pi x)\cos(\pi y)t^2 \end{bmatrix}.$$

The rectangular domain, Ω, was then discretized into a structured mesh of trian-

gles of equal size (see Figure 4.1). Each subsequent refinement kept the same structure to ensure consistency of the mesh throughout the convergence rates tests.

Figure 4.1. Exemplary mesh for $h = 1/4$

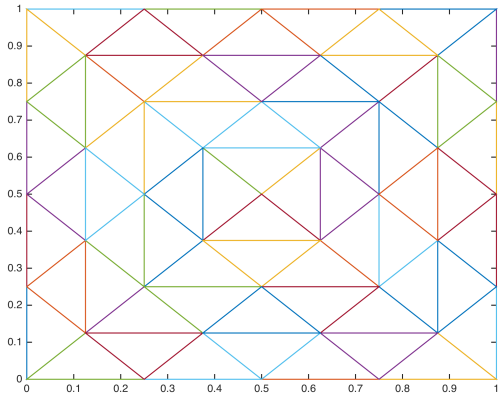

Table 4.1. Mesh size convergence rates in various norms for $T = 1$, $p = 1$, and $\Delta t = .0001$

$h =$	$\|\|\boldsymbol{e}_0\|\|_\infty$	Rate:	$\|\|\boldsymbol{e}_0\|\|_{L^2}$	Rate:	$\|\|\boldsymbol{e}_h\|\|_{wc}$	Rate:
1/4	1.0909E-01	–	8.8990E-02	–	7.4883E-01	–
1/8	3.0025E-02	1.8613	2.4674E-02	1.8507	3.5480E-01	1.0776
1/16	7.6767E-03	1.9676	6.3395E-03	1.9606	1.7373E-01	1.0302
1/32	1.9300E-03	1.9919	1.5959E-03	1.9900	8.6353E-02	1.0085
1/64	4.8318E-04	1.9980	3.9968E-04	1.9975	4.3111E-02	1.0022

4.7 Conclusions

We developed a weak Galerkin finite element method for the time-dependent Maxwell's equations. Stability and error convergence results were proved for both

Table 4.2. Mesh size convergence rates in various norms for $T = 1$, $p = 2$, and $\Delta t = .0001$

$h =$	$\|\|\boldsymbol{e}_0\|\|_\infty$	Rate:	$\|\|\boldsymbol{e}_0\|\|_{L^2}$	Rate:	$\|\|\boldsymbol{e}_h\|\|_{wc}$	Rate:
1/4	1.3579E-02	–	7.5105E-03	–	5.6149E-02	–
1/8	1.7486E-03	2.9571	9.7734E-04	2.9420	1.3996E-02	2.0042
1/16	2.1656E-04	3.0134	1.2296E-04	2.9907	3.4970E-03	2.0008
1/32	2.6888E-05	3.0097	1.5374E-05	2.9996	8.7413E-04	2.0002
1/64	3.3515E-06	3.0041	1.9206E-06	3.0009	2.1853E-04	2.0000

Table 4.3. Mesh size convergence rates in various norms for $T = 1$, $p = 3$, and $\Delta t = .0001$

$h =$	$\|\|\boldsymbol{e}_0\|\|_\infty$	Rate:	$\|\|\boldsymbol{e}_0\|\|_{L^2}$	Rate:	$\|\|\boldsymbol{e}_h\|\|_{wc}$	Rate:
1/4	5.5154E-04	–	5.3120E-04	–	4.0012E-03	–
1/8	3.7533E-05	3.8772	3.3526E-05	3.9859	4.9760E-04	3.0074
1/16	2.3819E-06	3.9780	2.0929E-06	4.0017	6.2121E-05	3.0018
1/32	1.3661E-07	4.1240	1.3013E-07	4.0075	7.7628E-06	3.0004

a semi-discrete scheme and a fully-discrete scheme were demonstrated with a few examples for $p = 1, 2$ and 3. The WG method is characterized by the usage of two main concepts, the discrete weak curl and the stabilization term.

The use of the discrete weak curl approximates the curl of the solution through a separate function space. This allows the scheme to be more flexible, allows for solutions that are discontinuous across elements, and better accommodates common problems such as nonconforming meshes. Similar to other discontinuous Galerkin methods, this scheme needs a way to transmit information across discontinuities through a flux-like term. The stabilization term fills that role in this scheme, computing a type of flux between each element interior and its associated boundary.

The numerical results for the WG scheme show that the scheme has the standard

Table 4.4. Time step convergence rates in various norms for $T = 1$, $p = 4$, and $h = 1/8$

$\Delta t =$	$\|\|\boldsymbol{e}_0\|\|_\infty$	Rate:	$\|\|\boldsymbol{e}_0\|\|_{L^2}$	Rate:	$\|\|\boldsymbol{e}_h\|\|_{wc}$	Rate:
0.02	1.2121E-01	–	6.9579E-02	–	8.7562E-02	–
0.01	2.5733E-02	2.2358	1.3366E-02	2.3801	1.6468E-02	2.4106
0.005	6.5050E-03	1.9840	3.1227E-03	2.0977	3.8431E-03	2.0993
0.0025	1.7991E-03	1.8543	7.6889E-04	2.0219	9.4510E-04	2.0237
0.00125	5.4699E-04	1.7177	1.9558E-04	1.9750	2.3882E-04	1.9845

Figure 4.2. Convergence plots for the WG method in time and space.

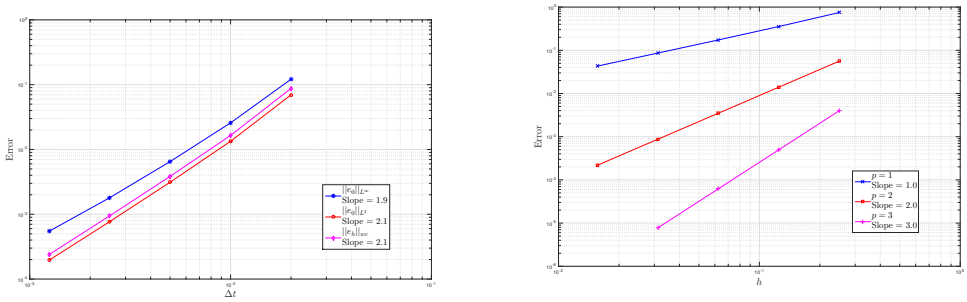

(a) Time convergence in various norms. **(b)** Spatial error in the weak curl norm for $p = 1, 2, 3$.

optimal order of convergence in the L^2, L^∞, and appropriate energy norms. Additionally, the scheme is shown to have the expected second order convergence in time in all three norms.

However, all of this added flexibility in the scheme does not come without its costs. The WG scheme requires substantially more degrees of freedom when solving the system. Although the global matrix that is fairly sparse, it still can slow down the algorithm considerably while time stepping. This can be reduced through the use of the Schur complement, whose implementation is outlined in Mu et al. (2015a). With

the Schur complement, we can simplify the scheme to only solve for the boundary degrees of freedom, reducing the computational costs drastically.

Although the WG method for Maxwell's equations does not provide any advantage in computational costs, it has the benefit of being a fairly flexible and unconditionally stable scheme while keeping an optimal order of error convergence. Future work for this scheme will include reducing time error, investigating the possibilities of superconvergence, showing the optimal convergence rate in the L^2 and L^∞ norms, and increasing the computational efficiency.

CHAPTER 5

CONCLUSIONS AND FUTURE WORK

5.1 Summary

This dissertation focused on the development and analysis of three different numerical methods for three different formulations of the time-dependent Maxwell's equations. For each model, an appropriate numerical method was chosen to solve the application at hand. In chapter 2, a Yee scheme finite difference time-domain (FDTD) method was used to simulate the backwards wave propagation through negative-index metamaterials due to the rectangular shape of the domain. Additionally, the non-uniform grid was utilized to simulate the metamaterial slab with a finer mesh than the surrounding vacuum. Chapter 3 then focuses on the modeling of signal propagation in corrugated coaxial cables. Because the domain in this application is more complex, and therefore more difficult to model with an FDTD method, a nodal discontinuous Galerkin (nDG) method was used to solve the axisymmetric Maxwell's equations on a 2-D cross-section of the dielectric of the cable. The nDG has an advantage over FDTD methods for applications such as this one due to the ability to spatially discretize the domain into triangles instead of rectangles. Finally, in chapter 4 we developed a new type of discontinuous Galerkin method named the weak Galerkin (WG) method. Because this method is still in its infancy, we decided to create a framework for future applications by developing this method for the standard Maxwell's equations.

Stability analysis as well as various error convergence rates were then performed on each of these three schemes. For the fully-discrete non-uniform Yee scheme we were able to find the necessary conditions for stability as well as prove optimal order convergence for space and time in the L^2 norm. In the case of the cable model, we proved stability in the semi-discrete scheme and the optimal order of convergence for space in the L^2 norm. Finally, we proved that the fully-discrete WG method for the standard time-domain Maxwell's equations was unconditionally stable. Additionally, we showed that this scheme achieved optimal order of convergence in the so-called discrete weak curl norm. These results were subsequently confirmed through numerical experiments for all three schemes.

5.2 Future Work

For each of the chapters presented in this dissertation there are many potential avenues to explore. Because many cloaking metamaterial models are very similar in nature to the metamaterial model presented in chapter 2, the method and analysis of chapter 2 could potentially be extended to cloaking models. Additionally, the cable model in chapter 3 is far from complete. This cable assumed ideal, perfect conductors and a lossless dielectric. A future, more comprehensive model might attempt to model skin effect losses in the conductor as well as dielectric losses. The model presented also assumes homogeneity in all materials used in the cable, where this is often not the case. Another potential avenue from the cable model would be to perform uncertainty quantification on the cable in the form of uncertainty added to the dielectric and the

conductors.

Since little to no work has been done with weak Galerkin methods on time-dependent problems, there are many possible extensions of the work done in chapter 4. For example, the method could be applied to the time-domain metamaterial and cable models presented in chapters 2 and 3. While at a first glance the WG methods looks to be computationally less efficient than the nDG methods with the same accuracy, the WG method might have some other unexplored advantages over the nDG method. An interesting comparison between the WG method and the nDG method on various Maxwell's equations models might give more insight as to any potential usage of the WG method.

APPENDIX

COPYRIGHTS

Chapter 2 reprinted from Numerische Mathematik, 134, J. Li and S. Shields, "Superconvergence analysis of Yee scheme for metamaterial Maxwell's equations on non-uniform rectangular meshes", 741-781, Copyright (2016), with permission from Springer, license number 4052701271733.

Chapter 3 reprinted from Journal of Computational and Applied Mathematics, 309, J. Li, E. A. Machorro and S. Shields, "Numerical study of signal propagation in corrugated coaxial cables", 230–243, Copyright (2017), with permission from Elsevier, license number 4052720454260.

BIBLIOGRAPHY

Adjerid, S. and Baccouch, M. (2007). The discontinuous galerkin method for two-dimensional hyperbolic problems. part i: superconvergence error analysis. *J. Sci. Comput.*, 33:75–113.

Arnold, D. and Winther, R. (1982). A superconvergent finite element method for the korteweg-devries equation. *Math. Comp.*, 38:23–36.

Arnold, D. N., Brezzi, F., Cockburn, B., and Marini, L. D. (2001/02). Unified analysis of discontinuous galerkin methods for elliptic problems. *SIAM J. Numer. Anal.*, 39:1749–1779.

Assous, F., Jr., P. C., and Labrunie, S. (2002). Theoretical tools to solve the axisymmetric maxwell equations. *Math. Methods Appl. Sci.*, 25:49–78.

Babuśka, I., Baumann, C., and Oden, J. (1999). A discontinuous hp finite element method for diffusion problems: 1-d analysis. *Comput. Math. Appl.*, 37:103–122.

Bank, R. and Xu, J. (2004a). Asymptotically exact a posteriori error estimators, part i: Grids with superconvergence. *SIAM J. Numer. Anal.*, 41:2294–2312.

Bank, R. and Xu, J. (2004b). Asymptotically exact a posteriori error estimators, part ii: General unstructured grids. *SIAM J. Numer. Anal.*, 41:2313–2332.

Belhachmi, Z., Bernardi, C., and Deparis, S. (2006). Weighted clément operator and application to the finite element discretization of the axisymmetric stokes problem. *Numer. Math.*, 105:217–247.

Bermúdez, A., Gómez, D., Rodrguez, R., and Venegas, P. (2015). Numerical analysis of a transient non-linear axisymmetric eddy current model. *Comput. Math. Appl.*, 70:1984–2005.

Bermúdez, A., Reales, C., Rodrguez, R., and Salgado, P. (2010). Numerical analysis of a finite-element method for the axisymmetric eddy current model of an induction furnace. *IMA J. Numer. Anal.*, 30:654–676.

Blank, E., Busch, K., Dörfler, W., König, M., and Niegemann, J. (2013). The discontinuous galerkin method applied to bor maxwell's equations. *preprint, Karlsruher Institut für Technologie (KIT)*.

Böcklin, C., Kaufmann, T., Hoffmann, J., Fumeaux, C., and Vahldieck, R. (2009). Simulation of corrugated coaxial cables using the meshless radial point interpolation time-domain method. In *20th Int. Zurich Simposium on EMC, Zurich 2009*.

Bokil, V. and Gibson, N. (2012). Analysis of spatial high-order finite difference methods for maxwell's equations in dispersive media. *IMA J. Numer. Anal.*, 32:926–956.

Cao, W. (2014). On the superconvergence patch recovery techniques for the linear finite element approximation on anisotropic meshes. *J. Comp. Appl. Math.*, 265:33–51.

Celiker, F., Zhang, Z., and Zhu, H. (2012). Nodal superconvergence of sdfem for singularly perturbed problems. *J. Sci. Comput.*, 50:405–433.

Chan, J., Heuer, N., Bui-Thanh, T., and Demkowicz, L. (2014). A robust dpg method for convection-dominated diffusion problems ii: Adjoint boundary conditions and mesh-dependent test norms. *Comput. Math. Appl.*, 67:771–795.

Chen, C. and Huang, Y. (1995). *High Accuracy Theory of Finite Element Methods (in Chinese)*. Hunan Science Press, China.

Chen, H., Ewing, R., and Lazarov, R. (1998). Superconvergence of mixed finite element methods for parabolic problems with nonsmooth initial data. *Numer. Math.*, 78:495–521.

Chen, L., Wang, J., Wang, Y., and Ye, X. (2015). An auxiliary space multigrid preconditioner for the weak galerkin method. *Comput. Math. Appl.*, 70:330–344.

Chen, W., Li, X., and Liang, D. (2008). Energy-conserved splitting fdtd methods for maxwells equations. *Numer. Math.*, 108:445–485.

Chung, E., Du, Q., and Zou, J. (2003). Convergence analysis of a finite volume method for maxwell's equations in nonhomogeneous media. *SIAM J. Numer. Anal.*, 41:1:37–63.

Chung, E., Jr., P. C., and T.F, Y. (2013). Convergence and superconvergence of staggered discontinuous galerkin methods for the three-dimensional maxwells equations on cartesian grids. *J. Comp. Phys.*, 235:14–31.

Ciarlet, P., Jr, N. F., and Labrunie, S. (2000). Un résultat de fermeture pour les équations de maxwell en géométrie axisymétrique. *C. R. Academie Science Paris*, 331:293–298.

Cockburn, B., Gopalakrishnan, J., and Lazarov, R. (2009). Unified hybridization of discontinuous galerkin, mixed, and continuous galerkin methods for second order elliptic problems. *SIAM J. Numer. Anal.*, 47:1319–1365.

Cockburn, B. and Shu, C.-W. (1998). The local discontinuous galerkin method for time-dependent convection-diffusion systems. *SIAM J. Numer. Anal.*, 35:2440–2463.

Craster, R. and Guenneau, S., editors (2013). *Acoustic Metamaterials: Negative Refraction, Imaging, Sensing and Cloaking*. Springer, New York.

Demkowicz, L. and Gopalakrishnan, J. (2011). Analysis of the dpg method for the poisson equation. *SIAM J. Numer. Anal.*, 49:1788–1809.

Demkowicz, L. and Li, J. (2013). Numerical simulations of cloaking problems using a dpg method. *Comp. Mech.*, 51:661–672.

D.M.Copeland, Gopalakrishnan, J., and Oh, M. (2010). Multigrid in a weighted space arising from axisymmetric electromagnetics. *Math. Comp.*, 79:2033–2058.

D.M.Copeland and J.E.Pasciak (2006). A least-squares method for axisymmetric div-curl systems. *Numer. Linear Algebra Appl.*, 13:733–752.

Engheta, N. and Ziolkowski, R., editors (2006). *Electromagnetic Metamaterials: Physics and Engineering Explorations*. Wiley.

Fezoui, L., Lanteri, S., Lohrengel, S., and Piperno, S. (2005). Convergence and stability of a discontinuous galerkin time-domain methods for the 3d heterogeneous maxwell equations on unstructured meshes. *Model. Math. Anal. Numer.*, 39(6):1149–1176.

Gao, L. and Zhang, B. (2011). Stability and superconvergence analysis of the fdtd scheme for the 2d maxwell equations in a lossy medium. *Science China Mathematics*, 54:2693–2712.

Grote, M., Schneebeli, A., and Schötzau, D. (2007). Interior penalty discontinuous galerkin method for maxwell's equations: energy norm error estimates. *J. Comput. Appl. Math.*, 204:375–386.

Guo, W., Qiu, J.-M., and Qiu, J. (2015). A new laxwendroff discontinuous galerkin method with superconvergence. *J. Sci. Comput.*, 65:299–326.

Hesthaven, J. and Warburton, T. (2008). *Nodal Discontinuous Galerkin Methods*. Springer.

Hong, J., Ji, L., and Kong, L. (2014). Energy-dissipation splitting finite-difference time-domain method for maxwell equations with perfectly matched layers. *J. Comp. Phys.*, 269:201–214.

Huang, Y., J. Li, W. Y., and Sun, S. (2011). Superconvergence of mixed finite element approximations to 3-d maxwells equations in metamaterials. *J. Comput. Phys.*, 230:8275–8289.

Huang, Y., Li, J., and Lin, Q. (2012). Superconvergence analysis for time-dependent maxwell's equations in metamaterials. *Numer. Methods Partial Differential Eq.*, 28:1794–1816.

Huang, Y., Li, J., and Yang, W. (2013). Modeling backward wave propagation in metamaterials by the finite element time-domain method. *SIAM J. Sci. Comput.*, 35:B248–B274.

Imperiale, S. and Joly, P. (2014). Mathematical modeling of electromagnetic wave propagation in heterogeneous lossy coaxial cables with variable cross section. *Appl. Numer. Math.*, 79:42–61.

Krizek, M., Neittaanamäki, P., and Stenberg, R., editors (1998). *Finite Element Methods: Superconvergence, Postprocessing and A Posteriori Estimates*. Marcel Dekker, New York.

Li, J. (2007). Error analysis of mixed finite element methods for wave propagation in double negative metamaterials. *J. Comp. Appl. Math.*, 209:81–96.

Li, J. (2009). Numerical convergence and physical fidelity analysis for maxwells equations in metamaterials. *Comput. Methods Appl. Mech. Engrg.*, 198:3161–3172.

Li, J. and Hesthaven, J. (2014). Analysis and application of the nodal discontinuous galerkin method for wave propagation in metamaterials. *J. Comp. Phys.*, 258:915–930.

Li, J. and Huang, Y. (2013). *Time-Domain Finite Element Methods for Maxwell's Equations in Metamaterials, Springer Series in Computational Mathematics, vol.43*. Springer.

Li, J., Machorro, E. A., and Shields, S. (2017). Numerical study of signal propagation in corrugated coaxial cables. *J. Comp. and App. Math.*, 309:230–243.

Li, J. and Shields, S. (2016). Superconvergence analysis of yee scheme for metamaterial maxwell's equations on non-uniform rectangular meshes. *Numer. Mat.*, 134:741–781.

Li, J., Waters, J., and Machorro, E. (2012). An implicit leap-frog discontiunous galerkin method for the time-domain maxwell's equations in metamaterials. *Comput. Methods Appl. Mech. Eng.*, 223-224:43–54.

Li, J. and Wheeler, M. (2000). Uniform convergence and superconvergence of mixed finite element methods on anisotropically refined grids. *SIAM J. Numer. Anal.*, 38:770–798.

Li, Q. and Wang, J. (2013). Weak galerkin finite element methods for parabolic equations. *Numer. Methods Partial Differential Equations*, 29(6):2004–2024.

Li, W., Liang, D., and Lin, Y. (2013). A new energy-conserved s-fdtd scheme for maxwell's equations in metamaterials. *Int. J. Numer. Anal. Model*, 10:775–794.

Lin, Q. and Li, J. (2008). Superconvergence analysis for maxwell's equations in dispersive media. *Math. Comp.*, 77:757–771.

Lin, Q. and Yan, N. (1996). *The Construction and Analysis of High Accurate Finite Element Methods (in Chinese)*. Hebei University Press, Hebei, China.

Lin, Q. and Yan, N. (1999). Global superconvergence for maxwell's equations. *Math. Comp.*, 69:159–176.

Lu, T., Zhang, P., and Cai, W. (2004). Discontinuous galerkin methods for dispersive and lossy maxwell's equations and pml boundary conditions. *J. Comp. Phys.*, 200:549–580.

Machorro, E. (2007). Discontinuous galerkin finite element method applied to the 1-d spherical neutron transport equation. *J. Comp. Phys.*, 223:67–81.

Monk, P. (1994). Superconvergence of finite element approximations to maxwells equations. *Numer. Methods Partial Differential Eq.*, 10:793–812.

Monk, P. and Süli, E. (1994). A convergence analysis of yee's scheme on nonuniform grids. *SIAM J. Numer. Anal.*, 32:393–412.

Mu, L., J. Wang, X. Y., and Zhang, S. (2015a). A weak galerkin finite element method for the maxwell equations. *J. Sci. Comput.*, 65:363–386.

Mu, L., Wang, J., Wang, Y., and Ye, X. (2013). A computational study of the weak galerkin method for second-order elliptic equations. *Numerical Algorithms*, 63(4):753–777.

Mu, L., Wang, J., and Ye, X. (2014). Weak galerkin finite element methods for the biharmonic equation on polytopal meshes. *Numer. Methods Partial Differential Equations*, 30(3):1003–1029.

Mu, L., Wang, J., and Ye, X. (2015b). Weak galerkin finite element methods on polytopal meshes. *Int. J. Numer. Anal. Model.*, 12:31–53.

Nicolaides, R. and Wang, D.-Q. (1998). Convergence analysis of a covolume scheme for maxwell's equations in three dimensions. *Math. Comp.*, 67:947–963.

Oden, J., Babuśka, I., and Baumann, C. (1998). A discontinuous hp finite element method for diffusion problems. *J. Comp. Phys.*, 146:491–519.

Qiao, Z., Yao, C., and Jia, S. (2011). Superconvergence and extrapolation analysis of a nonconforming mixed finite element approximation for time-harmonic maxwell's equations. *J. Sci. Comput.*, 46:1–19.

Ramo, S., Whinnery, J., and Duzer, T. V. (1994). *Fields and Waves in Communications Electronics, 3rd ed.* John Wiley & Sons.

S.Borm and R.Hiptmair (2002). Multigrid computation of axisymmetric electromagnetic fields. *Adv. Comput. Math.*, 16:331–356.

Scheid, C. and Lanteri, S. (2013). Convergence of a discontinuous galerkin scheme for the mixed time domain maxwell's equations in dispersive media. *IMA J. Numer. Anal.*, 33:432–459.

Schüppert, B. (1988). Microstrip/slotline transitions: Modeling and experimental investigation. *IEEE Transactions on Microwave Theory and Techniques*, 36.

Sen, B. and Wheeler, R. L. (1998). Skin effects models for transmission line structures using generic spice circuit simulators. unpublished manuscript.

Shi, D. and Pei, L. (2009). Low order crouzeix-raviart type nonconforming finite element methods for the 3d time-dependent maxwells equations. *Appl. Math. Comp.*, 211:1–9.

Shields, S., Li, J., and Machorro, E. A. (Under Review). Weak galerkin methods for time-dependent maxwell's equations. *Comp. and Math. with App.*

Ulaby, F. (2007). *Fundamentals of Applied Electromagnetics, 5th ed.* Prentice Hall.

Wahlbin, L. (1995). *Superconvergence in Galerkin Finite Element Methods*. Springer, Berlin.

Wang, B., Xie, Z., and Zhang, Z. (2010). Error analysis of a discontinuous galerkin method for maxwell equations in dispersive media. *J. Comp. Phys.*, 229:8552–8563.

Wang, C. and Wang, J. (2015). A hybridized weak galerkin finite element method for the biharmonic equation. *Int. J. Numer. Anal. Model.*, 12(2):302–317.

Wang, J., Xie, Z., and Chen, C. (2015). Implicit dg method for time domain maxwells equations involving metamaterials. *Adv. Appl. Math. Mech.*, 7:796–817.

Wang, J. and Ye, X. (2001). Superconvergence of finite element approximations for the stokes problem by projection methods. *SIAM J. Numer. Anal.*, 39:1001–1013.

Wang, J. and Ye, X. (2013). A weak galerkin finite element method for second-order elliptic problems. *J. Comput. Appl. Math.*, 241:103–115.

Wang, J. and Ye, X. (2014). A weak galerkin mixed finite element method for second-order elliptic problems. *Math. Comp.*, 83:2101–2126.

Wang, J. and Ye, X. (2016). A weak galerkin finite element method for the stokes equations. *Adv. Comput. Math.*, 42(1):155–174.

Ziolkowski, R. (2003). Pulsed and cw gaussian beam interactions with double negative metamaterial slabs. *Optical Express*, 11:662–681.

VITA

Graduate College
University of Nevada, Las Vegas, USA

Sidney Shields

Degrees:

Bachelor of Science in Mathematics, 2011
Pacific Union College, Angwin, CA

Publications:

J. Li, and S. Shields. "Superconvergence analysis of Yee scheme for metamaterial Maxwells equations on non-uniform rectangular meshes." Numerische Mathematik (2016) 134: 741-781.

J. Li, E. A. Machorro, and S. Shields. "Numerical study of signal propagation in corrugated coaxial cables." Journal of Computational and Applied Mathematics 309 (2017): 230-243.

S. Shields, J. Li, and E. A. Machorro. "Weak Galerkin methods for time-dependent Maxwell's equations." Computers and Mathematics with Applications (Under Review).

Thesis Title:

Novel methods for the time-dependent Maxwell's equations and their applications

Thesis Examination Committee:

Chairperson, Jichun Li, Ph.D.
Committee Member, Monika Neda, Ph.D.
Committee Member, Hongtao Yang, Ph.D.
Committee Member, Pengtao Sun, Ph.D.
Graduate Faculty Representative, Yi-Tung Chen, Ph.D.